OPEN HEART: ECG Based Cardiac Disease Analysis & Diagnosis System

By

FAYYAZ UL AMIR AFSAR MINHAS

(Thesis submitted in partial fulfillment of requirements for MS Systems Engineering)

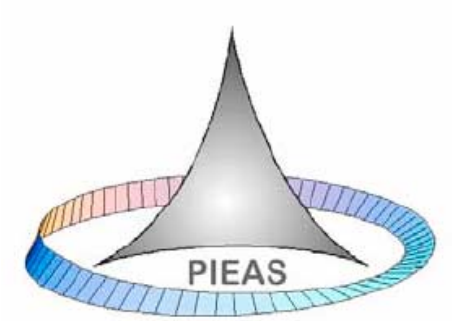

Department of Electrical Engineering
Pakistan Institute of Engineering and Applied Sciences
Nilore-45650, Islamabad
August, 2007

Allah says

Ah! Ye are those who love them, but they love you not, though ye believe in the whole of the Book. When they meet you, they say, "We believe": But when they are alone, they bite off the very tips of their fingers at you in their rage. Say: "Perish in you rage; Allah knoweth well all the secrets of the heart."

Al-Qur'an, 003.119 (Aal-E-Imran [The Family of Imran])

Declaration of Originality

I hereby declare that the work contained in this thesis and the intellectual content of this thesis are the product of my own work. This thesis has not been previously published in any form nor does it contain any verbatim of the published resources which could be treated as infringement of the international copyright law.

I also declare that I do understand the terms ‘copyright’ and ‘plagiarism,’ and that in case of any copyright violation or plagiarism found in this work, I will be held fully responsible of the consequences of any such violation.

Signature: _____

Name: Fayyaz-ul-Amir Afsar Minhas

Date: _____

Place: _____

CERTIFICATE OF APPROVAL

This is to certify that the work contained in this thesis entitled

"*OPEN HEART*: ECG Based Cardiac Disease Analysis & Diagnosis System"

was carried out by

Mr. Fayyaz-ul-Amir Afsar Minhas

Under my supervision and that in my opinion, it is fully adequate, in scope and quality, for the degree of MS Systems Engineering from Pakistan Institute of Engineering and Applied Sciences (PIEAS).

Approved By:

Signature:_____

Supervisor: ***Dr. Muhammad Arif***

PE, DCIS

PIEAS

To

The loving memory of my Father,

The love of my Mother,

My Brothers, Munir and Shahid,

My very Dear, Loving and Caring Sister, Shaista,

And

All My Teachers at school and college, especially, Mr. Sajid Mehmood and Mr. Sadaqat Hayat

As a gesture of gratefulness to all the dedication, love and care they rendered to me!

ACKNOWLEDGEMENTS

Praise be to Allah Almighty for He bestowed upon us intelligence, gave us the mental strength to demystify the secrets of the universe, conferred to us the will and the strength to explore and the power to aim for and achieve our goals.

I would like to especially thank my project supervisor, Dr. Muhammad Arif, DCIS, PIEAS without whom this thesis would not exist. During the course of the project it was his intelligence, patience and persistent moral and technical support which acted as a beacon for me to move on.

I am also very grateful To Mr. Yousuf Kakakhel, DNM and Dr. Muhammad Tufail, DEE, PIEAS, who were my project examiners, for their keen interest and extremely fruitful suggestions.

I must also thank Dr. Anila Usman and Dr. Javed Khusrshid, DCIS, PIEAS for the provision of Special Compuatational Lab Facilites and workplace for the project.

I owe a great deal to Mr. Rahat Abbas, Mr. Atiq A. Tahir, Mr. Rafiullah Chamlawi and Mr. Imran Usman, PhD. Scholars, DCIS, PIEAS for providing technical and moral support for the project.

I would also like to thank Brig. Imran Majeed, M.D, Armed Forces Institute of Cardiology (Rawalpindi, Pakistan) and Dr. Kee-Ho Yu, Division of Mechanical and Aerospace Systems Engineering, Chonbuk National University (Jeonju, Korea) for sharing their medical and technical knowledge for the project, especially in its initial phases.

Lastly, many thanks to Ms. Shahzadi Farah, for helping me in the project and in the proof reading of this thesis.

Fayyaz ul Amir Afsar Minhas

PIEAS, Nilore, Islamabad

Table of Contents

List of Figures

List of Tables

Executive Summary

Cardiac disease is one of the leading causes of death all over the world. With the inception of fast signal processing and computing hardware, techniques for the automatic detection of cardiac disorders through ECG has stemmed up as one of the most promising methodologies in Clinical Decision Support Systems. Such a system can offer rapid, accurate and reliable diagnosis to a variety of cardiac diseases and can reduce the work load for cardiac experts along with providing a facility for the simultaneous monitoring of multiple patients. In this work we have developed techniques for the automatic processing and analysis of the ECG. The work is divided into three major parts: Part-I involving study and implementation of methods for removal of artifacts from the ECG. These include baseline and noise removal techniques. In this work we have compared different baseline removal techniques, such as use of digital FIR and IIR filters and 3 different polynomial fitting approaches, to find out that the use of a two stage first order polynomial fitting based method introduces least distortion in the ECG while effectively compensating the ECG baseline. For Noise removal, we compare and contrast three different techniques, i.e. Use of Digital filters, Independent Component Analysis (ICA) and Local Nonlinear Projective Filtering. We conclude that nonlinear projective filtering performs well in removing noise from the ECG, whereas the potential of ICA for this purpose has been explored.

Part-II involves the segmentation of different ECG components, i.e. P, QRS and T-waves using methods based on digital filters, Continuous Wavelet Transform (CWT) and the Discrete Wavelet Transform. A new method for QRS detection and delineation through CWT has been developed which compares well with existing research offering Sensitivity/Specificity of ~99.8% for detection of QRS with ~10ms error in determining its onset and offset. The accuracy of an existing DWT based method has been improved through the use of Genetic Algorithms (GA). We conclude that the use of DWT with parameter optimization through GA proves to be the most effective technique for ECG Segmentation giving equally good accuracy in terms of detection and delineation.

Part-III is concerned with the classification of different types of heart rhythms (Normal, Atrial Premature Beats, Ventricular Premature Beats, Paced Rhythms, Left

and Right Bundle Branch Blocks) and the detection of ST Segment deviations connected to Ischemic Heart Disease. For the purpose of classification of different arrhythmias we have compared DWT based features with those obtained from the Discrete Fourier Transform (DFT) to conclude that DWT is more effective in the classification of different types of heart rhythms. We have achieved 99.1% accuracy through implementing a DWT based technique for feature extraction and using k-Nearest Neighbor classifiers. These results have been compared with those obtained through the use of Probabilistic Neural Networks (PNN) and Learning Vector Quantization (LVQ) Neural Networks. We have also compared the performance of different types of feature extraction and classification techniques for the detection of ischemic ST deviation episodes, such as time-domain features with a rule based classifier, use of Principal Component Analysis (PCA) based features with a Backpropagation Neural Network, a Neural Network Ensemble and a Support Vector Machine (SVM) ensemble classifier. We have achieved a Sensitivity/Positive Predictivity of ~90% with the use of a novel Neural Network Ensemble which uses lead specific principal components as features. These results are highest in terms of accuracy when compared with the existing literature with the novelty lying in the use of lead specific KLT Bases and Ensemble Neural Classifiers for each lead.

The work reported in this thesis can be used to establish the foundations of a practical stand-alone system for patient monitoring and the design of a multiple patient monitoring system as required in hospitals.

List of Publications:

1) Afsar, F.A. and M. Arif, *QRS Detection and Delineation Techniques for ECG Based Robust Clinical Decision Support System Design*, in *National Science Conference*. June, 2007: Lahore, Pakistan.
2) Afsar, F.A. and M. Arif, *QRS Detection and Delineation through Continuous Wavelet Transform*
   [Under Development for the Sixth IASTED International Conference on Biomedical Engineering]
3) Afsar, F.A., M. Arif, and M. Yousuf, *A Comparison of Wavelet and Fourier Domain Features for Beat Classification in the Electrocardiogram* [Under Development for the Sixth IASTED International Conference on Biomedical Engineering]

4) Afsar, F.A. and M. Arif, *Detection of ST Segment Deviation Episodes in the ECG using KLT with an Ensemble Neural Classifier*, in *International Conference on Emerging Technologies (ICET 2007)*. 2007: Islamabad, Pakistan. [submitted: under review]
5) Afsar, F.A. and M. Arif, *Use of Lead Specific KLT Bases and Ensemble Classifiers for the Detection of Ischemic ST Segment Episodes* [Extended version of (4) for the Journal *Physiological Measurements*, Under Development]

CHAPTER 1
INTRODUCTION

Electrocardiogram (ECG or EKG) is a noninvasive tool that has been in use for determining the cardiac status of a subject for almost a century. ECG presents an effective means of analyzing the heart rhythm and studying the conduction pathways in the heart. The in-depth examination of the ECG enables us to derive a number of informative measurements from the characteristic ECG waveforms. ECG analysis is the archetype for the timely detection of dangerous cardiac conditions in clinical settings. Such an examination or analysis is carried out practically by specially trained medical experts. Because of its systematic nature and the large amount of time spent in performing the task manually, ECG analysis is a good candidate for automation and comprises an important component in the field of biomedical signal processing.

1.1 Impetus & Objectives of the Project

This project is aimed at the development of an initially offline ECG Analyzer and an expert system for the classification and prediction of cardiac disorders. The incentive behind development of such a system is to aid a medical expert in interpreting the ECG by providing the ability of reliable and fast feature extraction (such as heart rate etc.) from the ECG, thus saving plenty of time and effort by the valued cardiac expert. The system is also to incorporate disease classification and prediction. These features of the system enable medical experts to respond to emergencies and monitor a larger number of patients simultaneously. These features can also help an average physician (one who is not a cardiac expert) to handle cardiac patients much more easily, effectively and accurately. Moreover, such a system also finds its application as a teaching aid for doctors and medical staff.

The applications of such a system are difficult to summarize here, however one may easily deduce about the efficacy of the system, by keeping in mind that heart diseases are the dominant cause of natural deaths all over the world. In Pakistan, the major contributor to the short average life span is the development of cardiac diseases at relatively young ages and a lack of awareness amongst the masses. The situation is

worsened by the presence of only a small number of cardiac experts per unit of population and the lack of proper equipment in the hospitals. Commercial analysis software and Expert systems are costly and therefore are viewed only as prohibitive alternatives. In such a situation, locally developed software is bound to be of extreme assistance to the cardiac experts and the general physician alike.

1.2 System Architecture

The proposed architecture of the system comprises of the following major components:

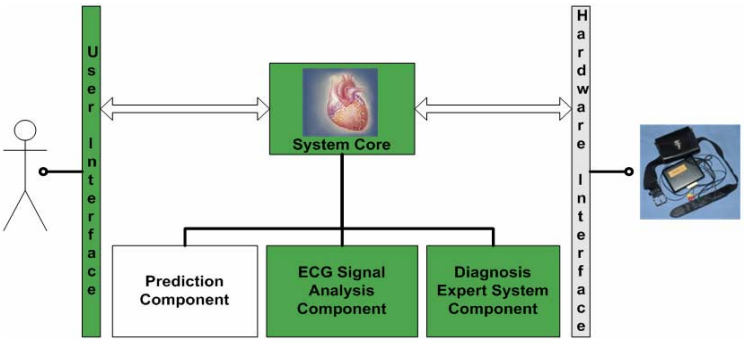

fig. 1-1 System Components

Below a description of each of the sub systems is presented:

1.2.1 User Interface

It presents a high level interface to the medical expert for carrying out tasks such as marking and viewing annotations, viewing decision results and diagnosis reports etc.

1.2.2 ECG Signal Analysis Component

The objective of this component is to develop a subsystem which would calculate different time domain parameters from the given ECG signals after detection and removal of different artifacts (such as baseline wandering and noise etc.) to produce an analysis report which can be displayed to the medical expert using a user interface. This component is divided in to three further components.

- Signal Conditioning

Signal conditioning involves the application of techniques for the removal of different types of artifacts (Baseline wandering, Noise etc.) from the ECG Signal.

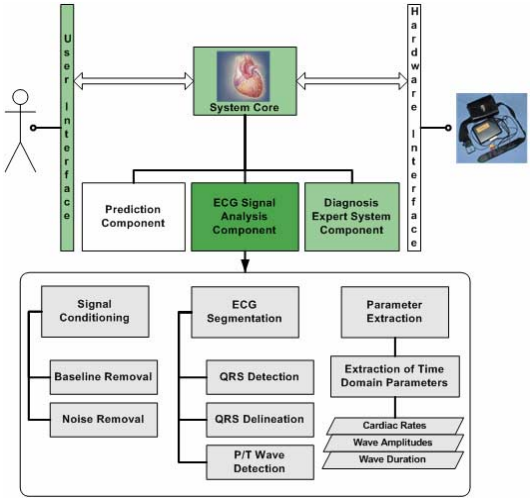

fig. 1-2 ECG Signal Analysis

- **ECG Segmentation**

ECG Segmentation is related the detection and delineation (determination of onset and offset) of the QRS Complex and the P/T waves which is required for subsequent feature extraction techniques.

- **Parameter Extraction**

Parameter extraction relates to the extraction of time domain parameters (such as cardiac rates, wave amplitudes and durations etc.) from the ECG using the information obtained from ECG Segmentation. A list of these parameters is given below:

- *Beat Level Parameters*

These include the following parameters:

  - P/T/U-Wave Parameters: Peak Location, Amplitude, Morphology of the P/T/U-wave
  - QRS Complex Parameters: Reference Point, Morphology, Axis, Q-Wave Location, Amplitude and Duration, R-Wave Location, Amplitude and Duration, S-Wave Location, Amplitude and Duration
  - Detection and Extraction of ST Segments
  - Calculation of QT, and PR Intervals

- *Multi-beat Parameters*

These include the following features:

- Heart Rate (HR or RR-Interval) Variability
- PR Interval Variability
- QT Interval Variability

1.2.3 Diagnosis Expert System Component

This component is aimed at the development of an expert system that would utilize the time domain features extracted during the analysis phase and combine with them other disease specific characteristics to detect the presence of different cardiac disorders in the given ECG Signals. The different categories to be considered at different stages during this phase include:

- Arrhythmias

  E.g. Tachycardia, Bradycardia, Artrial and Ventrical Fibrillations and flutters etc.
- Coronary Artery Diseases

  E.g. Myocardial Ischemia, Injury and Infarctions etc
- Hypertrophies
- Inflammations of the Heart

  E.g. Myocarditis and Pericarditis
- Conduction Problems

  E.g. Heart Blocks, Bundle Branch Blocks etc

This component logically comprises of two modules, i.e. Feature Extraction and Classification (see figure below).

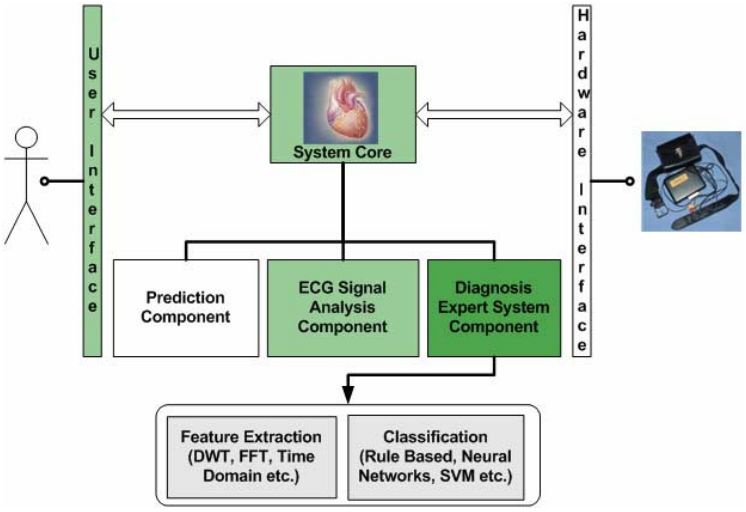

fig. 1-3 Diagnosis Expert System Component

A variety of feature extraction techniques such as Discrete Wavelet Transform, Discrete Fourier Transform, and Principal Component Analysis etc. can be employed along with time domain features obtained from the analysis phase. For the purpose of classification we can use Rule Based Classification, Fuzzy Inference Systems, Neural Networks, Support Vector Machines etc.

1.2.4 Prediction Component

This is the fourth component of the system in which the temporal probability values for the occurrence of specific cardiac events or disorders are to be calculated before time. This component in the overall system design has not been considered in this thesis.

1.2.5 Hardware Interface

This component involves the integration of the system with a commercially available ECG Machine. This phase has not been considered for implementation in this thesis.

1.2.6 System Core

The task of this component is to coordinate the flow of information between different system level components.

1.3 Organization of the Thesis

This document serves as a detailed description of the project and presents in detail, different steps involved in the development of the ECG Signal Analysis and Diagnosis Components. Chapter-1 presents the introduction to the project. Chapter-2 gives an introduction to the working of the heart. Chapter-3 provides an overview of the characteristics of different datasets used in this work. Chapter-4 describes different techniques for the removal of artifacts from the ECG techniques for ECG with chapter-5 describing the QRS Detection and Delineation Strategies. Chapter-6 explains the procedures for the detection and Feature extraction in relation to the T and P-waves whereas in chapter-7, Methods for the classification of different types of

arrhythmias are given. Chapter-8 gives the details techniques implemented for the detection of ST Segment Deviation Episodes. Chapter-9 presents the conclusions and future work. Each chapter describes the objectives and importance of the task it addresses, presents a review of the existing methodologies, describes in detail the implemented schemes, and gives a programmer function reference and quality evaluation for the implemented techniques.

CHAPTER 2
HEART & THE ECG

In this chapter we describe the structural and functional working of the heart along with a detailed overview of electrical activity within the heart that leads to rhythmic operation of the heart and can be observed, non-invasively, through the electrocardiogram. We also delineate different types of ECG systems that are used for ECG acquisition. An account of the diagnostic use of the ECG and its limitations is also given.

2.1 Anatomy and working of the Heart

The heart is a four-chambered pump, located in the chest cavity surrounded by a membrane called pericardium, which serves two purposes: to move oxygen depleted blood to the lungs to exchange CO_2 and O_2, and to move oxygen rich blood from the lungs to the rest of the body, including the heart itself. The top two chambers of the heart are called the *atria*, which receive blood from the veins of the circulatory system. The lower two chambers are called the *ventricles* and provide the main pumping force needed to push the blood to the lungs or the rest of the body.

In general, blood moves through the heart in following series of steps, as shown in Figure 2.1.

- First un-oxygenated blood moves into the Right Atria (3) of the heart through the Superior (1) and Inferior (2) Vena Cava.
- The Atria then contracts and pushes the blood through a one-way valve (called the Tricuspid valve (4)) into the Right Ventricle (5).
- The Right Ventricle then contracts, pushing the blood out of the heart to the pulmonary arteries (7) to the lungs for the exchange of CO_2 for O_2.
- The blood then returns to the heart's Left Atria (9) via the pulmonary veins (8).
- The Atria again contracts and push the blood through another one-way valve (called the Mitral valve (10) into the left Ventricle (11).

- The left Ventricle then contracts, pushing the blood out of the heart to the Aorta (13), which then branches off to the rest of the arteries of the human body.

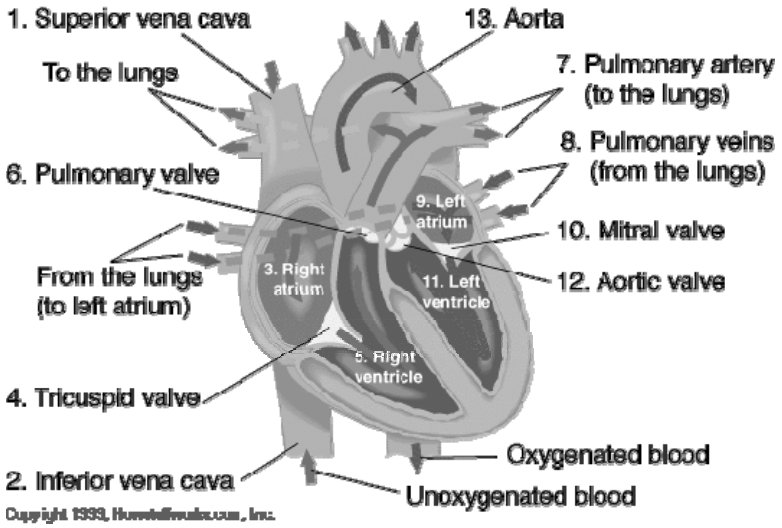

fig. 2-1 Blood Flow in the Heart

The heart gets its own blood supply through the coronary arteries which stem from the aorta as shown below.

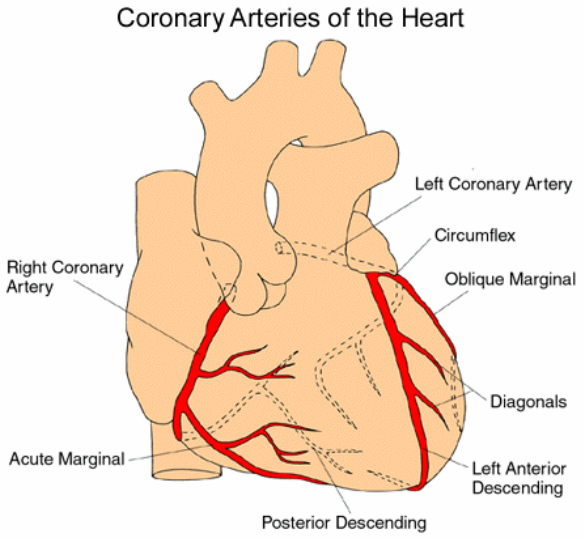

fig. 2-2 Coronary Arteries

2.2 Electrical Activity in the Heart

In this section we describe how the pumping action of the heart is triggered by electric impulses generated from within the heart. We first detail the concept of action potentials and the way these action potentials cause muscular contraction in the heart muscle producing the pumping action of the heart. We then discuss how these

impulses are generated and conducted to the heart muscle by explaining the functioning of cardiac pacemakers and the electrical conduction system of the heart.

2.2.1 Action Potentials and the Heart Muscle (Myocardium)

The most important function of heart cells is to contract rhythmically and systematically. The contraction of the heart as a whole is as a direct result of the contraction of all of the tiny cells of the heart muscle. These contractions are triggered by an electrical impulse known as the *action potential [1]*. Before discussing the cardiac action potential, we must first know what an action potential is.

A thin membrane surrounds each cell in our body. Different ions (small charged molecules can move across the cell membrane through the special ion channels. The channels can freely let one type of ions go through the membrane and block passage of other types of ions. Due to such a specific permeability a concentration gradient is established across the cellular membrane. Because ions are charged molecules, an electrical gradient is also established across the cell membrane. This imbalance in electrical charge across the cell membrane is known as the *membrane potential*. Every cell in our body is slightly more negative inside then outside with a resting membrane potential of approximately (- 0.1 V or -100mV).

Some of the cells (called *excitable cells*) are capable to rapidly reverse their resting membrane potential from negative resting values to slightly positive values. This rapid change in membrane potential is called an action potential. The action potential is brought on by a rapid change in membrane permeability to certain ions. Excitable cells include neurons (nerve cells) and muscle cells.

Cardiac muscle has some similarities to neurons and muscle cells, as well as important unique properties. Like a neuron, a given myocardial cell has a negative membrane potential when at rest. Stimulation above a threshold value induces the opening of voltage-gated ion channels and a flood of cations into the cell. When the threshold is met, an action potential initiates. This causes the positively charged ions to enter the cell [depolarization]. Like skeletal muscle, depolarization causes the opening of voltage-gated calcium channels and entry of Ca^{2+}. This influx of calcium causes calcium-induced calcium release from the calcium storing sarcoplasmic reticulum in the cell, and the increase in myoplasmic free Ca^{2+} concentration causes muscle contraction. After a delay (the absolute refractory period), Potassium channels

reopen and the resulting flow of K+ out of the cell causes repolarization to the resting state.

The standard model used to understand the cardiac action potential is the action potential of the ventricular myocyte. The action potential has 5 phases (numbered 0-4). Phase 4 is the resting membrane potential, and describes the membrane potential when the cell is not being stimulated.

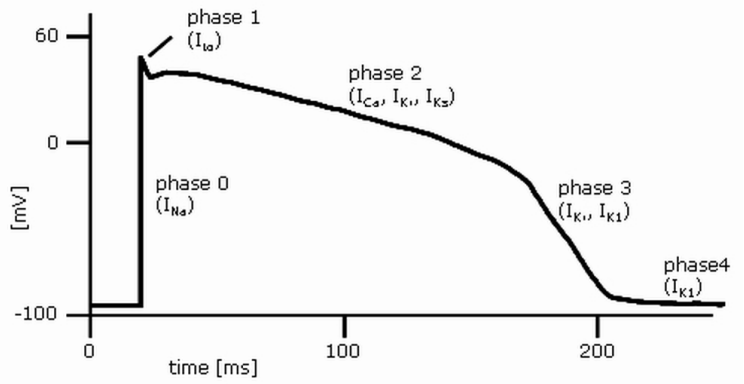

fig. 2-3 Action Potentials in the Heart

Once the cell is electrically stimulated (typically by an electric current from an adjacent cell), it begins a sequence of actions involving the influx and efflux of multiple cations and anions that together produce the action potential of the cell, propagating the electrical stimulation to the cells that lie adjacent to it. In this fashion, an electrical stimulation is conducted from one cell to all the cells that are adjacent to it, to all the cells of the heart.

2.2.1.1 Phase 4

Phase 4 is the resting membrane potential. This is the period that the cell remains in until it is stimulated by an external electrical stimulus (typically an adjacent cell). This phase of the action potential is associated with diastole of the chamber of the heart.

2.2.1.2 Phase 0

Phase 0 is the rapid depolarization phase. The slope of phase 0 represents the maximum rate of depolarization of the cell and is known as Vmax. This phase is due to the opening of the fast Na^+ channels causing a rapid increase in the membrane

conductance to Na^+ (GNa) and thus a rapid influx of Na^+ ions (I_{Na}), also known as *funny* current, into the cell; a Na^+ current.

The ability of the cell to open the fast Na^+ channels during phase 0 is related to the membrane potential at the moment of excitation. If the membrane potential is at its baseline (about -85 mV), all the fast Na^+ channels are closed, and excitation will open them all, causing a large influx of Na^+ ions. If, however, the membrane potential is less negative, some of the fast Na^+ channels will be in an inactivated state insensitive to opening, thus causing a lesser response to excitation of the cell membrane and a lower V_{max}. For this reason, if the resting membrane potential becomes too positive, the cell may not be excitable, and conduction through the heart may be delayed, increasing the risk for arrhythmias.

2.2.1.3 Phase 1

Phase 1 of the action potential occurs with the inactivation of the fast Na^+ channels. The transient net outward current causing the small downward deflection of the action potential is due to the movement of K^+ and Cl^- ions, carried by the I_{to1} and I_{to2} currents, respectively. Particularly the I_{to1} contributes to the "notch" of some ventricular cardiomyocyte action potentials.

2.2.1.4 Phase 2

This "plateau" phase of the cardiac action potential is sustained by a balance between inward movement of Ca^{2+} (I_{Ca}) through L-type calcium channels and outward movement of K^+ through the slow delayed rectifier potassium channels, I_{Ks}.

2.2.1.5 Phase 3

During phase 3 of the action potential, the L-type Ca^{2+} channels close, while the slow delayed rectifier (I_{Ks}) K^+ channels are still open. This ensures a net outward current, corresponding to negative change in membrane potential, thus allowing more types of K^+ channels to open. These are primarily the rapid delayed rectifier K^+ channels (I_{Kr}) and the inwardly rectifiyng K^+ current, I_{K1}. This net outward, positive current (equal to loss of positive charge from the cell) causes the cell to repolarize. The delayed rectifier K^+ channels close when the membrane potential is restored to

about -80 to -85 mV, while I_{K1} remains conducting throughout phase 4, contributing to set the resting membrane potential.

2.2.2 Initiation of Action Potentials: Pacemakers

The rhythm of the heart is initiated by action potentials generated by certain cells of the heart that have the ability to undergo spontaneous depolarization, in which an action potential is generated without any influence from nearby cells. This is also known as *automaticity*. The cells that can undergo spontaneous depolarization the fastest are the primary *pacemaker* cells of the heart, and set the heart rate. Usually, these are cells in the SA node of the heart. Electrical activity that originates from the SA node is propagated to the rest of the heart. The fastest conduction of electrical activity is via the *electrical conduction system* of the heart shown in the figure below.

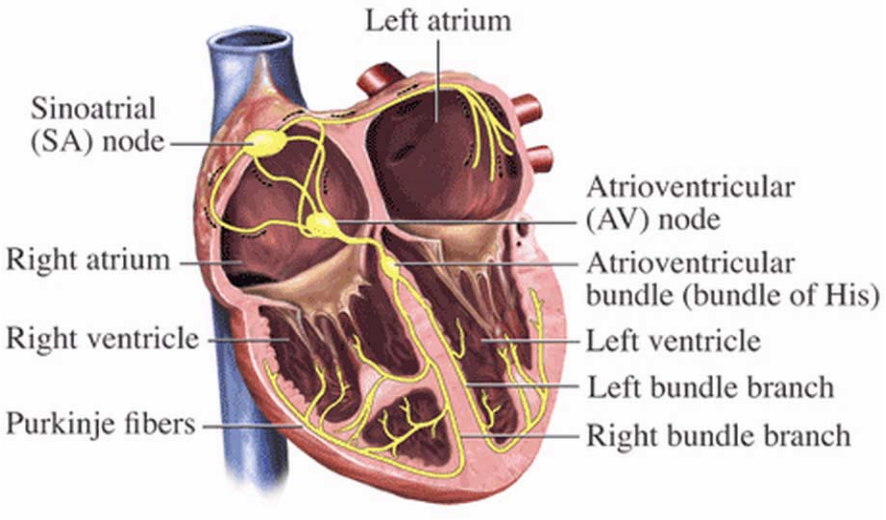

fig. 2-4 Electrical Conduction Pathways in the Heart

Although all of the heart's cells possess the ability to generate these electrical impulses (or action potentials), a specialized portion of the heart, called the sinoatrial node, is responsible for the whole heart's beat.

The sinoatrial node (SA node) is a group of cells positioned on the wall of the right atrium, near the entrance of the superior vena cava. These cells are modified cardiac myocytes. They possess some contractile filaments, though they only contract relatively weakly.

Cells in the SA node will spontaneously depolarize, resulting in contraction, approximately 100 times per minute. This native rate is constantly modified by the activity of sympathetic and parasympathetic nerve fibers, so that the average resting

cardiac rate in adult humans is about 60 beats per minute. Because the sinoatrial node is responsible for the rest of the heart's electrical activity, it is sometimes called the primary pacemaker.

If the SA node doesn't function, or the impulse generated in the SA node is blocked before it travels down the electrical conduction system, a group of cells further down the heart will become the heart's pacemaker, this is known as an ectopic pacemaker. These cells form the atrioventricular node (AV node), which is an area between the atria and ventricles, within the atrial septum.

The cells of the AV node normally discharge at about 40-60 beats per minute, and are called the secondary pacemaker.

Further down the electrical conducting system of the heart, the Bundle of His, the left and right branches of this bundle, and the Purkinje fibres, will also produce a spontaneous action potential if they aren't inhibited by other electrical activity. These tertiary pacemakers fire at a rate of 30-40 per minute.

Even individual cardiac muscle cells will contract rhythmically by themselves.

The reason the SA node controls the whole heart is that its action potentials are released most often; this triggers other cells to generate their own action potentials. In the muscle cells, this will produce contraction. The action potential generated by the SA node, passes down the cardiac conduction system, and arrives before the other cells have had a chance to generate their own spontaneous action potential.

2.2.3 Generation of Action Potentials in Pacemaker Cells

There are three main stages in the generation of an action potential in a pacemaker cell. Since the stages are analogous to contraction of cardiac muscle cells, they have the same naming system. This can lead to some confusion. There is no phase one or two, just phases zero, three and four.

2.2.3.1 Phase 4 - Pacemaker potential

The key to the rhythmical firing of pacemaker cells is that, unlike muscle and neurons, these cells will slowly depolarize by themselves. As in all other cells, the resting potential of a pacemaker cell (-60mV to -70mV) is caused by a continuous outflow or "leak" of potassium ions through ion channel proteins in the membrane that surrounds the cells. The difference is that this potassium permeability decreases

as time goes on, partly causing the slow depolarization. As well as this, there is a slow inward flow of sodium, called the *funny* current. This all serves to make the cell more positive. This relatively slow depolarization continues until the threshold potential is reached. Threshold is between -40mV and -50mV. When threshold is reached, the cells enter phase 0.

2.2.3.2 Phase 0 - Upstroke

Though much faster than the depolarization caused by the funny current and decrease in potassium permeability above, the upstroke in a pacemaker cell is relatively slow compared to that in an axon. The SA and AV node do not have fast sodium channels like neurons, and the depolarization is mainly caused by a slow influx of calcium ions. (The funny current also increases). The calcium is let into the cell by voltage-sensitive calcium channels that opened when the threshold was reached.

2.2.3.3 Phase 3 - Repolarization

The calcium channels are rapidly inactivated, soon after they opened. Sodium permeability is also decreased. Potassium permeability is increased, and the efflux of potassium (loss of positive ions) slowly repolarizes the cell.

2.2.4 Transmission of Electrical Activity in the Heart

Electrical activity in the heart can be shown in the figure below. As we can see that first the electrical potential is originated in SA node. This SA node then depolarizes and electrical activity goes rapidly to AV node. Conduction through AV node is very slow but then depolarization moves rapidly through ventricular conducting system to the apex of heart from where depolarization moves upward and outward through the Purkinje fiber. The Epicardium is the last part of the ventricular wall to receive the depolarization stimulus. The generated potential difference is propagated to the surface of the body through the tissues in contact with the heart and this fact can be used to monitor electrical activity in the heart, non-invasively.

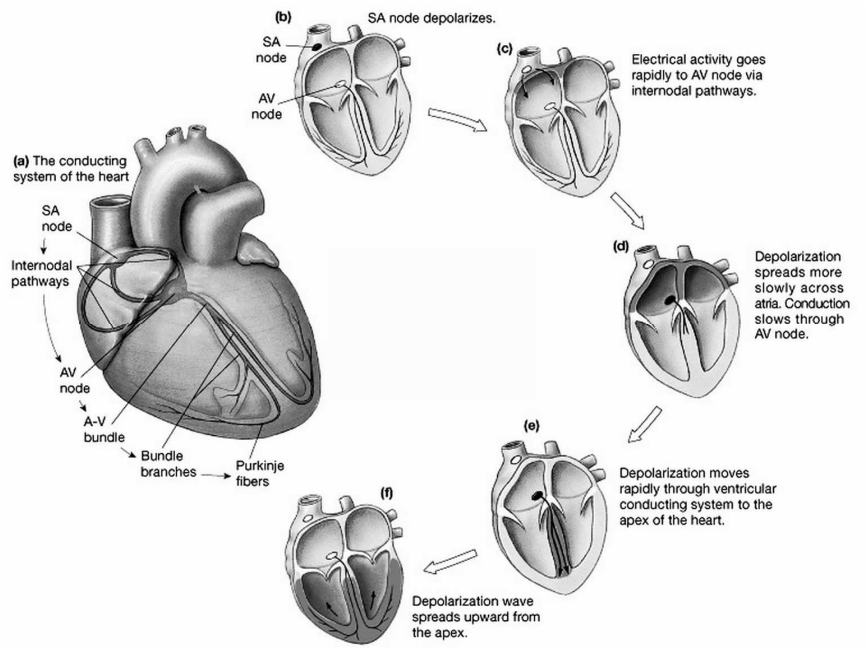

fig. 2-5 Electrical Activity in the Heart

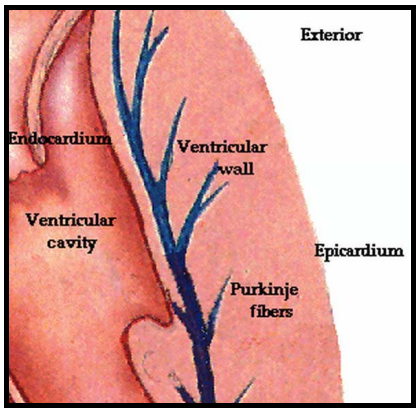

fig. 2-6 The Epicardium

2.3 Measurement of Cardiac Electrical Activity: ECG

The electrical activity in the heart can be measured, non-invasively, with the use of the electrocardiogram which records this electrical activity over time. The ECG device was invented in 1901 by Willem Einthoven, working in Leiden, The Netherlands who used the string galvanometer invented by him along with electromechanical recording and display equipment to record the electrical activity of the heart as shown below. Einthoven assigned the letters P, Q, R, S and T to the various deflections in the ECG, and described the electrocardiographic features of a number of cardiovascular disorders. In 1924, he was awarded the Nobel Prize in Medicine for his achievement.

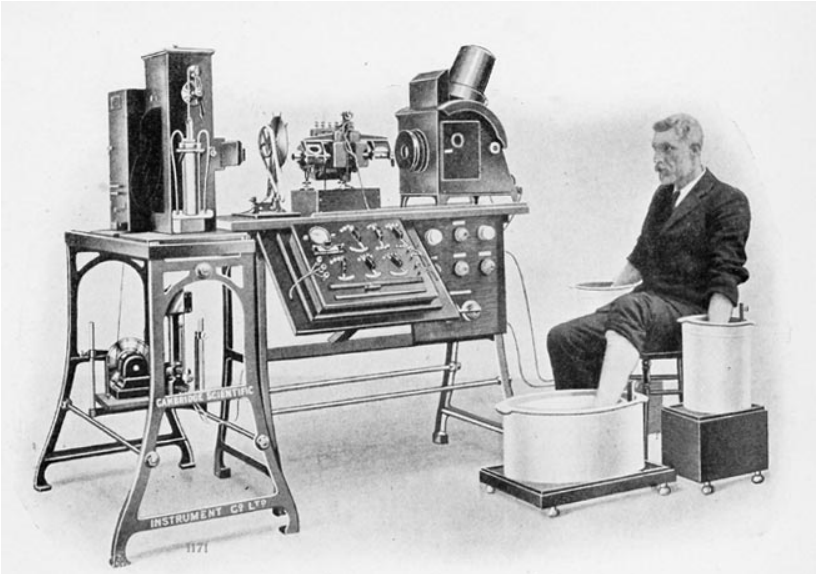

PHOTOGRAPH OF A COMPLETE ELECTROCARDIOGRAPH, SHOWING THE MANNER IN WHICH THE ELECTRODES ARE ATTACHED TO THE PATIENT, IN THIS CASE THE HANDS AND ONE FOOT BEING IMMERSED IN JARS OF SALT SOLUTION

fig. 2-7 The ECG Machine by Einthoven [2]

An electrocardiogram is obtained by measuring electrical potential between various points of the body using a biomedical instrumentation amplifier. A lead records the electrical signals of the heart from a particular combination of recording electrodes which are placed at specific points on the patient's body. As a depolarization wavefront (or mean electrical vector) moves toward a positive electrode, it creates a positive deflection on the ECG in the corresponding lead. When a depolarization wavefront (or mean electrical vector) moves away from a positive electrode, it creates a negative deflection on the ECG in the corresponding lead. When a depolarization wavefront (or mean electrical vector) moves perpendicular to a positive electrode, it creates an equiphasic (or isoelectric) complex on the ECG. It will be positive as the depolarization wavefront (or mean electrical vector) approaches (A), and then become negative as it passes by (B). This phenomenon is shown in the figure below.

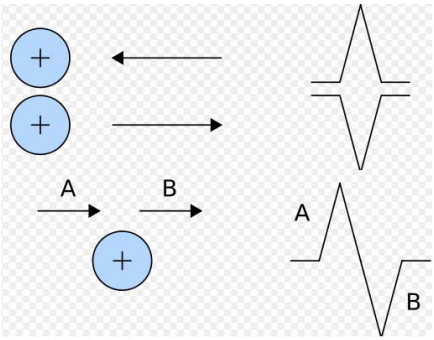

fig. 2-8 Effect of the Movement of Electrical Impulse towards and away from an electrode [2]

The electrical activity of the specialized conduction tissues is not apparent on the surface electrocardiogram (ECG). This is due to the relatively small mass of these tissues compared to the myocardium.

2.4 ECG Systems

In this section we detail different types of ECG systems in use for medical diagnosis.

2.4.1 The 12-Lead ECG System

The 12-lead ECG system consists of 12 leads that are placed on the limbs and the chest. In this system there are two types of leads—*unipolar* and *bipolar*. The former have an indifferent electrode at the center of the Einthoven's triangle (which can be likened to a 'neutral' of the wall socket) at zero potential. The direction of these leads is from the "center" of the heart radially outward and includes the precordial (chest) leads and limb leads— VL, VR, & VF. The latter, in contrast, have both the electrodes at some potential and the direction of the corresponding electrode is from the electrode at lower potential to the one at higher potential, e.g., in limb lead I, the direction is from left to right. These include the limb leads-I, II, and III. These leads are described in more detail in the following.

2.4.1.1 Limb Leads

Leads I, II and III are the so-called limb leads as their corresponding electrodes are placed on the limbs of the patient. They form the basis of what is known as Einthoven's triangle (see figure below). Eventually, electrodes were invented that could be placed directly on the patient's skin. Even though the buckets of salt water are no longer necessary, the electrodes are still placed on the patient's arms and legs to approximate the signals obtained with the buckets of salt water. They remain the first three leads of the modern 12 lead ECG.

- Lead-I is a dipole with the negative electrode on the right arm and the positive electrode on the left arm.
- Lead-II is a dipole with the negative electrode on the right arm and the positive electrode on the left leg.

- Lead-III is a dipole with the negative electrode on the left arm and the positive electrode on the left leg.

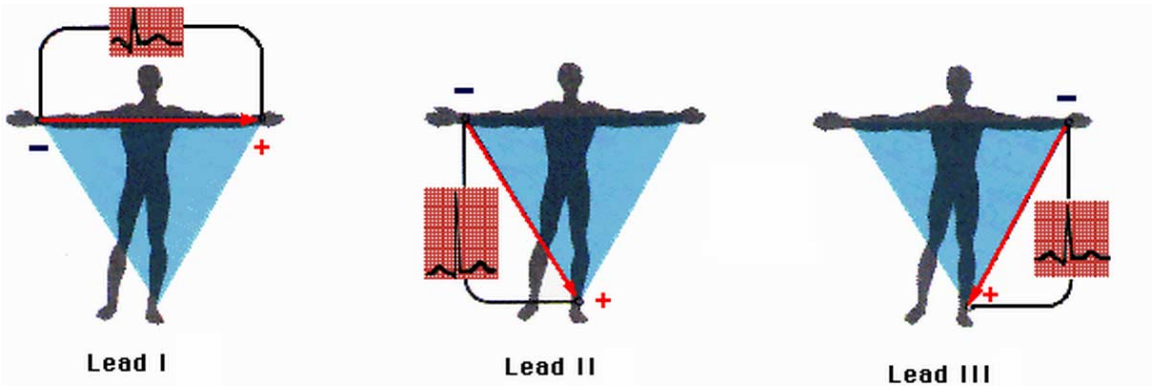

fig. 2-9 Limb Lead Placement

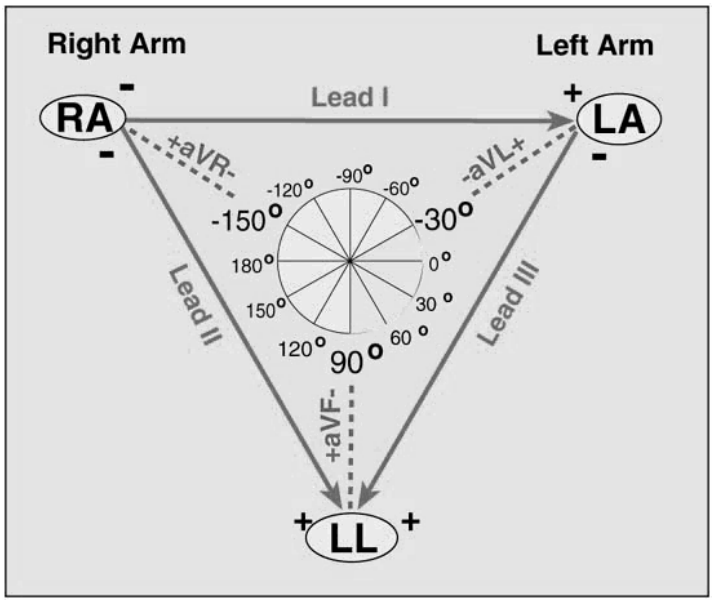

fig. 2-10 The Einthoven Triangle

2.4.1.2 Augmented Limb Leads

Leads aVR, aVL, and aVF are augmented limb leads. They are derived from the same three electrodes as leads I, II, and III. However, they view the heart from different angles (or vectors) because the negative electrode for these leads is derived by adding leads I, II, and III together and plugging them into the negative terminal to form Wilson's Central Terminal for the EKG machine. This zeroes out the negative electrode and allows the positive electrode to become the "exploring electrode" or a unipolar lead. This is possible because Einthoven's Law states that I + (-II) + III = 0. The equation can also be written I + III = II. It is written this way (instead of I + II + III = 0) because Einthoven reversed the polarity of lead II in Einthoven's triangle,

possibly because he liked to view upright QRS complexes. Wilson's central terminal paved the way for the development of the augmented limb leads aVR, aVL, aVF and the precordial leads V1, V2, V3, V4, V5, and V6.

- Lead aVR or "augmented vector right" has the positive electrode (white) on the right arm. The negative electrode is a combination of the left arm (black) electrode and the left leg (red) electrode, which "augments" the signal strength of the positive electrode on the right arm.
- Lead aVL or "augmented vector left" has the positive (black) electrode on the left arm. The negative electrode is a combination of the right arm (white) electrode and the left leg (red) electrode, which "augments" the signal strength of the positive electrode on the left arm.
- Lead aVF or "augmented vector foot" has the positive (red) electrode on the left leg. The negative electrode is a combination of the right arm (white) electrode and the left arm (black) electrode, which "augments" the signal of the positive electrode on the left leg.

The augmented limb leads aVR, aVL, and aVF are amplified in this way because the signal is too small to be useful when the negative electrode is Wilson's central terminal. Together with leads I, II, and III, augmented limb leads aVR, aVL, and aVF form the basis of the hexaxial reference system, which is used to calculate the heart's electrical axis in the frontal plane.

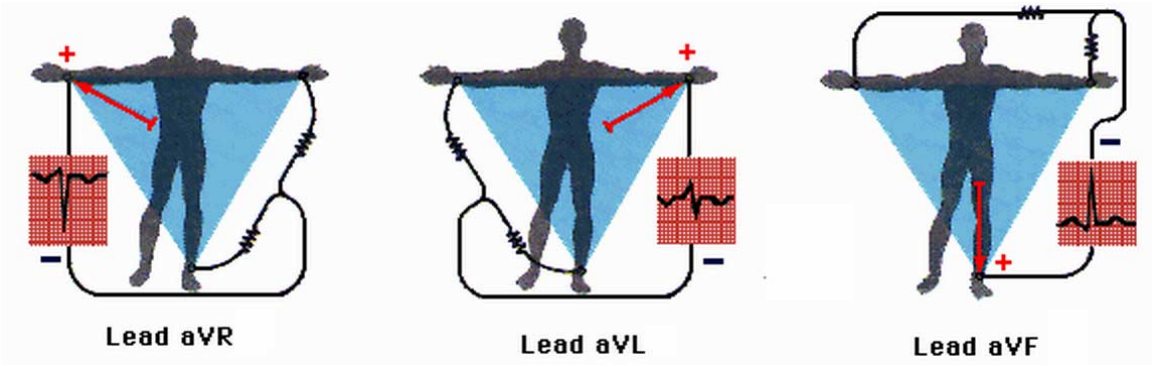

fig. 2-11 Augmented Limb Lead Placement

2.4.1.3 Precordial Leads

The precordial leads V1, V2, V3, V4, V5, and V6 are placed directly on the chest. Because of their close proximity to the heart, they do not require augmentation. Wilson's central terminal is used for the negative electrode, and these leads are considered to be unipolar. The precordial leads view the heart's electrical activity in

the so-called horizontal plane. The heart's electrical axis in the horizontal plane is referred to as the Z axis.

Leads V1, V2, and V3 are referred to as the right precordial leads and V4, V5, and V6 are referred to as the left precordial leads.

The QRS complex should be negative in lead V1 and positive in lead V6. The QRS complex should show a gradual transition from negative to positive between leads V2 and V4. The equiphasic lead is referred to as the transition lead. When the transition occurs earlier than lead V3, it is referred to as an *early transition*. When it occurs later than lead V3, it is referred to as a *late transition*. There should also be a gradual increase in the amplitude of the R wave between leads V1 and V4. This is known as *R wave progression*. Poor R wave progression is a nonspecific finding. It can be caused by conduction abnormalities, myocardial infarction, cardiomyopathy, and other pathological conditions.

- Lead V1 is placed in the fourth intercostal space to the right of the sternum.
- Lead V2 is placed in the fourth intercostal space to the left of the sternum.
- Lead V3 is placed directly between leads V2 and V4.
- Lead V4 is placed in the fifth intercostal space in the midclavicular line
- Lead V5 is placed directly between leads V4 and V6.
- Lead V6 is placed horizontal with V4 in the midaxillary line.

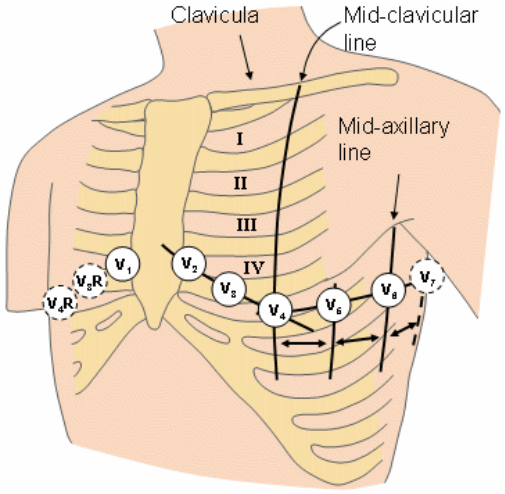

fig. 2-12 Precordial Lead Placement

Additional leads can be added by the physician if required.

2.4.1.4 Ground

An additional electrode is present in modern four-lead and twelve-lead ECGs. This is the ground lead and is placed on the right leg by convention, although in theory it can be placed anywhere on the body. With a three-lead ECG, when one dipole is viewed, the remaining lead becomes the ground lead by default.

2.4.1.5 Clinical Lead Groups

There are twelve leads in total, each recording the electrical activity of the heart from a different perspective, which also correlate to different anatomical areas of the heart for the purpose of identifying acute coronary ischemia or injury. Two leads that look at the same anatomical area of the heart are said to be contiguous as shown in the chart below.

- The inferior leads (leads II, III and aVF) look at electrical activity from the vantage point of the inferior (or diaphragmatic) wall of the left ventricle.
- The lateral leads (I, aVL, V5 and V6) look at the electrical activity from the vantage point of the lateral wall of left ventricle. Because the positive electrode for leads I and aVL are located on the left shoulder, leads I and aVL are sometimes referred to as the high lateral leads. Because the positive electrodes for leads V5 and V6 are on the patient's chest, they are sometimes referred to as the low lateral leads.
- The septal leads, V1 and V2 look at electrical activity from the vantage point of the septal wall of the left ventricle. They are often grouped together with the anterior leads.
- The anterior leads, V3 and V4 look at electrical activity from the vantage point of the anterior wall of the left ventricle.
- In addition, any two precordial leads that are next to one another are considered to be contiguous. For example, even though V4 is an anterior lead and V5 is a lateral lead, they are contiguous because they are next to one another.
- Lead aVR offers no specific view of the left ventricle. Rather, it views the inside of the endocardial wall from its perspective on the right shoulder.

I Lateral	aVR	V1 Septal	V4 Anterior
II Inferior	aVL Lateral	V2 Septal	V5 Lateral
III Inferior	aVF Inferior	V3 Anterior	V6 Lateral

fig. 2-13 Clinical Lead Groups

2.4.2 Modifications to the 12 lead System

In exercise ECG, the signal is distorted because of muscular activity, respiration, and electrode artifacts due to perspiration and electrode movements. The distortion due to muscular activation can be minimized by placing the electrodes on the shoulders and on the hip instead of the arms and the leg, as suggested by R. E. Mason and I. Likar (1966). The Mason-Likar modification is the most important modification of the 12-lead system used in exercise ECG. The accurate location for the right arm electrode in the Mason-Likar modification is a point in the infraclavicular fossa medial to the border of the deltoid muscle and 2 cm below the lower border of the clavicle. The left arm electrode is located similarly on the left side. The left leg electrode is placed at the left iliac crest. The right leg electrode is placed in the region of the right iliac fossa. The precordial leads are located in the Mason-Likar modification in the standard places of the 12-lead system.

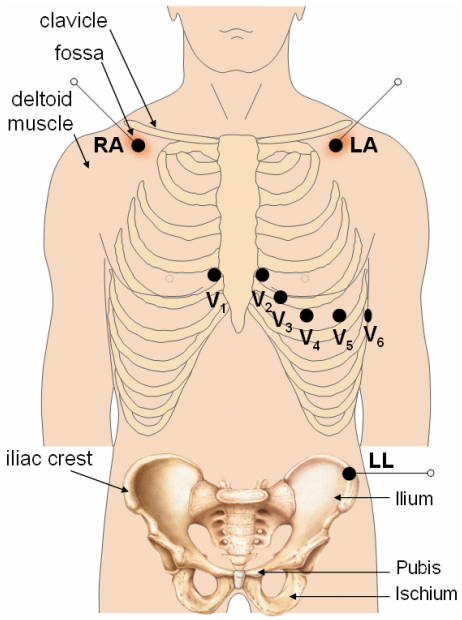

fig. 2-14 ML Lead Placement

In ambulatory monitoring of the ECG, as in the Holter recording, the electrodes are also placed on the surface of the thorax instead of the extremities.

2.4.3 Holter (or Ambulatory) ECG (H-ECG)

The Holter (after its inventor Dr. Norman J. Holter) or Ambulatory ECG is used for long-term monitoring the electrical activity of the heart. The number and position of leads varies by model, but most Holter monitors employ from two to eight.

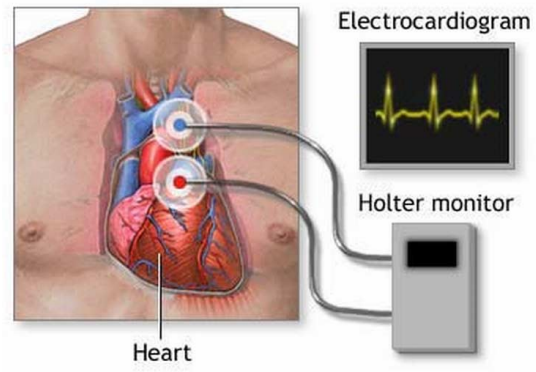

fig. 2-15 The H-ECG

H-ECG is the most widely used method to evaluate symptoms suggestive of cardiac rhythm disturbances (palpitations, dizziness, presyncope). H-ECG is also useful in diagnosis of type of arrhythmias and in identification of the likely underlying mechanism (particularly for supraventricular arrhythmias).

Post-myocardial infarction patients have an increase risk of sudden death, and H-ECG is usually performed before hospital discharge. Several studies performed before the advent of thrombolysis have demonstrated that presence of ventricular arrhythmias (frequent PVC and high grade ventricular ectopy, as repetitive, multiform PVC or VT) has been associated with a higher mortality rate among MI survivors.

Time and frequency domain analysis of HRV obtained through H-ECG is today a well recognized technique capable of providing information on autonomic modulation of the sinus node and of stratifying risk, particularly after myocardial infarction.

H-ECG has been widely used to evaluate the effects of anti-arrhythmic therapy. However, several limitations affect its usefulness, specifically: day-to-day variability in the frequency and type of arrhythmias in many patients, lack of correlation between arrhythmias suppression after an intervention and subsequent outcome, uncertain guidelines for the degree of suppression required to demonstrate an effect.

H-ECG is useful for documenting an adequate control of the ventricular rate in patients with continuous atrial arrhythmias, as chronic atrial fibrillation, because it provides data on the heart rate during the patient's typical daily activities.

Albeit its usefulness, H-ECG carries following demerits with its use when compared with the normal paper 12 lead ECG:

- We can't measure several diseases with H-ECG e.g. axis deviation for which we have to look at leads I and AVF and this is not possible in H-ECG.
- H-ECG cannot be used as screening tool for detecting coronary artery disease
- H-ECG cannot be used for evaluating severity of ischemia in individual patients
- We can detect ventricular hypertrophy using H-ECG but we can't distinguish left ventricle hypertrophy from that of right ventricle hypertrophy
- Before leaving the topic of H-ECG, it should be noted that although we can't use H-ECG for the diagnosis of certain diseases, but it is very useful for the research purpose and for the development of various ECG analyzers.

2.5 Waves and Intervals in the ECG

A typical ECG tracing of a normal heartbeat (shown below) consists of a P wave, a QRS complex and a T wave.

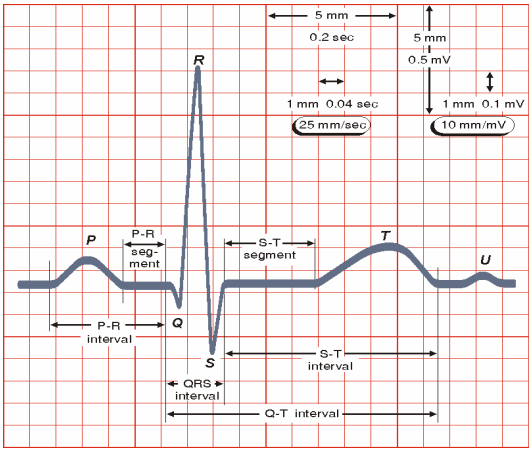

fig. 2-16 Components of a Typical ECG Signal on the ECG Paper

A small *U wave* is normally visible in 50 to 75% of ECGs. The baseline voltage of the electrocardiogram is known as the **isoelectric line**. Typically the isoelectric line is measured as the portion of the tracing following the T wave and preceding the next P wave.

2.5.1 P wave

During normal atrial depolarization, the mean electrical vector is directed from the SA node towards the AV node, and spreads from the right atrium to the left atrium (see figure below)

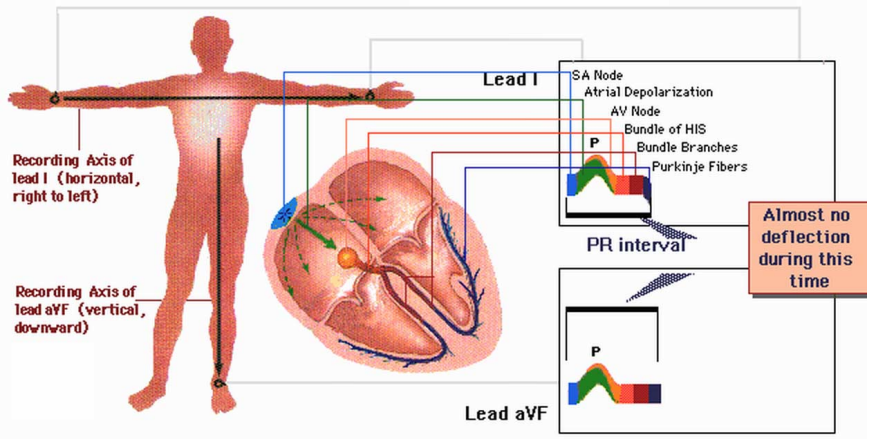

fig. 2-17 Generation of the P-wave

This turns into the P wave on the ECG, which is upright in II, III, and aVF (since the general electrical activity is going toward the positive electrode in those leads), and inverted in aVR (since it is going away from the positive electrode for that lead). A P wave must be upright in leads II and aVF and inverted in lead aVR to designate a cardiac rhythm as Sinus Rhythm.

- The relationship between P waves and QRS complexes helps distinguish various cardiac arrhythmias.
- The shape and duration of the P waves may indicate atrial enlargement.

2.5.2 PR interval

The PR interval is measured from the beginning of the P wave to the beginning of the QRS complex. It is usually 120 to 200 ms long.

- A prolonged PR interval may indicate a first degree heart block.

- A short PR interval may indicate a pre-excitation syndrome via an accessory pathway that leads to early activation of the ventricles, such as seen in Wolff-Parkinson-White syndrome.
- A variable PR interval may indicate other types of heart block.
- PR segment depression may indicate atrial injury or pericarditis.
- Variable morphologies of P waves in a single ECG lead is suggestive of an ectopic pacemaker rhythm such as wandering pacemaker or multifocal atrial tachycardia

2.5.3 QRS Complex

After brief delay at the AV node the impulse originating from the SA node traverses the common bundle of His and the left and right bundle branches and then enters the Interventricular septum causing myocardial depolarization with electric vextor directed right and downward causing a negative Q wave in Lead-I and an upward deflection in aVF. The Impulse continues along conduction system causing depolarization of ventricular (aptical) myocardium with electric vector directed down and left producing the R-wave. As depolarization progresses over ventricles, vector becomes to shift superiorly as well as to the left thus extending the R wave in lead-I and causing downward deflection in aVF. Thus The QRS complex is a structure on the ECG that corresponds to the depolarization of the ventricles. Because the ventricles contain more muscle mass than the atria, the QRS complex is larger than the P wave. In addition, because the His/Purkinje system coordinates the depolarization of the ventricles, the QRS complex tends to look "spiked" rather than rounded due to the increase in conduction velocity. A normal QRS complex is 0.06 to 0.10 sec (60 to 100 ms) in duration.

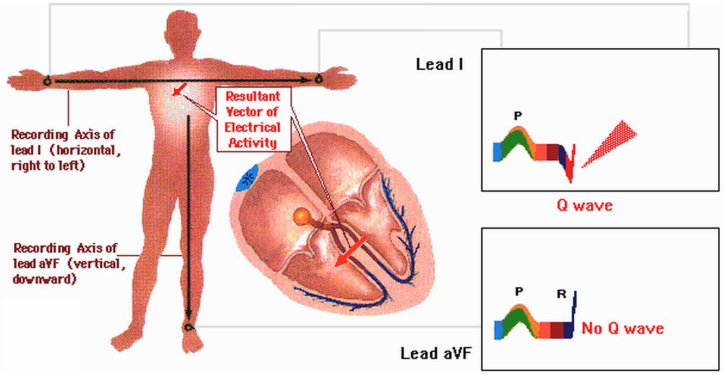

fig. 2-18 Generation of the Q-wave

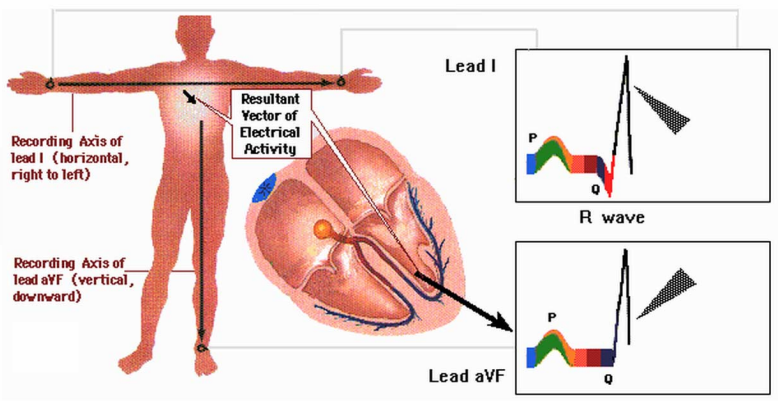

fig. 2-19 Generation of the R-wave

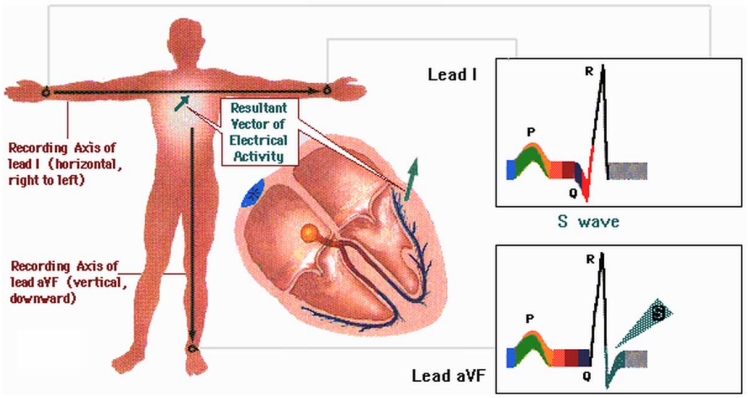

fig. 2-20 Generation of the S-wave

Not every QRS complex contains a Q wave, an R wave, and an S wave. By convention, any combination of these waves can be referred to as a QRS complex. However, correct interpretation of difficult ECGs requires exact labeling of the various waves. Some authors use lowercase and capital letters, depending on the relative size of each wave. For example, an Rs complex would be positively deflected, while a rS complex would be negatively deflected. If both complexes were labeled RS, it would be impossible to appreciate this distinction without viewing the actual ECG.

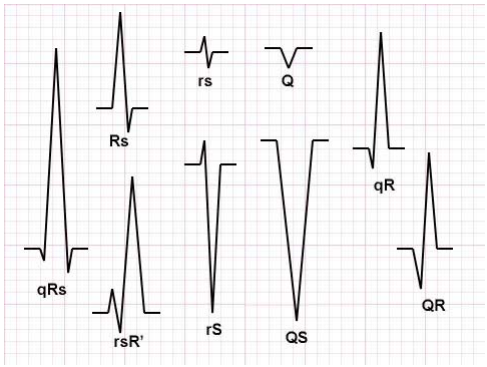

fig. 2-21 QRS Morphologies

- The duration, amplitude, and morphology of the QRS complex is useful in diagnosing cardiac arrhythmias, conduction abnormalities, ventricular hypertrophy, myocardial infarction, electrolyte derangements, and other disease states.
- Q waves can be normal (physiological) or pathological. Normal Q waves, when present, represent depolarization of the interventricular septum. For this reason, they are referred to as septal Q waves, and can be appreciated in the lateral leads I, aVL, V5 and V6.
- Q waves greater than 1/3 the height of the R wave, greater than 0.04 sec (40 ms) in duration, or in the right precordial leads are considered to be abnormal, and may represent myocardial infarction.

2.5.4 ST segment

The ST segment connects the QRS complex and the T wave and has a duration of 0.08 to 0.12 sec (80 to 120 ms). It starts at the J point (junction between the QRS complex and ST segment) and ends at the beginning of the T wave. However, since it is usually difficult to determine exactly where the ST segment ends and the T wave begins, the relationship between the ST segment and T wave should be examined together. The typical ST segment duration is usually around 0.08 sec (80 ms). It should be essentially level with the PR and TP segment.

- The normal ST segment has a slight upward concavity.
- Flat, downsloping, or depressed ST segments may indicate coronary ischemia.
- ST segment elevation may indicate myocardial infarction. An elevation of >1mm (0.1mV) and longer than 80 milliseconds following the J-point. This measure has a false positive rate of 15-20% (which is slightly higher in women than men) and a false negative rate of 20-30%.

2.5.5 T wave

The T wave represents the repolarization (or recovery) of the ventricles. When the heart is fully depolarized, there is no electrical activity for a brief period of time (ST Segment). Then repolarization begins in the epicardium and moves to the

endocardium causing the T-wave. The interval from the beginning of the QRS complex to the apex of the T wave is referred to as the absolute refractory period. The last half of the T wave is referred to as the relative refractory period (or vulnerable period).

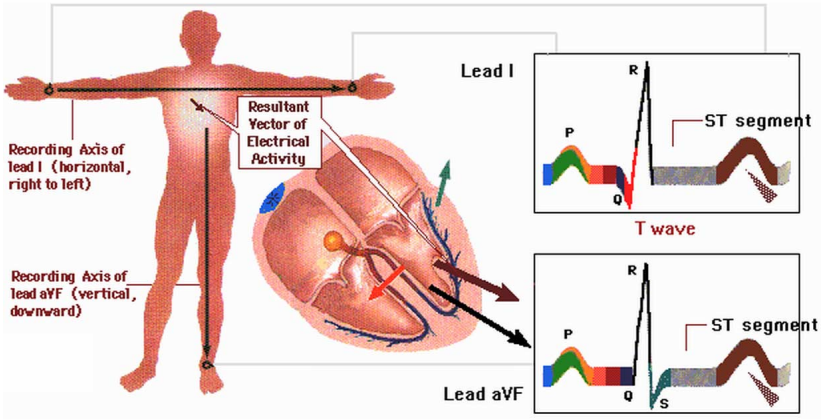

fig. 2-22 ST Segment and the T-wave

In most leads, the T wave is positive. However, a negative T wave is normal in lead aVR. Lead V1 may have a positive, negative, or biphasic T wave. In addition, it is not uncommon to have an isolated negative T wave in lead III, aVL, or aVF.

- Inverted (or negative) T waves can be a sign of coronary ischemia, Wellens' syndrome, left ventricular hypertrophy, or CNS disorder.
- Tall or "tented" symmetrical T waves may indicate hyperkalemia. Flat T waves may indicate coronary ischemia or hypokalemia.
- The earliest electrocardiographic finding of acute myocardial infarction is sometimes the hyperacute T wave, which can be distinguished from hyperkalemia by the broad base and slight asymmetry.
- When a conduction abnormality (e.g., bundle branch block, paced rhythm) is present, the T wave should be deflected opposite the terminal deflection of the QRS complex. This is known as appropriate T wave discordance.

2.5.6 QT interval

The QT interval is measured from the beginning of the QRS complex to the end of the T wave. A normal QT interval is usually about 0.40 seconds. The QT interval as well as the corrected QT interval are important in the diagnosis of long QT syndrome and short QT syndrome. The QT interval varies based on the heart rate, and various correction factors have been developed to correct the QT interval for the heart rate.

The most commonly used method for correcting the QT interval for rate is the one formulated by Bazett and published in 1920. Bazett's formula is,

$$QT_C = \frac{QT}{\sqrt{RR}}$$

where QTc is the QT interval corrected for rate, and RR is the interval from the onset of one QRS complex to the onset of the next QRS complex, measured in seconds. However, this formula tends to be inaccurate, and over-corrects at high heart rates and under-corrects at low heart rates.

2.5.7 U wave

The U wave is not always seen. It is typically small, and, by definition, follows the T wave. U waves are thought to represent repolarization of the papillary muscles or Purkinje fibers. Prominent U-waves are most often seen in hypokalemia, but may be present in hypercalcemia, thyrotoxicosis, or exposure to digitalis, epinephrine, and Class 1A and 3 antiarrhythmics, as well as in congenital long QT syndrome and in the setting of intracranial hemorrhage. An inverted U wave may represent myocardial ischemia or left ventricular volume overload.

2.5.8 ECG Axis

The heart's electrical axis refers to the general direction of the heart's depolarization wavefront (or mean electrical vector) in the frontal plane. It is usually oriented in a right shoulder to left leg direction, which corresponds to the left inferior quadrant of the hexaxial reference system, although -30^o to $+90^o$ is considered to be normal.

- Left axis deviation (-30^o to -90^o) may indicate left anterior fascicular block or Q waves from inferior Myocardial Infarction (MI).
- Right axis deviation ($+90^o$ to $+180^o$) may indicate left posterior fascicular block, Q waves from high lateral MI, or a right ventricular strain pattern.

In the setting of right bundle branch block, right or left axis deviation may indicate bifascicular block.

	Normal Axis 0 to 90	Left Axis Physiological 0 to -30	Left Axis Pathological -30 to -90	Right Axis 90 to 180	Extreme Axis -90 to -180	Indeterminate Axis ?
Lead I						
Lead II						
Lead III						

fig. 2-23 Axis Estimation

2.6 Diagnostic Utility of the ECG

The following disorders can be detected with the ECG:

- Abnormally fast or irregular heart rhythms.
- Abnormally slow heart rhythms.
- Abnormal conduction of cardiac impulses, which may suggest underlying cardiac or metabolic disorders.
- Evidence of the occurrence of a prior heart attack (myocardial infarction).
- Evidence of an evolving, acute heart attack.
- Evidence of an acute impairment to blood flow to the heart during an episode of a threatened heart attack (unstable angina).
- Adverse effects on the heart from various heart diseases or systemic diseases (such as high blood pressure, thyroid conditions, etc.).
- Adverse effects on the heart from certain lung conditions (such as emphysema, pulmonary embolus (blood clots to lung), etc.).
- Certain congenital heart abnormalities.
- Evidence of abnormal blood electrolytes (potassium, calcium, magnesium).
- Evidence of inflammation of the heart or its lining (myocarditis, pericarditis).

2.7 Limitations of the ECG

Some of the limitations of the ECG are given below.

- The ECG is a static picture and may not reflect severe underlying heart problems at a time when the patient is not having any symptoms. The most common example of this is in a patient with a history of intermittent chest pain due to severe underlying coronary artery disease. This patient may have an entirely normal ECG at a time when he is not experiencing any symptoms. In such instances, the ECG as recorded during an exercise stress test may reflect an underlying abnormality while the ECG taken at rest may be normal.
- Many abnormal patterns on an ECG may be non-specific, meaning that they may be observed with a variety of different conditions. They may even be a normal variant and not reflect any abnormality at all. These conditions can often be sorted out by a physician with a detailed examination, and occasionally other cardiac tests (e.g., echocardiogram, exercise stress test).
- In some instances, the ECG may be entirely normal despite the presence of an underlying cardiac condition that normally would be reflected in the ECG. The reasons for this are largely unknown, but it is important to remember that a normal ECG does not necessarily preclude the possibility of underlying heart disease. Furthermore, a patient with heart symptoms can frequently require additional evaluation and testing.

CHAPTER 3
ECG DATABASES

In this work we have used different ECG databases from Physionet [3] for assessing the quality of the algorithms developed. Physionet is a resource for biomedical signals and applications and it offers free access via the web to large collections of recorded physiologic signals (more than 40 databases) and related open-source software. In this chapter we give a brief description of different ECG databases used in this research in order to acquaint the reader with their acquisition methodologies and statistical characteristics.

3.1 The QT-Database

The QT Database [4] contains a wide variety of ECG morphologies and a significant number of patient records for performance evaluation of wave detection and segmentation algorithms for the ECG. The QT Database contains a total of 105 fifteen-minute excerpts of two channel ECGs, selected to avoid significant baseline wander or other artifacts. These records have been chosen primarily from among existing ECG databases, including the MIT-BIH Arrhythmia Database, the European Society of Cardiology ST-T Database, and several other ECG databases collected at Boston's Beth Israel Deaconess Medical Center along with new Holter ECG recordings. The table below shows the distribution of the 105 records as they are taken from other databases.

Table 3-1 Number of Subjects in QT Database as taken from other databases

MIT-BIH Arrhythmia database	MIT-BIH ST Database	MIT-BIH Supraventricular Arrhythmia Database	MIT-BIH Long Term Database	ESC ST-T Database	MIT-BIH NSR Database	Sudden Cardiac Death Database
15	**6**	**13**	**4**	**33**	**10**	**24**

Within each record, between 30 and 100 representative beats have been manually annotated by cardiologists, who identified the beginning, peak and end of the P-wave, the beginning and end of the QRS-complex (the QRS fiducial mark, typically at the R-wave peak, was given by an automated QRS detector), the peak and end of the T-wave, and (if present) the peak and end of the U-wave. In order to permit the study of beat-to-beat variations such as alternans, 30 consecutive beats of the dominant morphology have been annotated in each case if possible. In records with significant QRS morphology variation, up to 20 beats of each non-dominant morphology have also been annotated. Annotations exist only for those beats which along with their neighboring beats have been classified as Normal by the Aristotle Arrhythmia Detector [REF]. In all, 3622 beats have been annotated by cardiologists. These annotations have been carefully audited to eliminate gross errors, although the precise placement of each annotation was left to the judgment of the expert annotators. The current edition of the QT Database includes two independently derived sets of annotations for 11 records (to permit study of inter-observer variability). The remaining 94 records contain only a single set of expert annotations. All records have a sampling rate of 250Hz.

We have used this database for performance evaluation of different ECG segmentation algorithms described in chapter 5 and 6.

3.2 The European Society of Cardiology (ESC) ST-T Database

In order to evaluate the performance of algorithms designed for the detection of ST segment and T-wave changes indicative of Coronary Heart Disease (CHD), the ESC ST-T Database [5] is used as an international standard. It contains more than 200 ST Segment and almost 300 T-wave changes. The ST-T episodes have been defined as follows:

a. Minimum Duration: 30 seconds
b. ST Segment Changes: ST Segment Deviations of 0.1mV from the reference value, measured 80ms after the J-point, have been considered to start or end an ST Segment change. In Sinus Tachycardia (Heart Rate > 120bpm) ST deviations should be measured 60ms after the J point.

c. T wave Changes: T-wave amplitude deviations of 0.2mV from the reference values have been considered to start or end a T-wave change, whereas a 0.2mV threshold is applied for T-wave amplitude changes.
d. Successive episodes have been considered as separate only if there is a baseline interval of at least 30s.

Each of the 100 ECG records in this database contains 2-channel, 2-hour recordings taken at a sampling rate of 250Hz. Each record is accompanied by a clinical report including information concerning pathology, drug treatment, electrolyte imbalance and additional technical information. For each case, the two leads which were considered most likely to reveal ST-T changes have been recorded. Two cardiologists have independently annotated QRS Complexes, episodes of changes in ST segment or T wave morphology, rhythm changes, and signal quality. Episodes of ST segment and T wave changes have been identified in both leads and their onsets, extrema and offsets have been annotated. Differences in the annotations by the two cardiologists were resolved by a cardiologist in the database coordinating group. The database contains the following type of annotations:

a. Beat Annotations
    - Normal
    - Supraventricular Beat
    - Premature Ventricular Contractions (PVC)
b. Non Beat Annotations
    - ST segment elevations and Depressions (Start, End and Peak Amplitudes)
    - T-wave elevations and Depressions (Start, End and Peak Amplitudes)
    - Rhythm Changes
        i. Atrial Fibrillation
        ii. Atrial Flutter
        iii. Ventricular Bigeminy
        iv. Ventricular Tachycardia
    - Signal Quality Change Annotations
        i. Moderate Level Noise
        ii. High Level Noise

The table below shows summary of different main events in the database.

Table 3-2 Number of different events in the ESC ST-T Database

Total Number of Beats	**431524**
Supraventricular Beats	**640**
PVC	**1329**
Ventricular Couplets	**41**
Ventricular Runs	**25**
ST elevation Episodes	**81**
ST Depression Episodes	**143**
T Wave Elevation Episodes	**161**
T Wave Depression Episodes	**128**

Annotations by the pair of independent cardiologists have also been analyzed to evaluate reproducibility of the human expert opinions. The reference annotations were used to determine the Sensitivity (Se) and Positive Predictive Value (PPV) of each annotating cardiologist. The table below shows the Se/PPV for the best and the worst annotator in the database and points to the fact that ST deviation detection accuracy is higher than T-wave detection accuracy.

Table 3-3 Sensitivity and Positive Predictivity of ESC ST-T Database Annotators

Episode Type (Number)	**Best Annotator (Se/PPV)**	**Worst Annotator (Se/PPV)**
ST Elevation	83/90	70/85
ST Depression	80/93	71/85
T Wave Elevation	66/98	60/92
T Wave Depression	63/99	53/85

We have utilized the freely available part (comprising 48 records) of the ESC ST-T Database for the evaluation of ST segment change detection algorithms given in chapter-8.

3.3 The MIT-BIH Arrhythmia Database

The MIT-BIH Arrhythmia database [6] is used for evaluating the performance of arrhythmia detectors or beat classification systems. It comprises 48 records chosen at random from a set of over 4000 long term Holter recordings obtained by the Beth Israel Hospital Arrhythmia Laboratory between 1975 and 1979. Each of these recordings is slightly over 30 minutes long. The subjects were 25 mean aged 32 to 89

years and 22 women aged 23 to 89 years. The ECG are recorded using nine Del Mar Avionics model 445 two channel recorders digitized at 360Hz with a 11-bit ADC over a -5mV to +5mV range. The database contains approximately 109,000 annotated beats of different types as indicated below.

Table 3-4 Different Annotations in the MIT-BIH database

Beat Type	Number of Beats
Normal	73447
Left Bundle Branch Block (BBB)	8075
Right BBB	7258
BBB	1
Atrial Premature Beat (APB)	2514
Aberrated APB	53
Nodal Premature Beat (NPB)	82
Escape Beat	2
PVC	6930
Fusion of Ventricular & Normal Beat	801
Atrial Escape Beat	16
Nodal Escape Beat	219
Ventricular Escape Beat	106
Paced Beat	7028
Fusion of Paced & Normal Beat	3
Unclassifiable Beat	33
Non Beat Annotations	3076
Total	**~109644**

We have used this database for the evaluation of our beat classification techniques detailed in chapter-7.

3.4 Other Databases

Another database of interest is the Long Term ST-T database [7] which contain 15 lead data of 24 hour recordings and is used for the detection of ST and T wave deviations corresponding to ischemic and axes changes. This database has not been used in this work. A complete list of databases is available online [3].

CHAPTER 4
ARTIFACT REMOVAL FROM THE ECG

In this chapter we present an in depth description of the techniques implemented for removal of artifacts from the ECG. Different artifacts in the ECG distort the ECG signal, thus lowering the accuracy of the diagnosis process or leading to the increased need of applying robust machine learning algorithms for diagnosis, raising over-all system complexity. The ECG signal, in itself, has very interesting characteristics like its quasi-periodic nature that can aid in removal of these artifacts. The rest of the chapter is organized as follows: In section-1, a description of different types of ECG artifacts is given. Section-2 describes and compares different techniques that have been implemented for removal of baseline from the ECG Signal. Section-3 renders procedures for noise removal with section-4 giving an account of the techniques used for removal of Ectopic beats from the ECG.

4.1 Artifacts in the ECG

The ECG Signal can be corrupted by the following major types of external artifacts [8]:

- Power line interference: Power line interference presents itself as 50 ±0.2 Hz noise (or 60 Hz in many data sets) with an amplitude of up to 50% of the peak-to-peak ECG amplitude
- Electrode contact noise: This noise is caused by the loss of contact between the electrode and the skin and exhibits itself as sharp changes with saturation at peak amplitude levels for periods of around 1 second on the ECG
- Patient–electrode motion artifacts: The movement of the electrode relative to the patient changes the contact surface for the electrode causing changes in impedance between the electrode and the skin resulting in rapid (but continuous) baseline jumps or complete saturation (up to 0.5s long) gives rise to these artifacts
- Perspiration Induced Artifacts

- Perspiration also causes the impedance between the electrode and the skin change therefore it also produces artifacts similar to those caused by the motion of electrodes.
- Electromyographic (EMG) noise: EMG is caused by muscular contractions and produces artifacts in the ECG that are about 50ms long and lie in the frequency range of 0-10KHz with an average amplitude of 10% of the peak ECG amplitude
- Baseline drift: Usually from respiration with an amplitude of around 15% of the peak ECG amplitude at frequencies drifting between 0.15 and 0.3 Hz;
- Instrumentation noise: Artifacts generated by the signal processing hardware, such as signal saturation etc.
- Electrosurgical noise: It is the noise generated by other medical equipment present in the patient care environment at frequencies between 100 kHz and 1 MHz, lasting approximately 1 and 10 seconds
- Quantization noise and aliasing caused by digitization procedures.
- Signal processing artifacts (e.g., Gibbs oscillations) resulting from filtering with a high order filter.

The presence of these artifacts makes the task of diagnosis intricate. The figure below shows an example of a noisy ECG signal contaminated by a mix of Power line interference, baseline wandering and EMG variations.

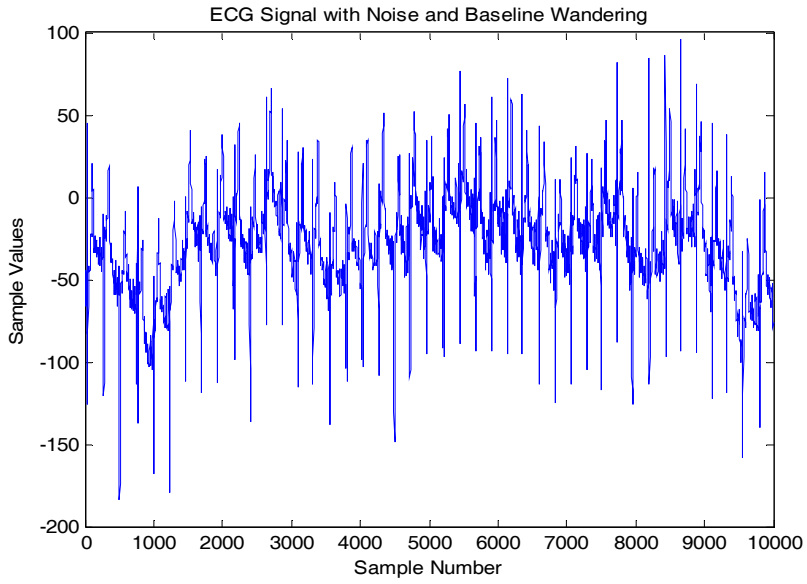

fig. 4-1 ECG Signal contaminated by a mixture of different noise sources

Here, reliable detection of different features for diagnosis, for instance, the J-point and the ST Segment etc, is very difficult due to the presence of noise. Therefore we need to remove these artifacts prior to the application of any diagnosis rules.

4.2 Baseline Removal

As described earlier, baseline wandering can result from the motion of electrodes, perspiration or respiration. It causes problems in analyzing ECG signals, especially the low frequency ST Segment. Therefore the removal of baseline wandering from the ECG is a critical step in ECG Signal Processing. The baseline removal scheme, while removing the baseline, should induce minimum distortion in the ECG. The isoelectric level in the signal that lies in the region after the end of the P-wave and before the start of the QRS complex is taken as the reference baseline.

4.2.1 Literature Survey

A large number of techniques exist in the literature for the removal of baseline wandering from the ECG. In a broad classification these techniques can be classified as:

a. Filtering Based Techniques

b. Polynomial Based Techniques

In filtering based approaches, a high pass filter is designed that removes slowly varying baseline from the signal. The cutoff frequency for the high pass filter is selected so as to minimize the distortion in the ECG Signal; therefore the lowest frequency component in the ECG is selected. The minimum heart rate is 40bpm (0.67Hz), therefore a cutoff frequency of around 0.5Hz is chosen. Linear phase characteristics are desirable in order to preserve the temporal characteristics in the ECG signal. Linear phase filtering can be achieved by the use of an FIR filter but it generally requires a very large filter order (700 to 2000) which causes a high computational load. In order to remove the filter delay, zero phase filtering can be implemented by forward-backward filtering. Another drawback of this method also stems from the high order of the filter, i.e., we are not able to remove the baseline over small datasets. The complexity, resulting from the high FIR filter order, can be avoided by using IIR forward-backward filtering, e.g. Chebyshev filters. More

sophisticated forms of filtering, for instance adaptive filtering has also been tried. Such techniques are described in [9, 10]. Another approach for the removal of the baseline is to first decimate the ECG signal, pass it through a low pass filter and then up-sample the sample to get an estimate of the baseline. This estimate is then subtracted from the ECG signal to get the baseline removed form. A more effective approach is to vary the cutoff frequency of the filter based on the heart rate, i.e. using a higher cutoff frequency when the heart rate is high and use a lower cutoff frequency otherwise. This helps in removing of higher frequency baseline wandering. A method for optimally selecting the cutoff frequency using the Short Time Fourier Transform (STFT) is given in [11]. Some approaches [12-14] utilize the wavelet transform for removal of baseline drift.

Linear filtering based methods can cause distortion in the ECG Signal especially when not using zero-phase forward-backward filtering as is required in real-time applications. This distortion is significant at the start and end of the QRS complex. Moreover the cutoff frequency (around 0.5Hz) effectively employed in the filtering techniques violates the American Health Association (AHA) recommendations [15] and the findings that the lowest frequency component of the ECG signal is around 0.05Hz [16]. Therefore any form of linear filtering beyond this frequency would cause some degree of distortion in the ECG. Filtering based approaches distort an ECG signal that has no baseline.

Polynomial fitting based approaches aim at fitting a curve on the ECG signal or some points from it. Polynomial based approaches, not being filters, do not cause distortion in the ECG signal as is caused by linear filtering. A popular approach is to use cubic spline fitting [17] by taking some representative knot points from the signal. Knots are selected from the isoelectric (PQ Segment) region. A cubic spline polynomial is fitted so that it passes through these knots in a smooth fashion. Such an approach can adapt automatically to the heart rate as more knots become available with increase in heart rate. However such an approach requires a proper definition of the knot points which must lie in the isoelectric region. This requirement, combined with over-fitting can distort the ECG signal and change the relative levels of different parts of the same beat. A low distortion technique based on the use of median and subsequent polynomial fitting is given in [18]. A simple approach that does not distort the relative levels of the ST and the PQ segment in a single cardiac cycle is given in [19] which uses a first order polynomial fitting to achieve this objective.

4.2.2 Implemented Techniques

The techniques implemented for Baseline removal are explained in this section and a comprehensive review of the characteristics of these algorithms is also described.

4.2.2.1 Baseline Removal Using High Pass Filters

As has been described earlier, Baseline is a slow varying component in the ECG signal and can be filtered out by the use of FIR high pass filters with cutoff frequency around 0.5Hz designed using window design method with hamming window. Filter order can be taken to be 700 to 2000 (even numbers).

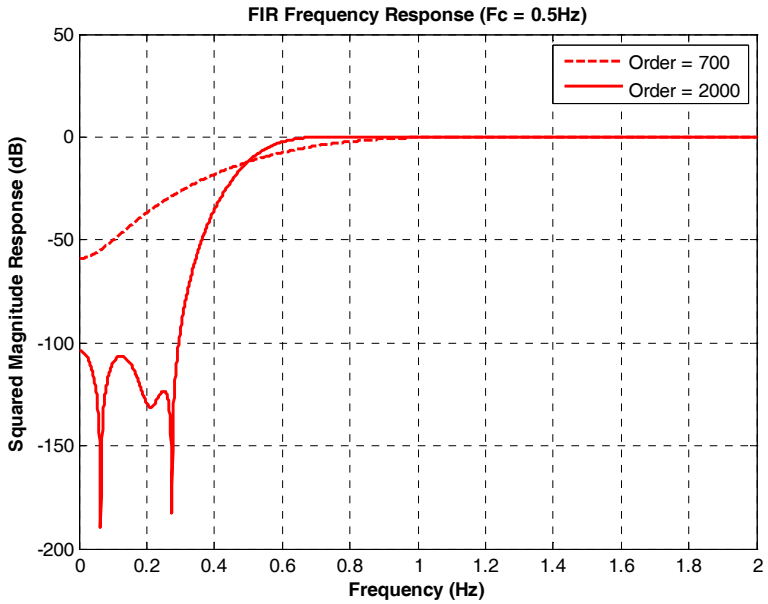

fig. 4-2 FIR Filter Frequency Response

Forward-backward filtering is used (for non-real-time applications) to produce a zero phase filtering effect to remove the tap delay inherent in the use of FIR filters. The squared response of these filters is shown below along with the results for baseline removal from an ECG signal artificially contaminated with a simulated sinusoidal baseline. The detailed figure shows negligible distortion in the ST segment whereas the baseline has been effectively compensated. These figures illustrate the effectiveness of the use of FIR high pass filters in the removal of baseline from the ECG due to their linear phase characteristics. .

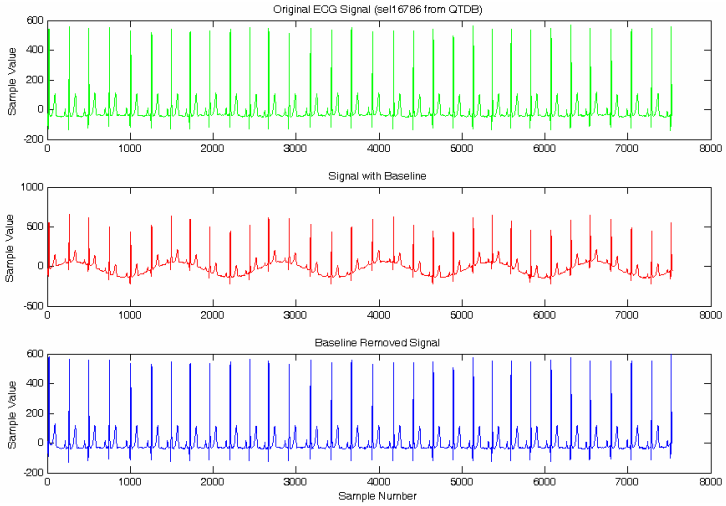

fig. 4-3 Removal of Artificial Baseline using FIR Filter (Order = 2000)

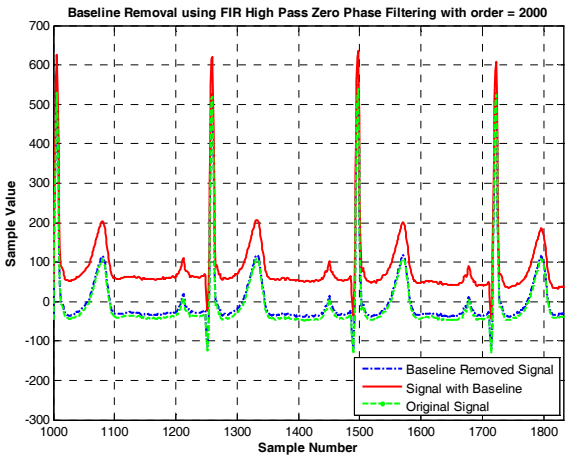

fig. 4-4 Baseline Removal using FIR Filter

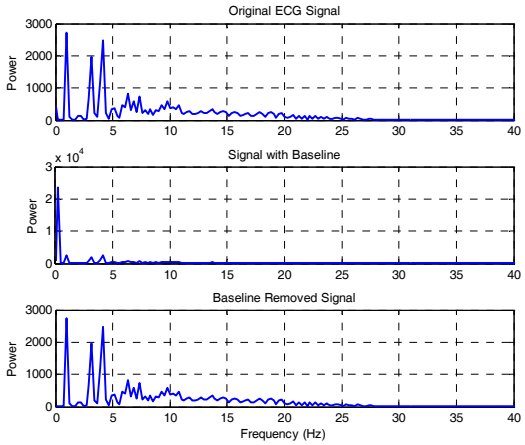

fig. 4-5 Frequency Spectrum for Baseline Removal using FIR Filtering

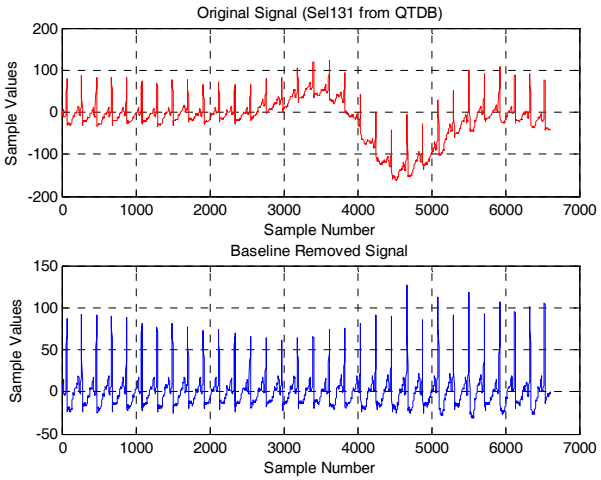

fig. 4-6 FIR Filtering Based Baseline Removal on Real ECG

Due to their high order, FIR filters present a computational load that can be eased through the use of forward-backward IIR filtering to make the filter response zero phase. The figures below illustrate the use of Butterworth and Chebyshev Type-II filters for baseline removal. It can be clearly noted that the application of these filters causes severe distortion in the ECG signal because of the nonlinear phase characteristics if only forward filtering is employed. The use of forward-backward filtering reduces the distortion but then it cannot be implemented in real-time. Another issue associated with the use of IIR filters is that their application becomes increasingly difficult at higher sampling rates as poles move closer to the unit circle, resulting in unstability. An improvement that can be made is to use heart rate dependent IIR filtering as described in the previous section.

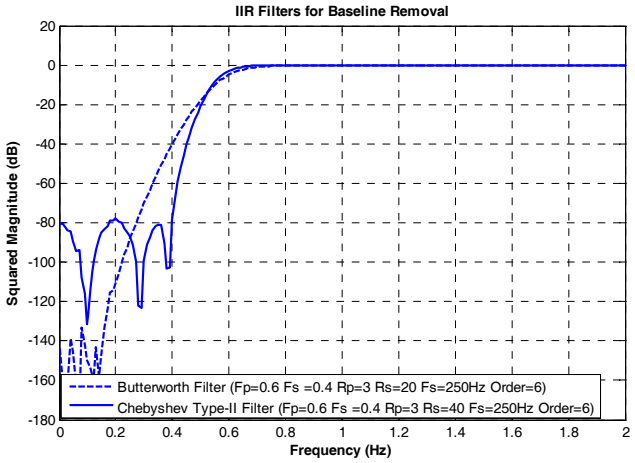

fig. 4-7 IIR Filter Frequency Response

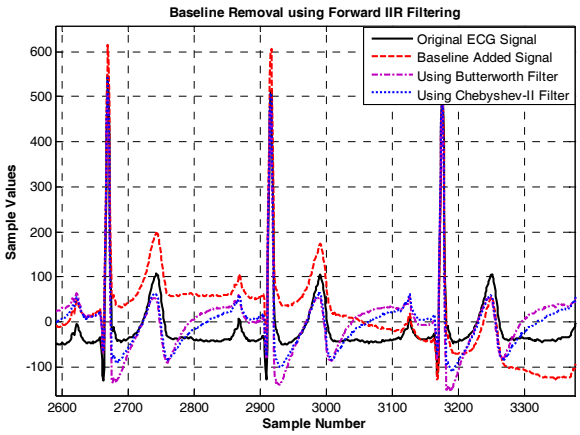

fig. 4-8 Effects of nonlinear phase in forward filtering

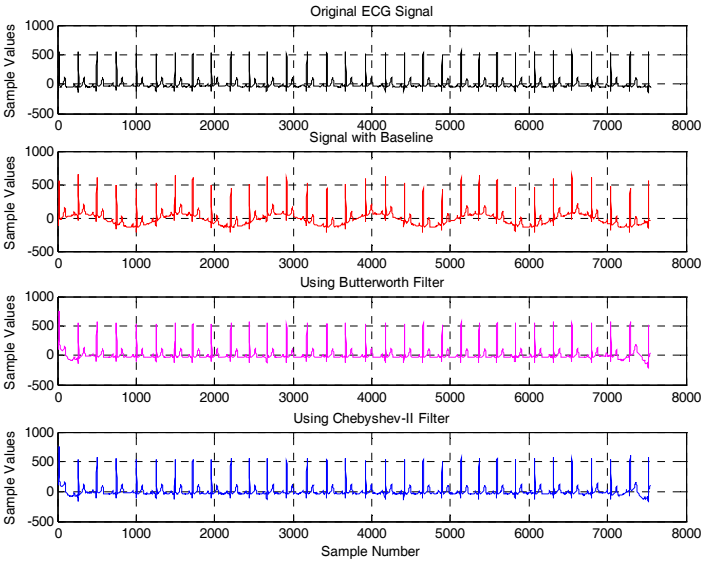

fig. 4-9 Baseline Removal using IIR Filters

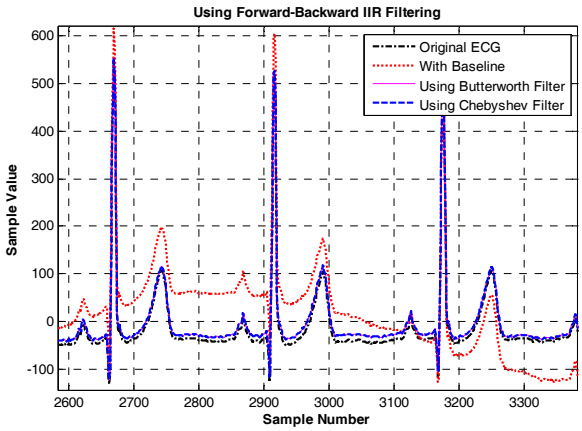

fig. 4-10 Baseline Removal using IIR Filters

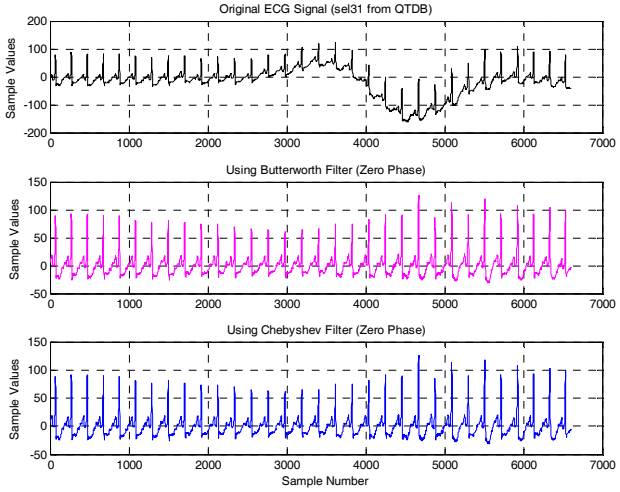

fig. 4-11 Baseline Removal on Actual ECG using IIR Filters

Function Reference

FIR Filtering

The filters used FIR filtering technique described earlier can be obtained by the use of `getFIRHPF.m`.

```
% File Name: getFIRHPF.m
% Author Name: Fayyaz ul Amir Afsar Minhas
% Date: 28May2007
% Description: Returns the Numerator Coefficients of the FIR High
Pass
% filter for use with baseline removal algorithm
% Usage:
%     BH=getFIRHPF(Fc_HPF,Forder,FS)
%     %Fc_HPF: Cutoff Frequency (0.5Hz)
%     %Forder: Filter Order (700)
%     %FS: Sampling Frequeny (250Hz)
%     BH: Numerator Coefficient in B(z)/A(z)
%Once the filter has been obtained using this function, either use
%filtfilt for zero phase (without delay) filtering or filter in
%realtime applications
```

IIR Filtering

The Chebyshev and Butterworth filters described above are stored in the mat files `chby_HPF.mat` and `butw_HPF.mat` that were developed using `SPTOOL` in Matlab.

4.2.2.2 Using Polynomial Fitting

Polynomial (splines) based approaches have the benefit of automatically to heart-rate because the number of knots is automatically increased when the heart rate is high so the polynomial can detect the baseline more effectively. We have implemented three approaches for baseline removal using polynomial based methods or its derivatives, which are described henceforth.

4.2.2.3 Using Cubic Splines

In the use of this procedure, the QRS onsets and offsets are extracted first using the algorithms described in the next chapter. Afterwards we find the average level of the region starting 40ms before QRS onset and ending 4ms after the QRS onset. This is done in order to nullify any noise related artifacts and account for any errors in QRS Delineation. With the knots defined at the QRS onset points with amplitudes equal to the average level found earlier, we fit a third order cubic spline polynomial on these knots to obtain an estimate of the baseline which is then subtracted from the original ECG signal to get the baseline removed signal.

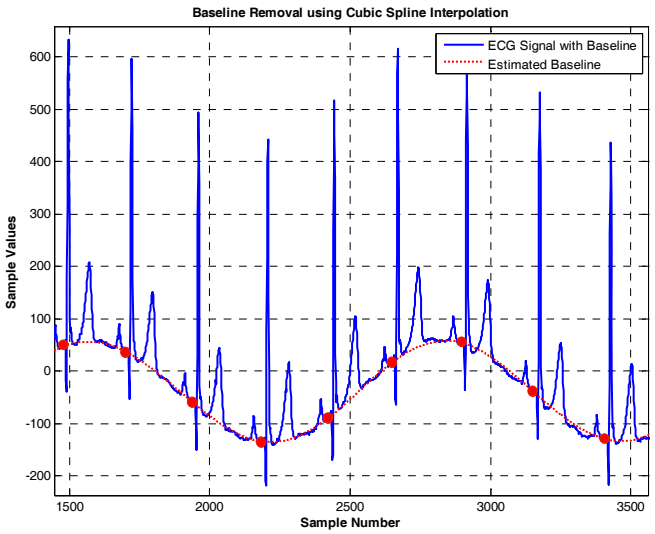

fig. 4-12 Spline Fitting for Baseline Removal

Results

The results of this technique are shown below. This method behaves poorly when only a small number of knots is available.

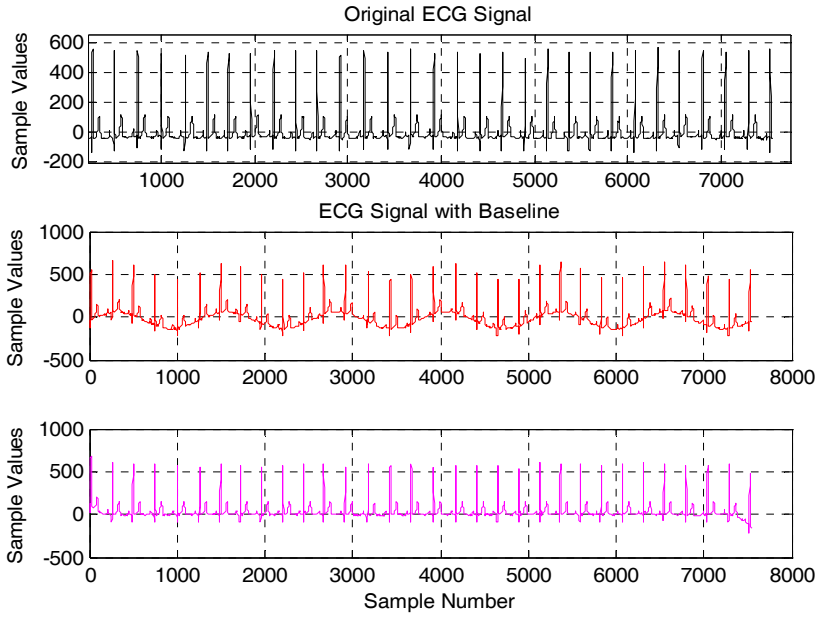

fig. 4-13 Baseline Removal using Spline Fitting

The major problem with the use of this polynomial based approach is that it is very sensitive to the detection accuracy of the knot points, which presents an issue in case of noisy ECG signals. An error made in the detection of QRS at a single beat

affects its neighboring beats as well if spline interpolation is used. An example of such an error is shown below.

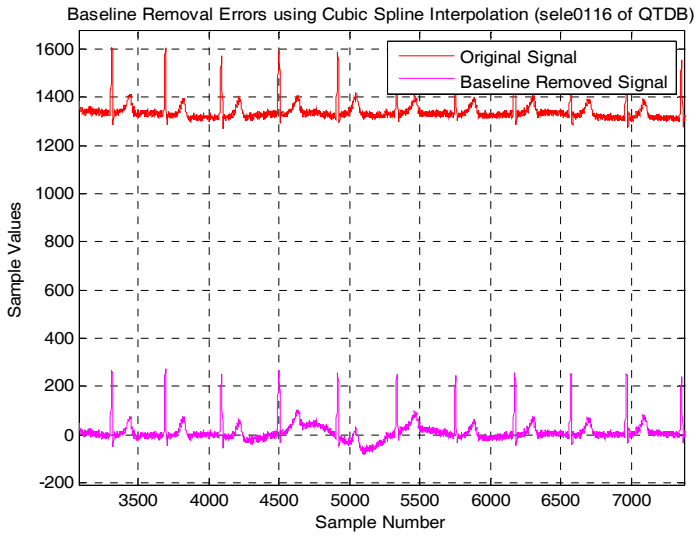

fig. 4-14 Problems with Spline Fitting

Function Reference

This technique has been implemented in the Matlab function `rmvBaseLine.m`.

```
% File Name: rmvBaseLine.m
% Author Name: Fayyaz ul Amir Afsar Minhas
% Date: 29Jan07
% Description: Baseline Removal using Spline Interpolation
% Usage:
%    [blr S]= rmvBaseLine(qrs_on,s,FS)
%     %qrs_on: QRS Start (1xno_of_qrs)
%     %s: Input ECG
%     %FS: Sampling Frequency [250Hz]
%     %S: Baseline
%     %blr: Baseline Removed ECG
```

4.2.2.4 Using Median Filtering

Chouhan et al. [18] give a technique for baseline removal using median filtering on the electrocardiogram. In this procedure we first compute the median of the signal values and subtract this median value from the signal, then a fifth order polynomial is fitted to this shifted waveform using least squares method to obtain a baseline estimate which is then subtracted from the ECG signal. The base line drift is further removed by applying median correction, one-by-one, in each RR interval. This method proposes modifications for handling false negatives in the QRS.

Results

The figure below shows the removal of baseline using this method.

The major advantage with the use of this method is that if no QRS drift is present in then the signal is not distorted as was the case with spline polynomials. Moreover it is computationally more efficient. However, it cannot adapt itself to very rapidly changing baseline variations. Moreover, it may change the difference the levels of the ST Segment and the PR interval.

Function Reference

This method has been implemented in the function `rmvBaseLineMed.m`.

```
% File Name: rmvBaseLineMed.m
% Author Name: Fayyaz ul Amir Afsar Minhas
% Date: 23May07
% Description: Baseline Removal Median Based Approach
% Usage:
%    [s]= rmvBaseLineMed(qrs_F,s)
%     %qrs_F: QRS Fiducial Point
%     %s: Input ECG
%     %s: Baseline Removed ECG
```

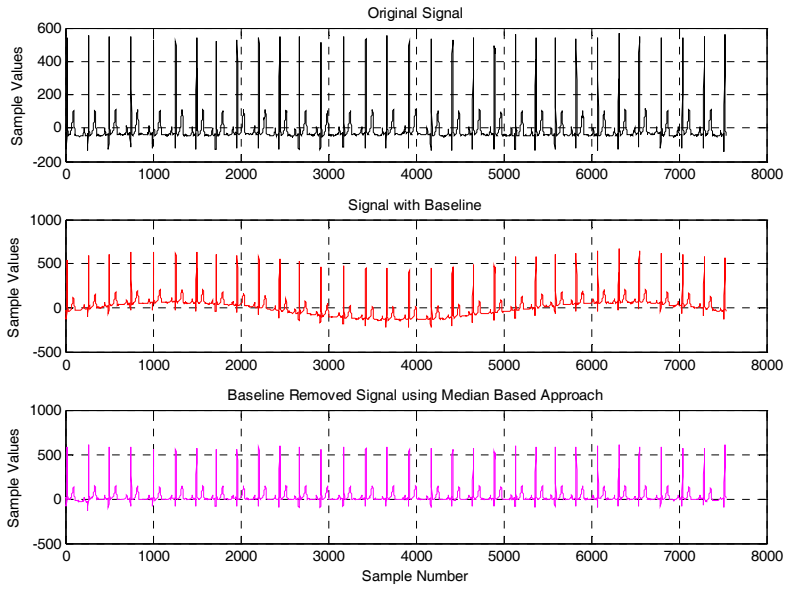

fig. 4-15 Median Based Baseline Removal

4.2.2.5 Using Linear Spline Fitting

In [19] an effective method for the removal of baseline from the ECG signal is given which is very well suited for use in diagnosis procedures using ST Segment analysis. This method takes the ECG Signal $s[n]$ and subtracts its mean from it to give $y[n]$, i.e.,

$$y[n] = s[n] - \bar{s} \tag{4.1}$$

This procedure translates the signal around zero level. Next a first order polynomial is fitted on each cardiac cycle in $y[n]$ and this is done in two sub-stages. In the first sub-stage we fit a first order polynomial to $y[n]$ itself and the values of this polynomial, $p[n]$, are subtracted from $y[n]$ to give $z[n]$,

$$z[n] = y[n] - p[n] \tag{4.2}$$

In the second sub-stage, the sample values to the QRS complex for each cardiac cycle are replaced by the corresponding values of $p[n]$ to yield $z^*[n]$. Thereafter, a region of each cardiac cycle starting 60ms before the P-wave and ending 60ms after the T-wave is taken from $z^*[n]$ and a first order polynomial is fitted to each of these regions which is subtracted from the corresponding region to produce a baseline removed cardiac cycle. The two sub-stages are necessary because the existence of the QRS complex slightly shifts the polynomial towards its main QRS polarity. If the QRS has a large R wave then the polynomial shifts upwards and the opposite happens when Q or S wave are large. This method has the advantage that in the absence of any baseline distortion in the original signal, this method does not distort the ECG and is highly efficient in removal of baseline as well without introducing any distortion in the ST Segment of the signal. However this method produces discontinuities at the end of a cardiac cycle; however no significant diagnostic information is contained in this region. In our implementation of the algorithm, we have used a simplifying approximation for the definition of a region of interest (ROI) as shown below.

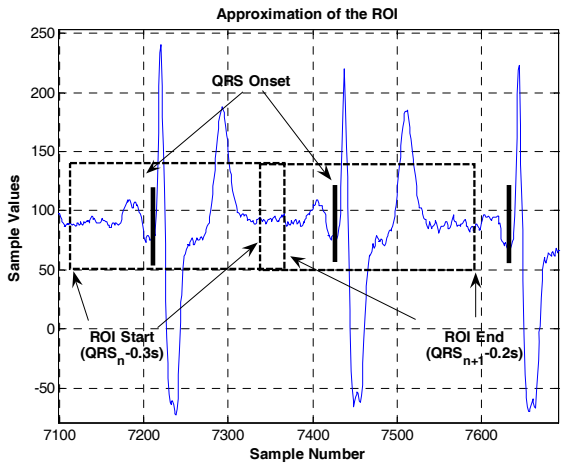

fig. 4-16 Approximation procedure used in the algorithm

This ROI is then used in the second sub-stage instead of the originally proposed cardiac cycle interval starting 60ms before the P-wave and ending 60ms after the T-wave. The results of this method are not reliable before the start of the P-wave and after the end of the T-wave. However this is not a significant loss, especially when dealing with the analysis of the ST-Segment.

Results

The results of baseline removal using this approach are given below:

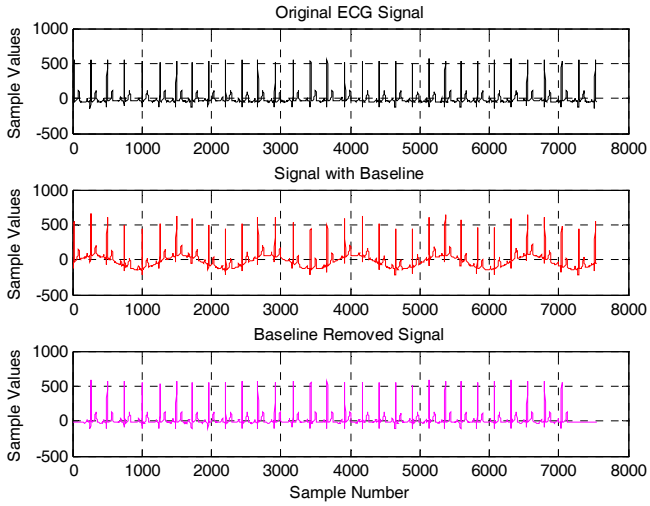

fig. 4-17 Baseline Removal

The figure below shows the distortion introduced by the baseline removal procedure.

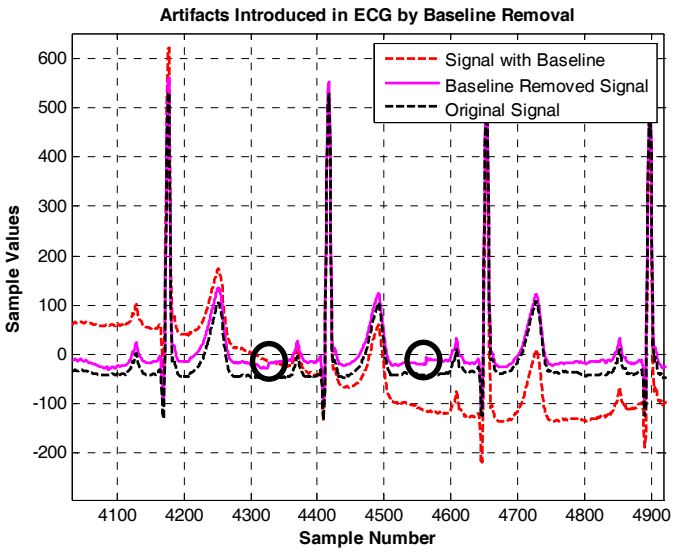

fig. 4-18 Artifacts in the ECG caused by Baseline Removal

Function Reference

This method has been implemented in the function `rmvBaseLinePolyMod.m`.

```
% Filename: rmvBaseLinePolyMod
% Author Name: Fayyaz ul Amir Afsar Minhas
% Date: 28May07
% Description: Baseline Removal using Two Stage First Order
Polynomial
% Fitting
% Usage:
%    [blr S]= rmvBaseLinePolyMod(s,qrs_on,qrs_off,FS)
%     %qrs_on: QRS Start (1xno_of_qrs)
%     %qrs_off: QRS End (1xno_of_qrs)
%     %s: Input ECG ECG
%     %FS: Sampling Frequency [250Hz]
%     %S: Baseline
%     %blr: Baseline Removed ECG
```

4.2.3 Conclusions

In this section, a wide variety of baseline removal techniques was described along with a visual comparison approach for analyzing the efficacy of these methods. Filtering based approaches, when implemented in non-real time environments (with forward-backward filtering) are highly effective in removing baseline from signals. However they may introduce distortion in the signal and are computationally inefficient for real time implementation. Use of cubic spline interpolation is good at automatically adapting to the heart rate but it introduces artifacts and distortion in the signal. Use of the median filtering based approach can remove only slowly varying baseline drift. However it does not distort the signal when no baseline drift is present. Using the two sub-stages for fitting a first order polynomial is able to cope up with fast baseline variations and introduces no artifacts in the diagnostically significant region of the ECG and is good choice for practical implementation, especially for the analysis of coronary artery disorders that manifest themselves in ST segment variations.

4.3 Noise Removal

Low SNR of the ECG signal causes performance degradation during diagnosis thereby making noise removal an imperative procedure in the design of a computer aided diagnosis expert system. A list of noise and noise related artifacts has been given in section 3.1. A large number of methods exist in the literature for removal of

noise from the ECG. In the following section we describe a literature survey of the different techniques that exist for this purpose. A detailed description of the implemented schemes and performance comparison is also given henceforth.

4.3.1 Literature Survey

The objective of a noise cancellation method for ECG is to produce a cleaned version of the signal without introducing distortion and ringing effects in the signal. ECG signal components, most sensitive to noise artifacts include the isoelectric regions, the P and the T-waves. The QRS complex is less affected by noise due to its relatively high amplitude. Major problems addressed in existing literature for noise removal from the ECG include removal of power line and Myo-Electric interferences. For the removal of Powerline interference, design of linear notch filters has been proposed, which filter out the 50/60Hz interference from the ECG Signal. However notch filters [20] cause undesirable distortion and ringing effects to be introduced in the ECG. Therefore they are generally not applied in practical applications. Nonlinear filtering can also be employed which builds on the idea of subtracting a sinusoid generated by a filter from the observed signal. A review of the subtraction procedure is given in [21]. Adaptive techniques for Powerline interference reduction [22, 23] are very effective in removing such interference. Wavelet Based Approaches [13, 24] also find application in removing Powerline interference and muscular noise from ECG.
As has been explained earlier, spectra of noise and the original ECG signal overlap, therefore any linear filtering method that removes noise from the signal also attenuates the signal. In order to overcome this difficulty, we have studied the use of Independent Component Analysis (ICA) and Nonlinear techniques for the removal of noise from the ECG. ICA is a tool for Blind Source Separation which can be adapted for ECG Noise Removal because different noise components in the ECG and the original ECG signal are statistically independent because the stem from different (independent) sources. Although ICA has been used extensively for feature extraction and noise reduction from the Electroencephalograph (EEG) and for separation of fetal ECG, its application to noise removal from the ECG has not been investigated in detail in the literature. Some of the methods described in the literature for noise removal from the ECG using ICA include [25-27].

Another approach studied for noise removal from ECG is nonlinear projective filtering which aims at first forming a reconstructed phase space from the ECG signal data. Some of the methods existing in the literature that utilize nonlinear techniques for ECG Noise removal include [28, 29].
Approaches using ICA and Nonlinear Noise reduction are described in greater details in the upcoming sections.

4.3.2 Implemented Approaches for Noise Removal

We have implemented three schemes for noise removal from the ECG. In this section we present a comparison of the performance of these techniques for the removal of noise artifacts from the ECG signal. In order to facilitate this comparison and present quantitative results we use artificially generated ECG obtained by the implementation of a dynamical model for the ECG [30] available as open source software at [31]. A summary of the ECG generation procedure and its characteristics are briefly described in this section.

4.3.2.1 Synthetic ECG Generation

The proposed method is based on a dynamical model comprising three coupled differential equations that is able to generate a desired ECG by specifying the mean and the standard deviation of the heart rate, morphology of the PQRST cycle and the power spectrum of the RR tachogram. Moreover both respiratory sinus arrhythmia at the high frequencies (HF) and Mayer waves at the low frequencies (LF) together with the LF/HF ratio are incorporated in the model.
This model generates a trajectory in a 3D state space with coordinates *(x, y, z)*. Quasi-periodicity in the ECG is reflected by the movement of the trajectory around an attracting limit cycle of unit radius in the *(x, y)* plane. Each revolution of this circle corresponds to one RR-interval or heart beat. Interbeat variation in the ECG signal is reproduced using the motion of the trajectory in the *z*-direction. Distinct points in the ECG, such as the P, Q, R, S and T are described by events corresponding to negative and positive attractors or repellors in the *z*-direction placed along the unit circle given by θ_P, θ_Q, θ_R, θ_S and θ_T as shown below. When the trajectory approaches one of these events, it is pushed upwards or downwards away from the limit cycle, and the as

it moves away from the limit cycle, and then as it moves away it is pulled back toward the limit cycle.

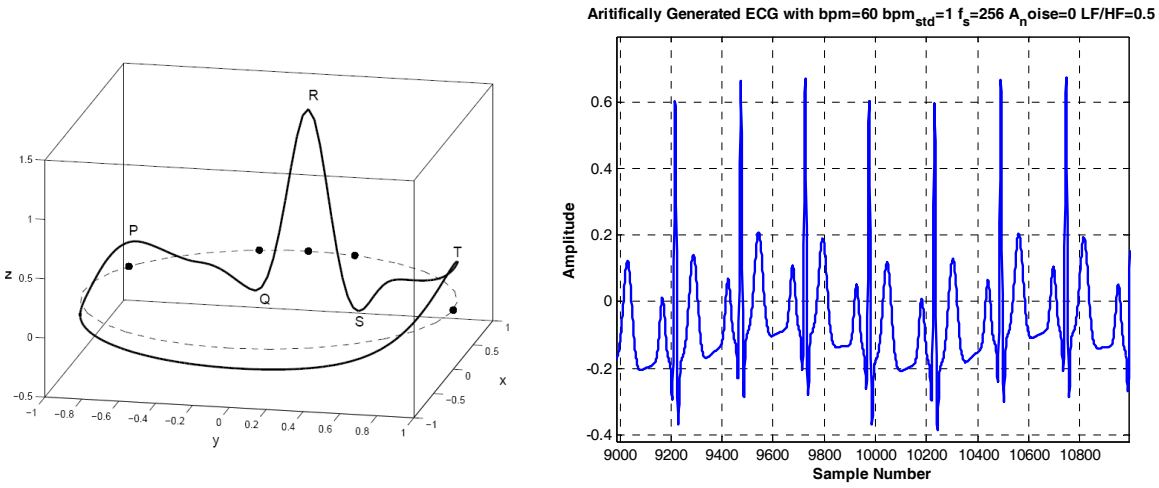

fig. 4-19 Artificial ECG Generation

The equations of the model are:

$$\begin{aligned}
\dot{x} &= \alpha x - wy \\
\dot{y} &= \alpha y + wx \\
\dot{z} &= -\sum_{i\in\{P,Q,R,S,T\}} a_i \Delta\theta_i \exp\left(\frac{-\Delta\theta_i^2}{2b_i^2}\right) - (z - z_0)
\end{aligned} \tag{4.3}$$

where

$$\begin{aligned}
\alpha &= 1 - \sqrt{x^2 + y^2} \\
\Delta\theta_i &= (\theta - \theta_i) \bmod 2\pi \\
\theta &= \operatorname{atan2}(y, x) \qquad \theta \in [-\pi \; +\pi] \\
z_0 &= A \sin(2\pi f_2 t)
\end{aligned}$$

Baseline wandering was introduced in the ECG using z_0 with f_2 being the respiratory frequency and $A=0.15mV$. The effects of Respiratory Sinus Arrhythmia (RSA) and Mayer waves which manifest themselves in the HF ($f_2 \sim 0.25Hz$) and LF ($f_1 \sim 0.1Hz$) regions of the power spectrum of RR-interval tachogram are modeled as a bimodal power spectrum consisting of the sum of two Gaussian Distributions

$$S(f) = \frac{\sigma_1^2}{\sqrt{2\pi c_1^2}} \exp\left(\frac{(f - f_1)^2}{2c_1^2}\right) + \frac{\sigma_2^2}{\sqrt{2\pi c_2^2}} \exp\left(\frac{(f - f_2)^2}{2c_2^2}\right)$$

The ratio of σ_1^2 / σ_2^2 models the LF/HF ratio is used as a measure of the sympathovagal balance for the autonomic nervous system. The RR Interval time series $T(t)$ is generated by taking the inverse Fourier Transform of complex numbers

with magnitude $\sqrt{S(f)}$ and phases randomly distributed between 0 and 2π. This time series is multiplied by an appropriate scaling constant and adding an offset value to have a required mean and standard deviation of the RR interval. This time series is used for defining the time dependent angular velocity $\omega(t)$ in the differential equation model as:

$$\omega(t) = \frac{2\pi}{T(t)}$$

These equations are solved using Runge-Kutta method with a fixed time step $\Delta t = 1/f_{sampling}$. The parameter values, originally given in the paper are:

Table 4-1 Dynamic Model Parameters for ECG Generation

Index (i)	P^{ECG}	Q^{ECG}	R^{ECG}	S^{ECG}	T^{ECG}
Time (secs)	-0.2	-0.05	0	0.05	0.3
θ_i (radians)	$-\frac{1}{3}\pi$	$-\frac{1}{12}\pi$	0	$\frac{1}{12}\pi$	$\frac{1}{2}\pi$
a_i	1.2	-5.0	30.0	-7.5	0.75
b_i	0.25	0.1	0.1	0.1	0.4

fig. 4-20 shows an ECG Generated using this method.

4.3.2.2 Evaluation Measures for Noise Reduction

In order to obtain a quantitative estimate of the level of noise reduction for a given algorithm we use artificial ECG with added noise. For the purpose of quantifying the level of noise in an ECG signal, we use the concept of SNR which is defined as:

$$\gamma = \frac{\sigma_{signal}}{\sigma_{noise}} \tag{4.4}$$

Where σ_{signal} and σ_{noise} are the standard deviations of the ECG signal and the noise respectively. An artificial ECG Signal was generated having a mean heart rate of 60bpm with a standard deviation of 1bpm and a sampling frequency of 256Hz. The position of the LF and HF components of the RR Interval spectrum were 0.1Hz and 0.25Hz respectively with a standard deviation of 0.01Hz and the LF/HF ratio was taken as 0.5.

Some of the samples from this ECG are shown below.

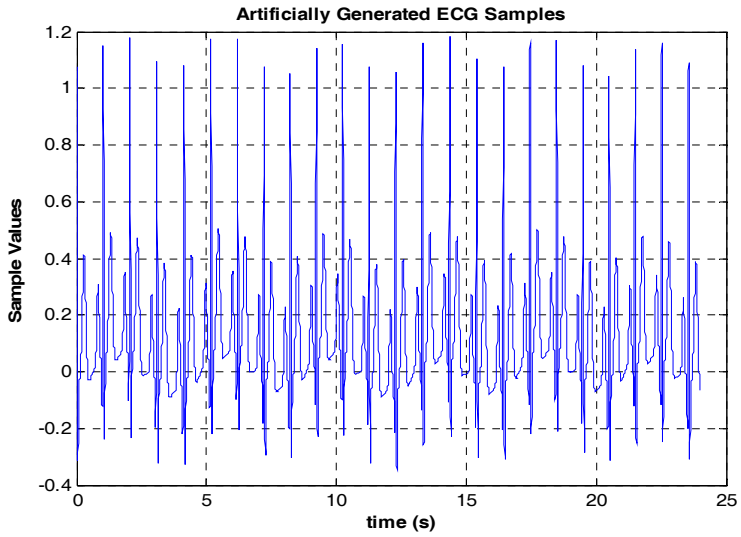

fig. 4-20 Artificial ECG Generated for Noise Removal Evaluation

Two types of noise were added to the ECG signal,

- Stochastic Noise, i.e. Gaussian Noise with zero mean
- Deterministic Noise, i.e. a model of finger tapping artifact generated with a 4Hz sinusoid at modulated by a hamming window with maximum noise magnitude at 0.1V.

The noise was considered to be additive. Let $x[n]$ be the original ECG signal and $\varepsilon[n]$ be the added noise, then the observed signal (with observational uncertainty) is:

$$y[n] = x[n] + \varepsilon[n] \tag{4.5}$$

For the purpose of evaluation of a noise reduction algorithm that generates a cleaned version of the signal, $z[n]$ we use two measures:

a. Noise Reduction Factor (NRF)

It is given by:

$$\chi = \sqrt{\frac{\left\langle \left(y[n] - x[n] \right)^2 \right\rangle}{\left\langle \left(z[n] - x[n] \right)^2 \right\rangle}} \tag{4.6}$$

Where $\langle \cdot \rangle$ denotes the average over time. The higher the value of the NRF the greater is the noise reduction. A NRF=1 implies no improvement in signal quality.

b. Correlation Coefficient (CC)

It is defined as:

$$\rho = \frac{\left\langle \left(x[n] - \mu_x \right)\left(z[n] - \mu_z \right) \right\rangle}{\sigma_x \sigma_z} \tag{4.7}$$

Where μ_x and μ_z are the mean values of $x[n]$ and $z[n]$ respectively and σ_x and σ_z are their standard deviations. A CC value of 1 implies that all noise has been removed from the ECG Signal.

4.3.2.3 Use of Linear Filtering Techniques

The simplest approach for noise removal from the ECG is based upon the use of digital filters. We know that the frequency content of the ECG signal does not exceed 40-45Hz. Therefore high frequency noise can be removed by the use of a simple low pass filter with cutoff at 45Hz. For this purpose we have designed a Butterworth IIR filter with order = 12. This filter is applied through forward-backward filtering to yield a zero phase response. The magnitude response of the filter is shown below:

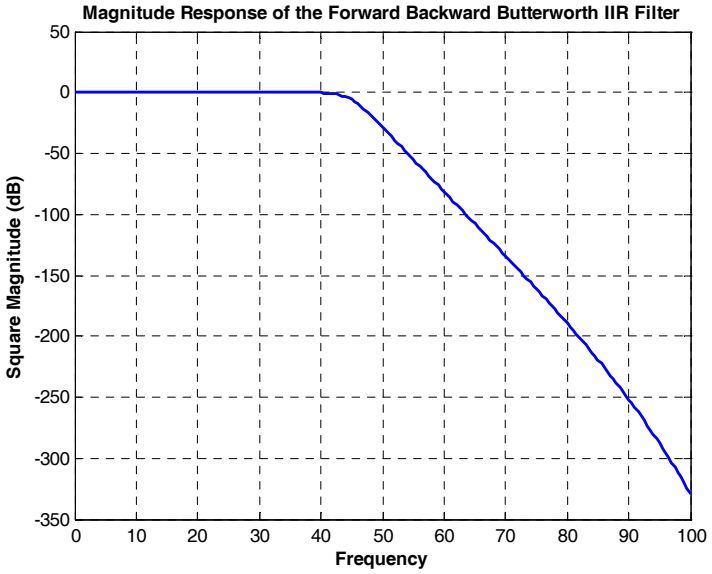

fig. 4-21 Magnitude Response of IIR LPF Filter

Results

The figure below shows the results of low pass filtering the artificial ECG along with the power spectrum density (PSD) obtained using Welch's Method [32]. The PSD shows that the LPF procedure is unable to retain the spectral characteristics of the ECG and to remove noise from the region where noise and signal spectra overlap.

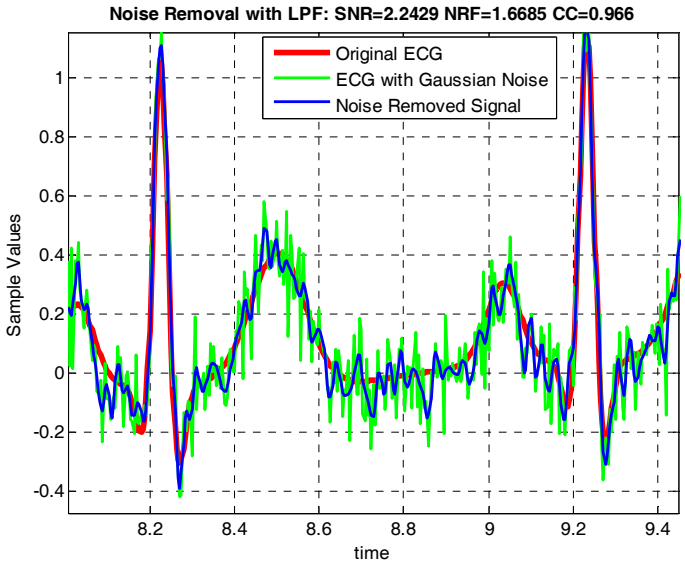

fig. 4-22 Noise Removal with LPF

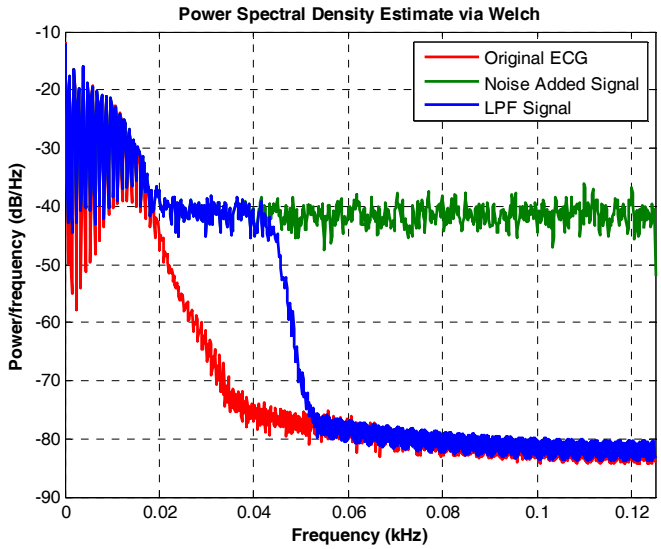

fig. 4-23 Change in Frequency Spectrum due to LPF

Function Reference

The filter described above was developed using SPTOOL in Matlab and is stored as `btw_LPF.mat` and can be used with `filtfilt` or `filter` commands in Matlab.

4.3.2.4 Independent Component Analysis for Noise Removal

In this section we investigate the effectiveness of using ICA for noise removal and the problems encountered in its application. For removal of noise artifacts from a single ECG channel we adapt the approach given in [33] which uses ICA in conjunction with Takens' theorem of Time Delay Embedding. Takens' theorem states

that it should be possible to reconstruct the dynamics of a deterministic system with the assumption is that the measured signal is due to nonlinear interactions of just a few degrees of freedom, with additive noise. This suggests the existence of an unobservable deterministic generator of the observed data. Takens' theorem allows the reconstruction of the unknown dynamical system that generated the measured time series by reconstructing a new state space based on successive observations of the time series. One of the methods for reconstructing a Dynamical Embedding (DE) matrix from the observed data $x(t)$ with unknown state $X(t)$ at a time *t* is given by:

$$X(t) = \left\{ x\left(t-\tau\right), x\left(t-2\tau\right), ..., x\left(t-\left(m-1\right)\tau\right) \right\} \in \Re \tag{4.8}$$

Where τ is the lag and m is the number of lags or the embedding dimension. This delay vector representation describes the observed signal values assuming that the data $x(t)$, $t = 1...N$ has been generated by a finite dimensional, nonlinear system of the form:

$$x(t) = f\left[X(t-1), X(t-2), ..., X(t-D)\right] + e_t \tag{4.9}$$

Where *D* is the degrees of freedom of the original system and e_t is independently and identically distributed (i.i.d), zero mean with unit variance.

Under quite general circumstances the attractor formed by the embedding is equivalent to the attractor in the unknown space in which the original system is living if the dimension of the delay coordinates space (*m*) is sufficiently large. To be precise, this is guaranteed if *m* is larger than twice the box counting dimension [34] of the attractor, i.e. roughly speaking larger than twice the number of active degrees of freedom. Several methods exist for finding the optimal time delay and the embedding dimension for given data (see [35, 36]). Once the values of optimal time delay and the embedding dimension have been chosen, the embedding matrix is formed from the ECG data as:

$$X = \begin{pmatrix} x_t & x_{t+\tau} & \cdots & x_{t+N\tau} \\ x_{t+\tau} & x_{t+2\tau} & \cdots & x_{t+(N+1)\tau} \\ \vdots & \vdots & \ddots & \vdots \\ x_{t+(m-1)\tau} & x_{t+m\tau} & \cdots & x_{t+(m+N-1)\tau} \end{pmatrix} \tag{4.10}$$

If the values of the time lag and the embedding dimension are chosen properly then we the estimated X contains sufficient information about the temporal structure of the measured data.

Now we attempt to span the embedding matrix with an appropriate basis with the aim of identifying the underlying sources in the embedding matrix. For this purpose we use ICA, which has the advantage of being able to identify non-orthogonal basis whereas PCA (using SVD) is limited to identifying orthogonal basis only. These non-orthogonal bases enables us carry out a blind separation of the statistically independent sources assuming linear mixing of the sources at the sensor.

Lets consider X to be a matrix of m observed random vectors, A a $m \times m$ square mixing matrix and S, the *m source* vectors such that

$$X = AS \tag{4.11}$$

ICA algorithms attempt to find a separating matrix W such that

$$S = WX \tag{4.12}$$

In practice, iterative methods are used to maximize or minimize a given cost function such as mutual information, entropy or kurtosis which leads to identifying the statistically independent components. In this study we considered two methods for performing ICA: Fast ICA [37] which optimizes kurtosis for finding the independent components and jadeR [38] which performs Multidimensional ICA and is based on the joint diagonalization of cumulant matrices thereby combining benefits of both PCA and ICA to provide a stable deterministic solution whereas ICA suffers from a scaling and column ordering problem due to indeterminacy of the solution to scalar multipliers and column permutations of the mixing matrix.

The next task after ICA is to select the appropriate independent components and project them back to the measurement space. For this purpose we use correlation of the observed ECG signal with the independent components and find the component that have the highest correlation with the original signal. In practice, selection of the relevant independent components should be done using a more generic approach.

Once the relevant independent component has been chosen, these components must be projected back to the measurement space such that

$$Y^i = a_i s_i^T \tag{4.13}$$

Where s_i is the selected independent component, a_i the corresponding column of the mixing matrix A and Y^i is the resulting embedding matrix. The projected time series is determined as:

$$y_i(t) = \frac{1}{m} \sum_{k=1}^{m} Y^i_{k,(t+k-1)} \tag{4.14}$$

for $t=1,2,...,N$, where $Y^i_{k,(t+k-1)}$ refers to the element of Y^i indexed by row k and column $(t+k-1)$. Here the assumption is that there is a single signal source and a single noise source which is very limited in application and must be generalized for better performance. Another issue is scaling and inversion indeterminacy problem. We can divide the actual output by the largest element of the original ECG signal. However this method is also not generic and these problems must be solved by the use of a more practical approach. The cleaned ECG produced by this method is delayed with respect to the source and noisy signal and must be corrected.

Results

The figure below shows the results of this algorithm for artificial ECG signals and it clearly demonstrates the problems associated with using ICA, i.e, delayed and scaled output.

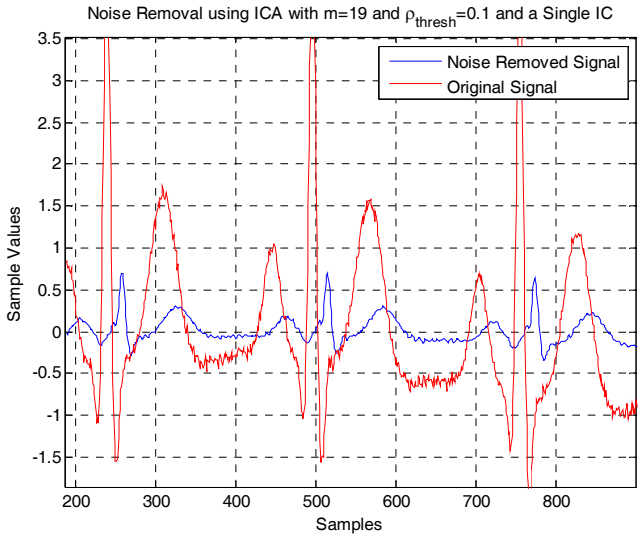

fig. 4-24 Noise Removal with ICA

Remarks

ICA presents a good method for removal of noise from ECG but the method needs to be investigated in more detail before it can be practically applied. The following issues need to be analyzed systematically:

a. Defining a procedure for detecting independent components related to ECG and noise
b. Defining multiple source signals and noise signals and combining the multiple source signals for better noise removal
c. Removal of delay and scaling issues for noise removed signals

d. Optimal selection of delay and embedding dimensions in Phase Space Reconstruction

Function Reference

This approach has been implemented in the file `ICANR_JADE.m`.

```
% Filename: ICANR_JADE.m
% Author Name: Fayyaz ul Amir Afsar Minhas
% Date: 06June07
% Description: Noise Reduction from ECG using ICA
% Usage:
%    [yy s]=ICANR_JADE(y,m)
%     %y: noisy signal
%     %m: Embedding Dimensions
%     %s: Scaled noisy signal
%     %yy: Noise Removed Signal
%     NOTED: This function requires getEmMat.m and jadeR.m
```

4.3.2.5 Nonlinear Noise Reduction by Projective Filtering

For nonlinear noise reduction in the ECG we have implemented the technique conferred in [28] which exploits the short term predictability in ECG with nonlinear projection method developed for chaotic signals. The variation in the RR interval of the ECG signal makes long term prediction impossible, although the dynamic evolution during one cycle is more or less confined to a typical shape resulting from the quasi periodic nature of the ECG signal. Due to random fluctuations of the cycle lengths the embedding theorems do not strictly hold, however this representation is very useful to exploit the structure hidden in the signal and the assumption of the embedding theorems may be well enough satisfied to allow practical use to be made of the embedding technique.

Consider a deterministic dynamical system written in m dimensional delay coordinates (as described in the previous section), $x_n = f\left(x_{n-m},...,x_{n-1}\right)$. We perform a measurement which is subject to random fluctuations $y_n = x_n + \varepsilon_n$. Rewriting the dynamics in implicit form as $f\left(x_{n-m},...,x_n\right) = 0$ shows that in an $m+1$ dimensional delay coordinate space the noise free dynamics is constrained to a m-dimensional hypersurface. The noise ε_n in the measurements causes an extension of a cloud of data points perpendicular to this hypersurface. Therefore one can identify the direction to correct the observed signal by projecting these points onto the hypersurface formed by the cleaned signal which is possible only if the variance of the noise is smaller than that of the signal. For this purpose in a $m+1$-dimesional embedding space we compute

the covariance matrix $C_{ij_{(m+1)\times(m+1)}}$ of a set of points $y_j \in U_n$ lying in the neighborhood of the *n*-th embedding vector as follows:

$$C_{ij} = \frac{1}{|U_n|}\sum_{k\in U_n} y_{k-m+i}y_{k-m+j} - \mu_i\mu_j \qquad i=0,...,m \qquad j=0,...,m \quad (4.15)$$

Where $|U_n|$ is the number of points in the neighborhood (with a minimum of $k_{\min} \geq 50$ points) and μ_i is the mean given by:

$$\mu_i = \frac{1}{|U_n|}\sum_{k\in U_n} y_{k-m+i} \qquad i=0,...,m \quad (4.16)$$

Then a transformed version of the covariance matrix is formed as:

$$\Gamma_{ij} = R_{ii}C_{ij}R_{jj} \quad (4.17)$$

Where $R_{ij}=0 \ \ (i\neq j)$, $R_{ii}=1 \ \ (i=2,...,m-1)$ and $R_{00}=R_{mm}=M$ where M is a large number. The Q orthonormal Eigen vectors of Γ with the smallest Eigen values are found and are given by $e_q, q=1,...,Q$. The projector onto the subspace spanned by these vectors is:

$$Q_{ij} = \sum_{q=1}^{Q} \varepsilon_{q,i}\varepsilon_{q,j} \quad (4.18)$$

Finally the *i*-th component of the correction,

$$\theta_{n.i} = \frac{1}{R_{ii}}\sum_{q=1}^{Q} Q_{ij}R_{jj}\left(\mu_j - y_{n-m+j}\right) \quad (4.19)$$

This gives the correction $b_\perp$ which can be added to each embedded vector to bring the point toward the manifold spanned by the *m+1-Q* largest Eigen vectors. We can summarize the procedure as:

$$\hat{\boldsymbol{y}}_{\boldsymbol{n}} = \mathbf{y_n} + \mathbf{R}^{-1}\sum_{\boldsymbol{q}=1}^{\boldsymbol{Q}} \boldsymbol{\varepsilon_q}\cdot\left[\boldsymbol{\varepsilon_q}\cdot\mathbf{R}\left(\boldsymbol{\mu_n} - \mathbf{y_n}\right)\right] \quad (4.20)$$

For details over the derivation of this method the reader can consult Kantz and Schreiber (2004) [35]. The penalty matrix **R** makes the largest two Eigen values lie in the subspace spanned by the first and last coordinates of the embedding space and prevents the correction vector from having any components in these directions. This correction is done for each embedding vector separately yielding a set of corrected vectors. Since each element of the scalar time series occurs as a component *m+1* different embedding vectors, we finally have as many different suggested corrections of which we take the average. Due to this averaging the resulting corrected vectors do

not precisely lie on the local subspaces but are only moved towards it. This procedure can be repeated multiple times to get better results.

Results and Remarks

The figures below show the results of this method. The values selected were $m=15,\ Q=13,\ k_{\min}=10,\ r_{neighborhood}=\text{Neighborhood Size}=0.4$ and $N_{iteration}=5$. With Gaussian noise this method was able to remove noise even when SNR<1 was taken.

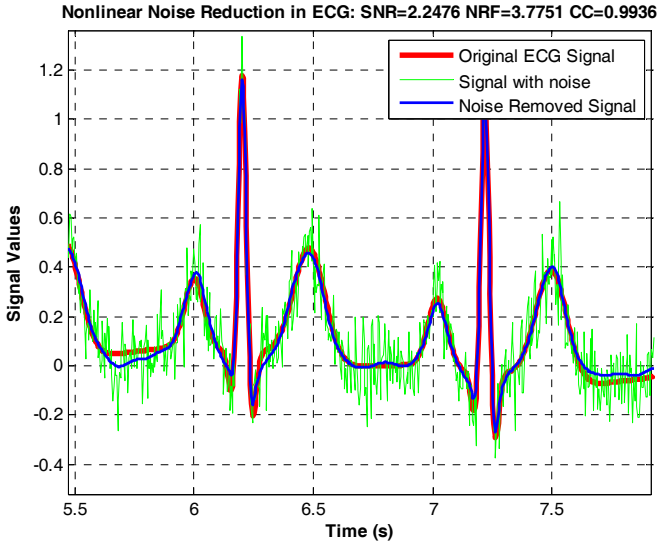

fig. 4-25 Nonlinear Noise Reduction (NLNR)

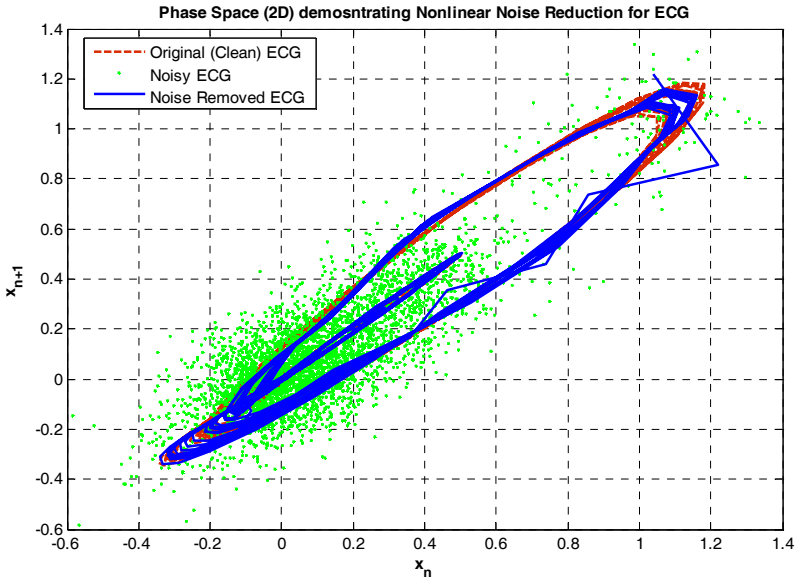

fig. 4-26 Phase Space Demonstration of Noise Removal Procedure

This clearly shows that this method is able to effectively remove noise that is orthogonal to the ECG signal and is able to retain the power spectrum of the true signal. However it does not behave well on non orthogonal noise (such as the 4Hz

sinusoid amplitude modulated by hamming window) as shown below. This is due to the fact that only orthogonal components were sought in the projection procedure and this problem can be remedied by using local ICA. Further enhancement can also be brought in by using a dynamic neighborhood size selection procedure [39] which would reduce the distortion caused in the QRS segment. Another issue associated with this method is its time complexity as this method requires about 10s for filtering a 5000 sample record sampled at 250Hz on a 1.8GHz PC with 512MB RAM with Matlab 7.1 and Windows XP Professional. This can be handled through the application of a noise detection procedure based on Principal Component Analysis [40].

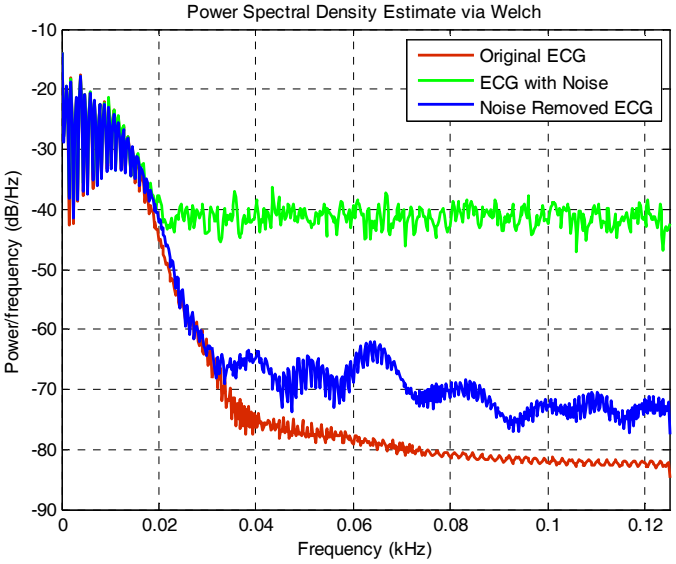

fig. 4-27 Frequency Characteristics after NLNR

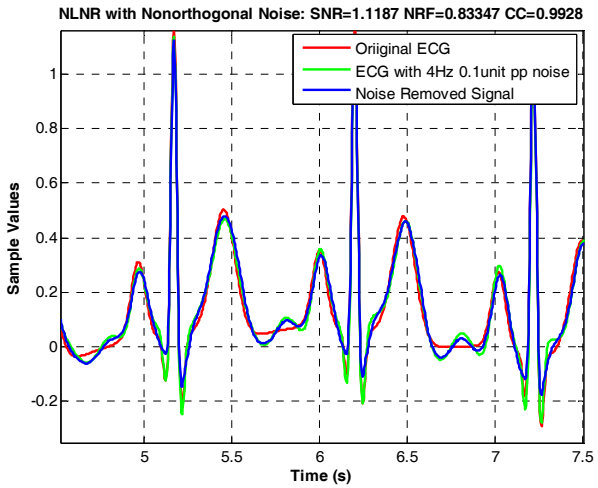

fig. 4-28 NLNR is unable to remove the non-orthogonal 4Hz finger tapping artifact

The figure below shows the results of nonlinear filtering with real ECG data and compares it with filtering using the LPF described in a previous section.

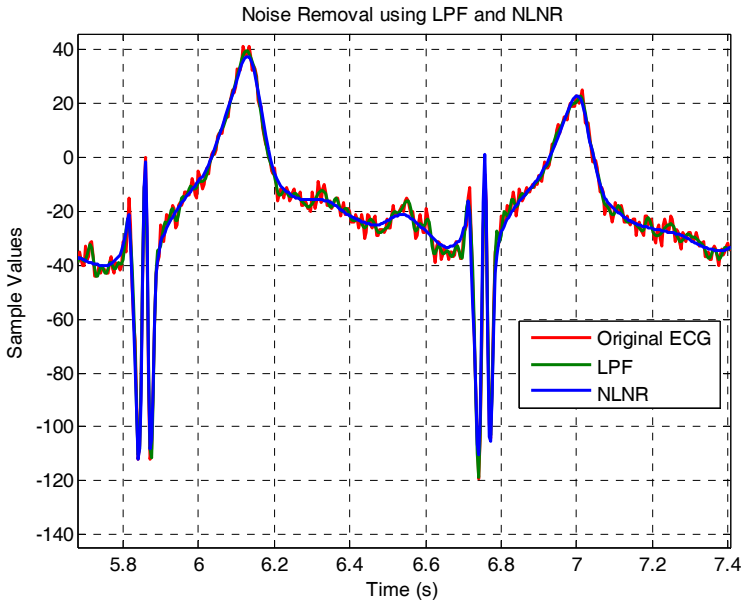

fig. 4-29 Comparison of NLNR and IIR LPF on real ECG

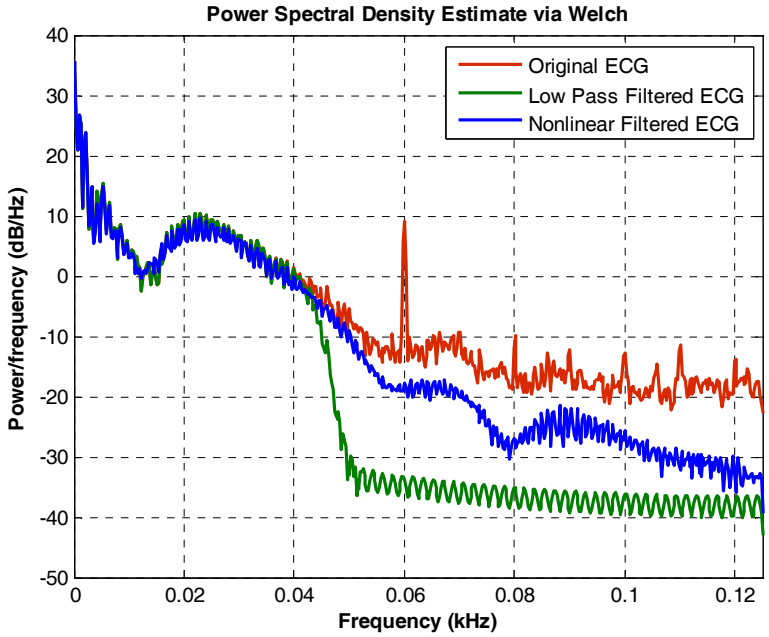

fig. 4-30 Frequency Spectrum Comparison of NLNR and IIR LPF

Function Reference

This approach has been implemented in the file `NLNR.m`.

```
% Filename: NLNR.m
% Author Name: Fayyaz ul Amir Afsar Minhas
% Date: 06June07
% Description: Noise Reduction from ECG using Nonlinear Projection
% Usage:
```

```
%     z=NLNR(y,m,p,r,kn,i)
%      %y: noisy signal
%      %m: Embedding Dimensions
%      %p: Selected Dimensions
%      %r: Neighborhood radius
%      %kn: Minimum number of neighbors
%      %i: number of iterations
```

CHAPTER 5
DETECTION AND DELINEATION OF THE QRS COMPLEX

In the ECG signal, the QRS complex is of fundamental importance. It indicates the ventricular depolarization and is characterized by the most dominant component of the beat, in terms of amplitude. Its detection is of vital importance in response to the sub sequent processing of the ECG signal such as calculation of the RR interval. In terms of disease classification, the QRS complex is of pathological importance. The detection of the QRS complex serves as an entry point for almost all automated ECG analysis algorithms.

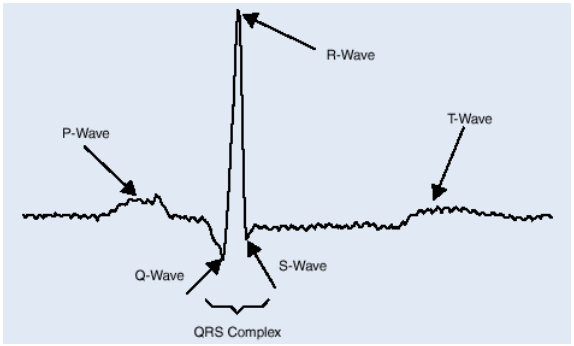

fig. 5-1 The QRS Complex

5.1 Objectives of QRS Detection and Delineation

The objectives of the QRS detection and Delineation process are described henceforth:

- Locate the start of the QRS Complex (Onset)
- Locate the end of the QRS Complex (Offset)
- Locate a reference point in the QRS (Not necessarily the R-Wave)
- Determine the Morphology of the QRS Complex (QR, QS, QRS, RS, RSR', R, or unknown)
- Locate the peaks of individual Q, R and S components

5.2 Problems in QRS Detection

The task of QRS detection is made intricate by the presence of noise in the ECG signal and the large variety of morphologies in which the QRS Complex can occur. Moreover the duration of the QRS complex can vary because of the presence of cardiac diseases related to the ventricles, which calls for the use of some adaptive techniques. A QRS detection and delineation process should be able to cope with all these problems.

5.3 Literature Survey

The figure below shows the architecture of a generic QRS Detector. It is divided into a preprocessing or feature extraction stage including linear and nonlinear filtering and a decision stage including peak detection and decision logic. Often an extra processing block is used for the exact determination of the temporal location of the assumed QRS candidate.

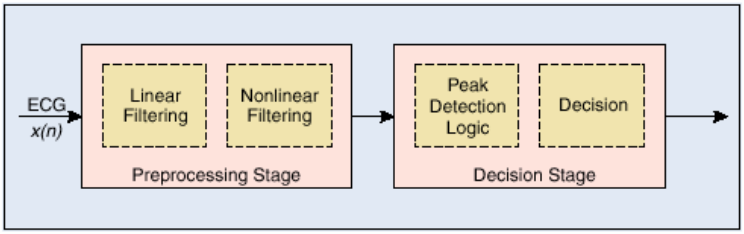

fig. 5-2 Architecture of a QRS Detection Algorithm

The peak detection logic is primarily based on heuristically comparing the output of the preprocessing stage against a threshold which can be adaptive. Therefore the QRS detection algorithms are mostly classified on the basis of their preprocessing stages. Kohler et al. [41] provide an excellent review of QRS detection and delineation strategies and divide the different algorithms used for this purpose into the following major categories:

- Derivative Based Algorithms

  These algorithms first apply derivative operators of different types on the given ECG signal and then compare the absolute value of the differentiated signal against certain thresholds. Some form of post processing is also required for accurately obtaining the QRS Complexes. However these methods are very sensitive to noise and moreover it is difficult to optimize the thresholds. An earlier implementation by [42] of such an algorithm indicates their deficiencies in the detection of the QRS.

- Algorithms based on Digital Filters

These algorithms use digital filters such as,

$$H(z) = (1 - z^{-K})(1 + z^{-1})^{L} \qquad K, L > 0 \tag{1.1}$$

- Algorithms based on the Wavelet Transform

Because of the non-stationary nature of the ECG Signals, multi-resolution methods such as wavelets provide a very effective means of analyzing the ECG signal. These algorithms utilize the CWT and the DWT for the detection of the QRS complex.

- Filter Bank Based Algorithms
- Neural Network Based Approaches
- Use of Adaptive Filters for QRS Detection
- HMM Based Approaches
- Approaches Based on Mathematical Morphology

These approaches use morphological operations such as opening and closing for the reliable extraction of the QRS Complex.

- Use of Matched Filters for QRS Detection
- GA Based Approaches
- Hilbert Transform Based Algorithms
- Length and Energy Transform Based Approaches
- Syntactic Approaches
- QRS Detection Based on Maximum A Posteriori (MAP) Estimation
- Zero Crossing Based Approaches

5.4 Implemented Schemes for QRS Detection/Delineation

The following methodologies for QRS detection have been implemented:

a. The Use of Length Transform for QRS Detection
b. Pan Tompkins's Algorithm for QRS Detection
c. Using CWT for QRS Detection
d. Use of DWT for QRS Detection

Each of these schemes is described in detail in this section.

5.4.1 Length Transform Based QRS Detection

QRS detection methods using length transforms have proven to be high performance detectors. They exploit the curve length concept. The following figure shows how the lengths L1 and L2 are able to characterize the shape of the curves, given a certain time interval *dt*.

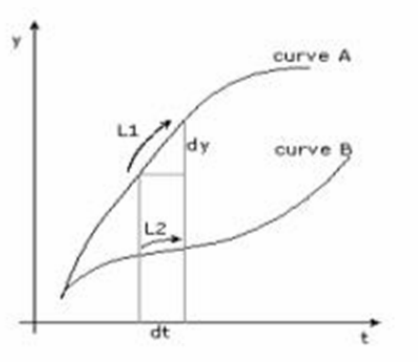

fig. 5-3 The Length Transform

This principle can be applied to detect the wave fronts that characterize the beginning and the end of an episode. Applying Pythagoras theorem in the discrete time domain we can approximate the arc- length relative to the i-th sample with the chord length, obtaining:

$$L = \sum_{i=0}^{n-1} l_i = \sum_{i=1}^{n} \sqrt{T_x^{\,2} + (y_i - y_{i-1})^2} \tag{5.2}$$

L is the total estimated length of the episode, T_x is the sampling interval, $y_i - y_{i-1}$ represents the *i*-th increment and *n* is a rough estimate of the duration of the episode (or waveform) to be detected: in our case *n* is an estimate of QRS duration.
L can also be written as

$$L = T_x \sum_{i=1}^{n} \sqrt{1 + \frac{(y_i - y_{i-1})^2}{T_x^2}} = T_x \sum_{i=1}^{n} \sqrt{1 + \frac{Dy^2}{T_x^2}} \tag{5.3}$$

Now, T_x being a constant and approximating the hypotenuse of successive triangles with their height we obtain:

$$U_1 = L \approx \sum_{i=1}^{n} Dy \tag{5.4}$$

It has been found by repeated experiments that taking the square of this quantity brings a better discriminator capacity. So we can define a new operator, called U2, as:

$$U_2 = \sum_{i=1}^{n} Dy^2 \tag{5.5}$$

Finally, centering the computational window on the i-th sample, and calling *w=n/2* we obtain a recursive low computational cost form which can be easily programmed.

$$U_{3i} = U_{3i-1} - (y_{i-w-2} - y_{i-w})^2 + (y_{i+w-2} - y_{i+w})^2 \quad (5.6)$$

Simple thresholding applied to the output of this operator leads to an efficient and reasonably accurate detection of QRS complexes in real time ECG signals.

5.4.1.1 Steps Involved

The different steps involved in QRS detection and onset/offset calculation using length transform have been slightly modified and are shown in the figure below. These include:

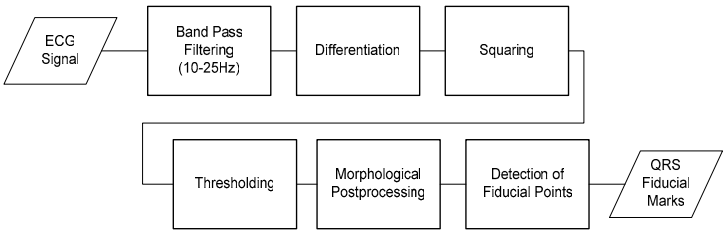

fig. 5-4 Steps involved in Length Transform Based QRS Detection

Band Pass Filtering

The frequency content of the QRS Complex lies in the range 10-25Hz [41]. A Band pass filter tuned to these frequencies would attenuate the P and T waves in comparison to the QRS complex, thus making QRS detection easier. Moreover it diminishes the effects of base line wandering which is taken to be low frequency noise and also removes any high frequency interferences from the ECG. Therefore the Prefiltered ECG signal is band pass filtered using a FIR 10-25Hz BPF of order 100 as shown below.

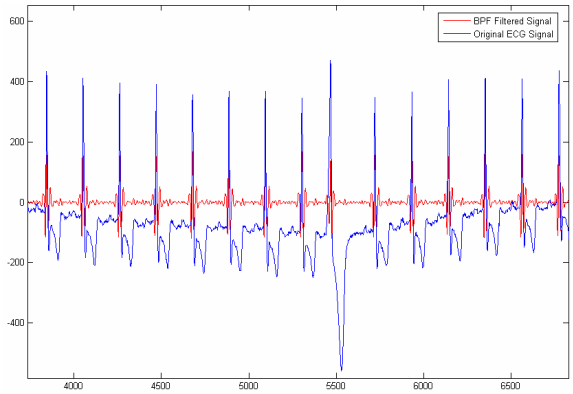

fig. 5-5 Effects of Band Pass Filtering

The signal is padded prior to BPF and the padding is removed afterwards in order to reduce the effects of border distortion.

Differentiation

Differentiation is carried out by the use of differencing as the sampling rate is considered to be constant. This step can be performed using the `diff` Matlab operator. But the use of an operator like $h=\frac{1}{8}[-2\ -1\ 1\ 2]$ gives better results because of a higher tolerance to noise.

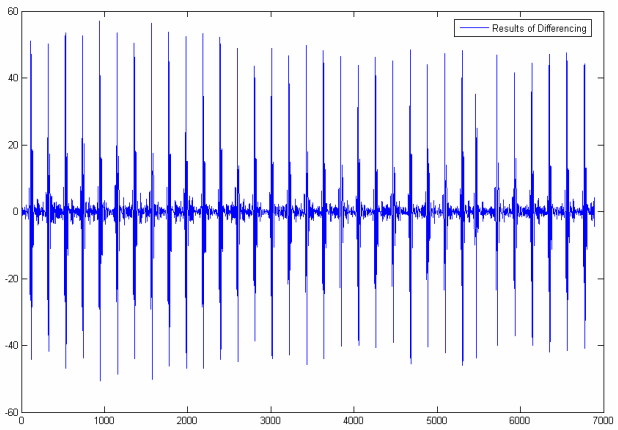

fig. 5-6 Effects of Differentiation

Squaring

The differenced signal is then squared in order to make the result positive and suppress small values.

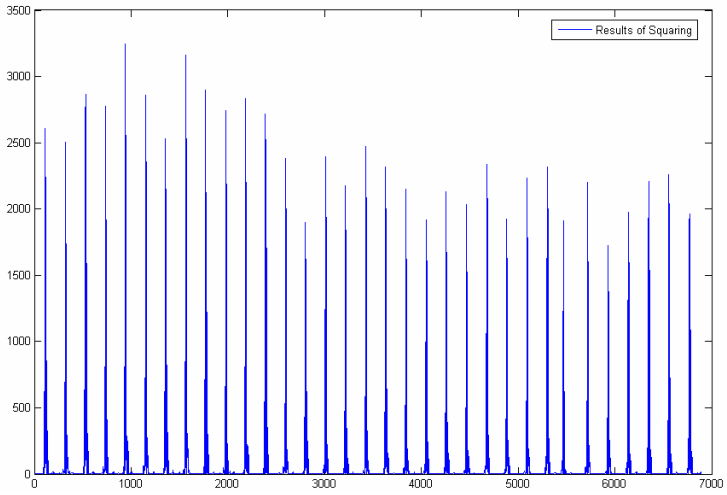

fig. 5-7 Effects of Squaring

Thresholding

The smoothed signal is then thresholded to detect the possible regions in which the QRS may occur. For this purpose an adaptive thresholding function is used which is proportional to the average value of the smoothed signal over a fixed window of duration 4s. For each of the windows over the signal, this threshold is calculated and

then compared with the smoothed signal to find the regions in which the QRS may lie. A parameter for noise tolerance can also be added to the thresholding function, which enables the flexibility of working with noisy signals.

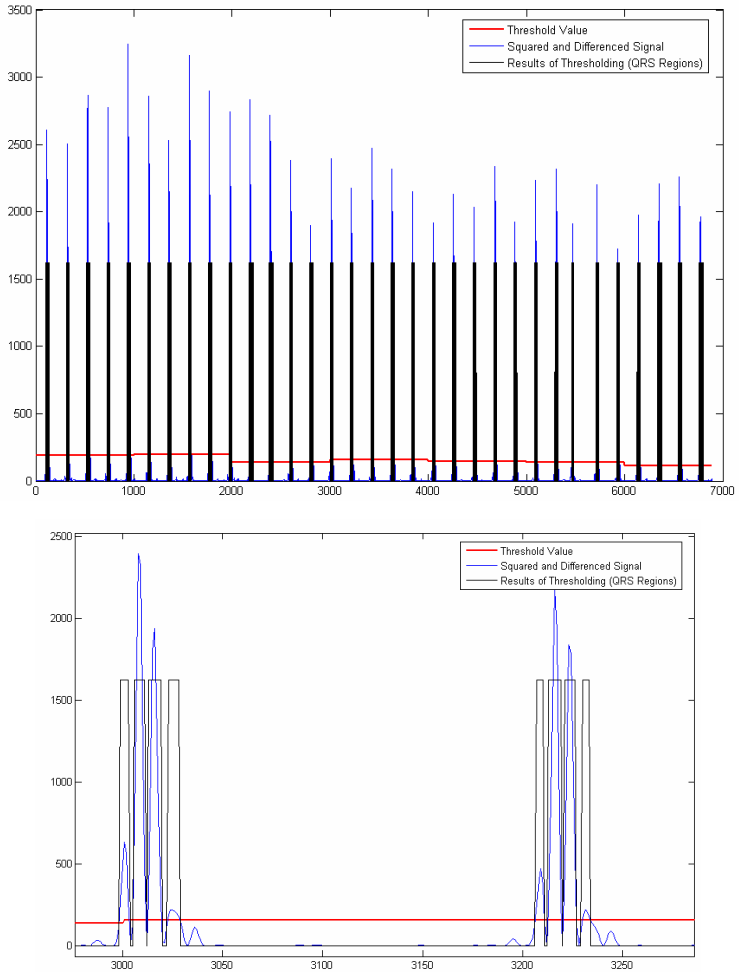

fig. 5-8 Effects of Thresholding

Morphological Post processing

The regions found during the thresholding process might suffer from the following problems:

a. The same QRS complex can be divided into multiple regions
b. Some regions might be crated due to the presence of noise and appear as small spikes, which must be removed

For this purpose, morphological opening and closing is used. The thresholded result is first subjected to morphological closing using a vector of ones of length 120ms (equal to the QRS average length, $0.12 f_s$) as the structuring element in order to remove breaks within a single QRS complex. Afterwards morphological opening is carried out with a

vector of ones of length equal to 40ms (one third of the average QRS length, $0.04 f_s$) to remove any regions smaller than 40ms. Isolated regions are also removed.

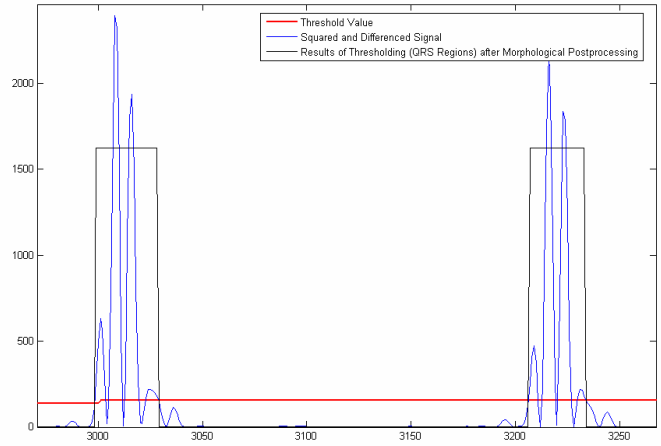

fig. 5-9 After Morphological Post processing

Detection of the Fiducial Points

The Fiducial point in each of the QRS regions detected is found by searching for the sample point within each region at which the local maximum of the band pass filtered signal w.r.t. that region lies.

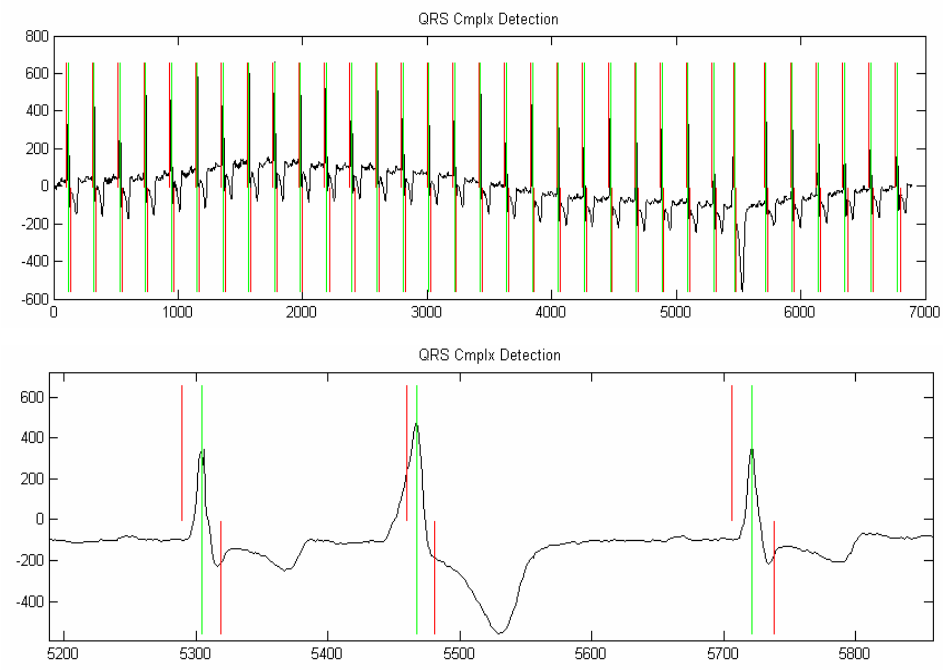

fig. 5-10 Detection of the QRS Fiducial Point

5.4.1.2 Function Reference

This algorithm is implemented in the Matlab-7 function `detectQRS_LT`.

```
[indxon indxoff R]=detectQRS_LT(s,FS,NOISEFAC)
% Author Name: Fayyaz ul Amir Afsar Minhas
```

```
% Date: 13Sep05, Modified: 14Oct05
% Description: QRS Detection using the length transform
% Usage:
%     [indxon indxoff R]=detectQRS_LT(s,FS,NOISEFAC)
%     %s: Input ECG Signal (nx1)
%     %FS: Sampling Freq (Hz)
%     %NOISEFAC: Noise filter multiplier
%       (thresholds all values below NOISEFAC*SquareSignal)
%        Optional: Default Value = 0
%     indxon: QRS Onsets (1 x number_of_qrs)
%     indxoff: QRS Offsets (1 x number_of_qrs)
%     R: Location of the Fiducial Point (1 x number_of_qrs)
% Internal Parameters:
%         F_order=100; %BPF Filter Order
%         Fc_LPF=25; %LPF Cutoff Freq (Hz)
%         Fc_HPF=10; %HPF Cutoff Freq (Hz)
%         MF=1.5; %Multiplier of mean in threshold function
%         SF=+0.0;Multiplier of stdev in threshold function
%                (MF*mu+SF*std)
%         T_win=4*FS;%Thresholding Window Size
%         QRS_Size=0.12*FS; %Approx QRS Complex Size
%         Min_QRS_Size=0.04*FS; %Minimum QRS Size
```

5.4.1.3 Results

This QRS Detection algorithm works accurately on a wide variety of signals and sampling frequencies. The algorithm takes 1 second for processing 74000 samples on a P-IV 1.8GHz processor with 248MB RAM. The algorithm was tested using the QTDB. The sensitivity and positive predictivity are both 99.90%, which indicate the high accuracy of the system.

5.4.1.4 Advantages

The main advantage of this algorithm is its high accuracy in terms of QRS Detection and its speed of operation. Moreover it has a very high tolerance to noise.

5.4.1.5 Problems and Deficiencies

However this algorithm suffers from the following problems:

a. It does not give accurate QRS onsets and offsets. However its detection accuracy is excellent.
b. It gives no information about the QRS morphology. Specific extensions are needed to detect the onset and offset and produce a decision about QRS morphology.

c. It is expected to detect P-waves as the QRS Complex if no QRS is present (Heart Blocks). This problem can be avoided by using a larger window during thresholding but then some of the QRS complexes might be missed.

5.4.2 Pan Tompkins's Algorithm for QRS Detection

Pan and Tompkins [43] proposed a real time QRS detection algorithm based on analysis of the slope, amplitude and width of QRS complexes. The algorithm includes a series of filters and methods that perform low pass, high pass, derivative, squaring, integration, adaptive thresholding, and search procedures. The following figure illustrates the steps of the algorithm in schematic form.

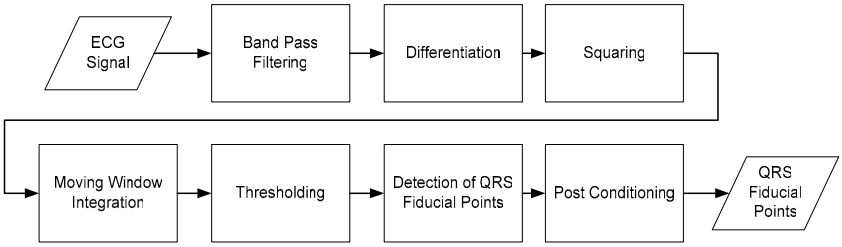

fig. 5-11 QRS Detection using Pan-Tompkins's Algorithm

The lowpass filter used in Pan-Tompkins algorithm has integer coefficients to reduce computational complexity, with the transfer function defined as

$$H(z) = \frac{1}{32}\frac{(1-z^{-6})^2}{(1-z^{-1})^2} \tag{5.7}$$

The output y(n) is related to the input x(n) as

$$y(n) = 2y(n-1) - y(n-2) + \frac{1}{32}[x(n) - 2x(n-6) + x(n-12)] \tag{5.8}$$

The high pass filter used in this algorithm is implemented as an allpass filter minus a lowpass filter. The lowpass component has the transfer function

$$H_{lp}(z) = \frac{(1-z^{-32})}{(1-z^{-1})} \tag{5.9}$$

The input-output relationship is

$$y(n) = y(n-1) + x(n) - x(n-32) \tag{5.10}$$

The transfer function of the highpass filter is specified as

$$H_{hp}(z) = z^{-16} - \frac{1}{32}H_{lp}(z) \tag{5.11}$$

Equivalently, the output p(n)of the highpass filter is given by the difference equation

$$p(n) = x(n-16) - \frac{1}{32}[y(n-1) + x(n) - x(n-32)] \tag{5.12}$$

with *x(n)* and *y(n)* being the input and output signals respectively.

The derivative operator used by Pan and Tompkins is specified as

$$y(n) = \frac{1}{8}[2x(n) + x(n-1) - x(n-3) - 2x(n-4)] \tag{5.13}$$

approximates the ideal differential operator between dc and 30 Hz. The derivative procedure suppresses the low frequency components of the P and T waves and provides a large gain to the high frequency components arising from the high slopes of the QRS complex.

The squaring operation makes the result positive and emphasizes large differences resulting from QRS complexes; the small differences arising from P and T waves are suppressed. The high frequency components in the signal related to QRS complex are further enhanced.

The output of a derivative based operation will exhibit multiple peaks within the duration of a single QRS complex. The Pan-Tompkins algorithm performs smoothing of the output of the preceding operations through a moving window integration filter as

$$y(n) = \frac{1}{N}[x(n-(N-1)) + x(n-(N-2)) + ... + x(n)] \tag{5.14}$$

The choice of the window width N is to be made with the following considerations: too large a value will result in the outputs due to the QRS and T waves being merged, whereas too small a value could yield several peaks for a single QRS.

5.4.2.1 Implementation

An open source implementation of a QRS detector based on the Pan Tompkins's Algorithm by G. D. Clifford was modified to remove the QRS Fiducial marks detected within 120ms (the post-conditioning stage). The original algorithm implements special rules for changing the thresholds adaptively based on the RR Intervals in case a beat is missed or falsely detected. However, such rules were not implemented because the performance of the algorithm was even then found to be outstanding.

This implementation divides the input signals into windows, for each of which QRS detection is carried out separately using different thresholds. Band pass filtering is carried out using cascaded LPF and HPF designed using SPTOOL instead of those proposed in the original paper. The differentiation is carried out using the diff operator

instead of using the operator specified in the original paper. Afterwards squaring is performed. The moving window integrator is implemented by using a 7 element (for FS = 250 Hz) summing filter. Afterwards thresholding is performed which is proportional to the maximum value of the integrated result within the window. This results in the detection of QRS regions in which the maximum value is to taken as the QRS Fiducial point. If multiple fiducial points are detected within 120ms of each other, only one is kept.

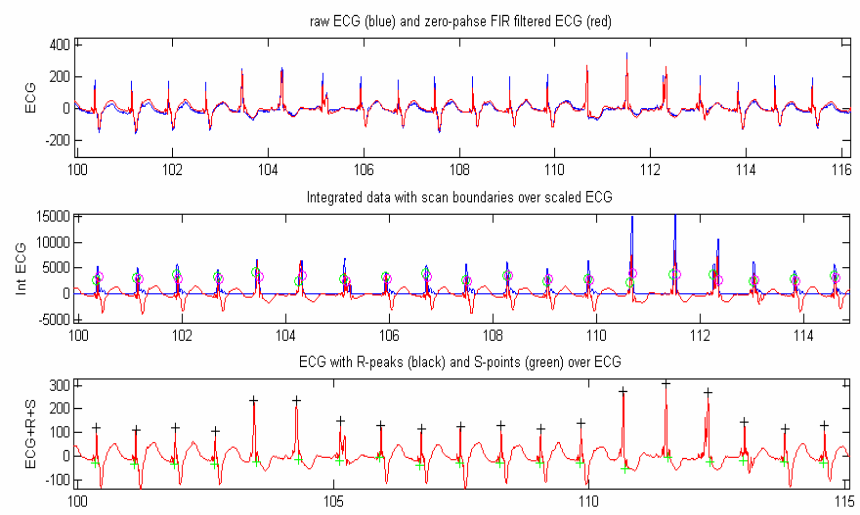

fig. 5-12 Different Steps in QRS Detection

5.4.2.2 Function Reference

This algorithm is implemented in the Matlab 7 file `detectQRS_PT`.

```
% Author Name: Fayyaz ul Amir Afsar Minhas
% Date: 14Sep05
%  Description:  Function  wrapper  to  Pan  Tompkin's  Algo
Implementation by Gari (modified to remove Fiducial Points lying
within 120ms of each other)
% Usage:
%     [R]=detectQRS_PT(s,FS)
%     %s: Input ECG Signal (nx1)
%     %FS: Sampling Freq (Hz)
%     R: Location of the Fiducial Point (1 x number_of_qrs)
% Internal Parameters:
%         thresh=0.12;  Threshold Value
%         testmode=0;  Shows graphs of different steps if 1
%         twind=1000;   Window Size in seconds
%         dt=0.12*FS;   Duration of the QRS
```

5.4.2.3 Results

This algorithm gives 99.98% sensitivity and positive predictivity on QTDB. It requires 1.5s for processing ~74000 samples at 250 Hz Sampling Frequency.

5.4.2.4 Advantages

The main advantage of this algorithm is its high accuracy in terms of QRS Detection and its speed of operation. Moreover it has a very high tolerance to noise.

5.4.2.5 Problems and Deficiencies

However this algorithm suffers from the following problems:

d. It does not give QRS onsets and offsets. However its detection accuracy is excellent.
e. It gives no information about the QRS morphology. Specific extensions are needed to detect the onset and offset and produce a decision about QRS morphology.

5.4.3 Use of Haar Wavelets for QRS Detection and Delineation

Gutierrez et al. [44] propose the use of the Haar wavelets for QRS detection. In this algorithm the input signal is subjected to CWT with a haar wavelet at scale 10 (for Sampling Frequencies up to 500Hz). The resultant waveform is then thresholded to obtain the QRS Fiducial points, no two of which are made to lie within 200ms of each other. The threshold is proportional to the maximum value of the result of the CWT.
This algorithm has been modified in a way that it gives both the QRS onsets and offsets and the fiducial points. The various steps in the modified implementation include:

a. Band Pass Filtering

Band Pass filtering (10-25Hz) is performed with cascaded LP and HP FIR filters of order 100.

b. Evaluation of the CWT

CWT is computed for the Prefiltered signal using Matlab's built-in function CWT. Prior to taking this CWT the signal is padded at both ends with replicated data from the signal, which is subsequently removed. The CWT is performed using the Haar wavelet at a scale of 12. The figure below shows the effects of taking the CWT.

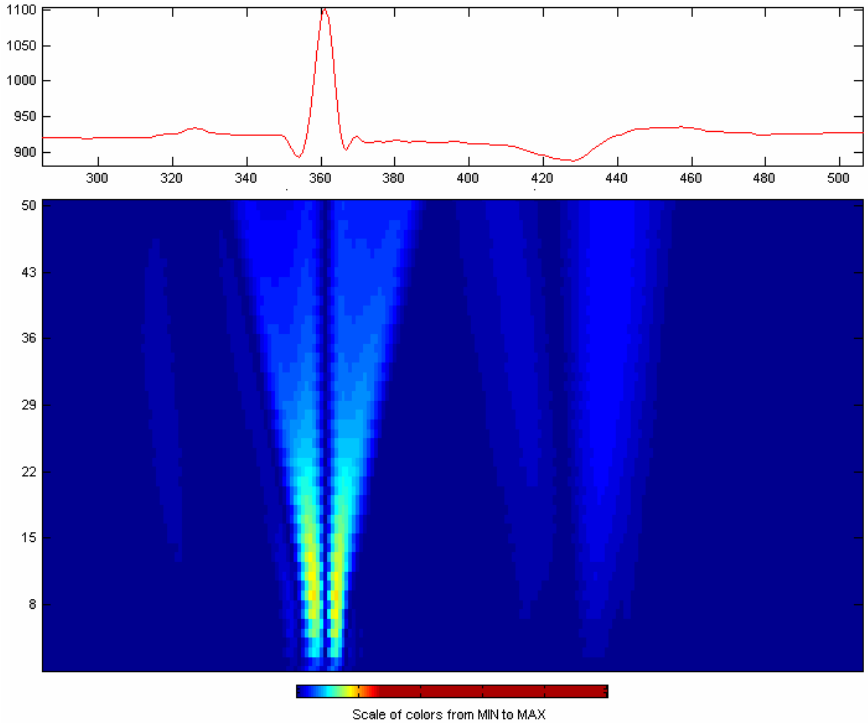

fig. 5-13 CWT of the ECG Signal

c. Differencing

The output of the CWT is then differentiated using the diff Matlab operator.

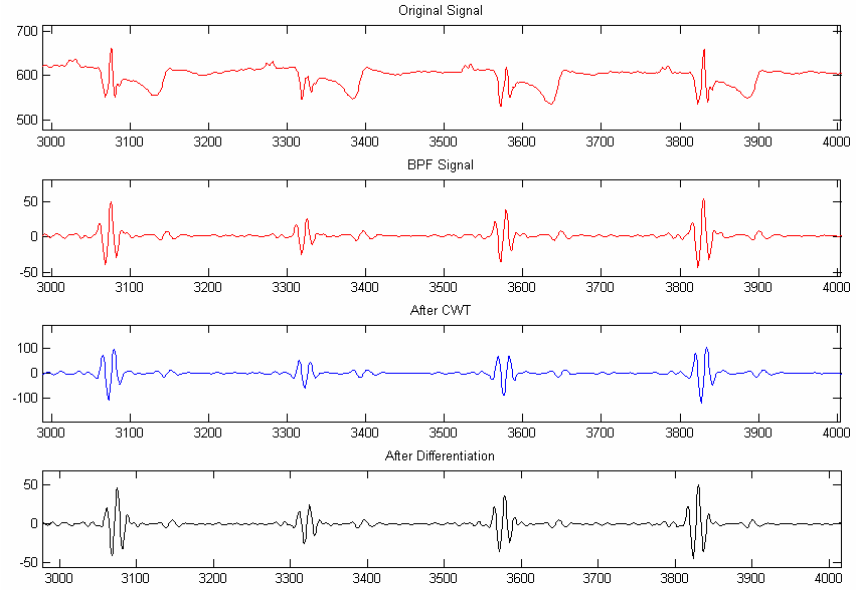

fig. 5-14 Different Steps in QRS Detection: BPF, CWT and Differencing

d. Squaring

The differenced result is then squared in order to suppress low values.

e. Thresholding

The RMS value of the squared result is computed for each window of 4s. The threshold is set proportional to this RMS value. Thresholding gives the QRS regions.

f. Morphological post processing

Morphological post-processing is carried out in a fashion similar to the one explained earlier.

g. Detection of the Fiducial Points

Fiducial point within the QRS is taken as the maximum value of the differentiated and squared result.

The figure below illustrates each of the steps in detail.

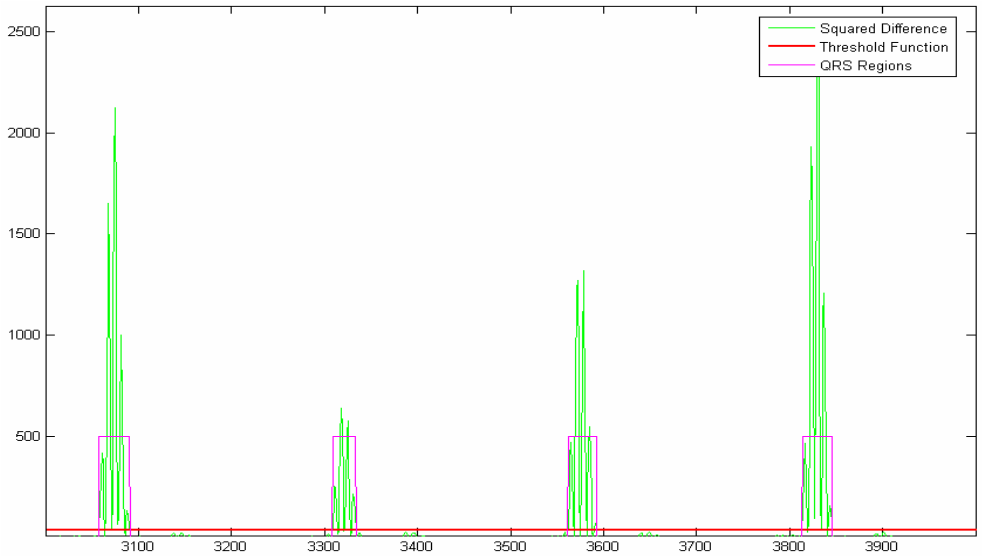

fig. 5-15 Squaring and Thresholding

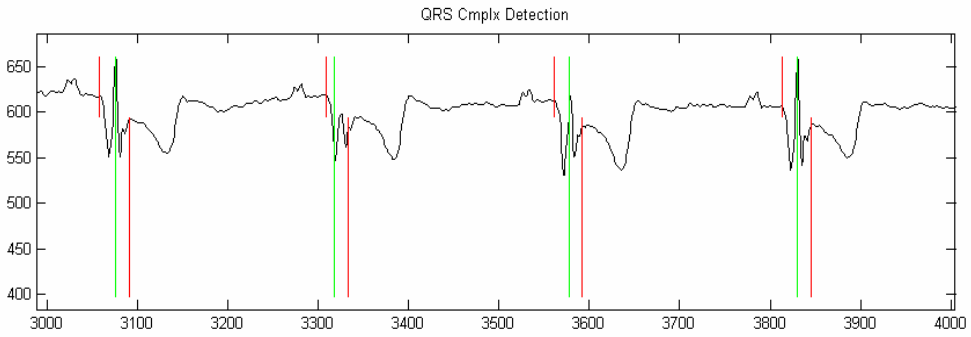

fig. 5-16 Detection of the QRS Fiducial Points

5.4.3.1 Function Reference

This function is implemented in the function Matlab -7 m-file `detectQRS_Haar2`.

```
   [indxon indxoff R]=detectQRS_Haar2(s,FS)
   % Author Name: Fayyaz ul Amir Afsar Minhas
   % Date: 15Sep05
   %   Description:   Haar   Wavelet   Based   QRS   Detector   using
Prefiltering and Morphological Post Processing
   % Usage:
   %     qrso=detectQRS_Haar2(s,FS)
```

```
%     %s: Input Coloumn Vector (ECG Signal)
%     %FS: Sampling Freq (Hz)
%     %indxon: Index of onset
%     %indxoff: Index of Offset
%     %R : Fiducial Marks for QRS
% Internal Parameters
%         F_order=100; %HPF & LPF Filter Order
%         Fc_LPF=25; %LPF Cutoff Freq (Hz)
%         Fc_HPF=10;  %HPF Cutoff Freq (Hz)
%         P=25; %Padding for CWT (P at start and P at end)
%         wname='haar'; %Wavelet Name
%         scale=12; %Scale
%         T=0.15; %Thresholding Function Multiplier
%         T_win=1000; %Threshold update window size
%         QRS_Size=0.12*FS; %Approx Size of QRS Complex
%         Min_QRS_Size=0.06*FS; %Min Size of QRS Complex.
```

5.4.3.2 Results

This method gives a detection Sensitivity/Specificity of 99.8% with onset and offset detection errors being 10ms and 12ms respectively. It takes 1s for processing ~74000 samples on a P-IV, 1.8GHz, 248MB RAM Machine.

5.4.3.3 Comments

This method demonstrates the efficacy of the system in QRS detection and delineation and it can also be extended to the detection and delineation of the P and T waves in the ECG. It offers high detection accuracy with low errors in determining the onset and offsets of the QRS complex with computation time comparable with the previously described algorithms.

5.4.4 Use of DWT for QRS Detection and Delineation

In [14], the authors have proposed a robust and highly accurate QRS detection and delineation system based on the DWT. It gives not only the QRS Fiducial points but also the complex's onsets and offsets along with the morphology. The theoretical and implementation details of this method are discussed in detail henceforth.

5.4.4.1 Theory of Operation

The DWT of a signal $x(t)$ is given by

$$W_a x(b) = \frac{1}{\sqrt{a}} \int_{-\infty}^{\infty} x(t)\psi\left(\frac{t-b}{a}\right)dt, \qquad a > 0 \tag{5.15}$$

The greater the scale factor a is, the wider is the basis function and consequently, the corresponding coefficients give information about the lower frequency component of the signal and vice versa. In this way, the temporal resolution is higher at higher frequencies than at low frequencies, achieving the property that the analysis window comprises the same number of periods for any central frequency. If the wavelet $\psi(t)$ is the derivative of a smoothing function $\theta(t)$, it can be shown that the wavelet transform of a signal $x(t)$ at a scale a is

$$W_a x(b) = -a\left(\frac{d}{db}\right)\int_{-\infty}^{+\infty} x(t)\theta_a(t-b)dt \tag{5.16}$$

Where $\theta_a(t) = \left(1/\sqrt{a}\right)\theta\left(t/a\right)$ is the scaled version of the smoothing function. The wavelet transform at scale a is proportional to the derivative of the filtered signal with a smoothing impulse response at scale a. Therefore, the zeros crossings of the WT correspond to the local maxima or minima of the smoothed signal at different scales, and the maximum absolute values of the wavelet transform are associated with maximum slopes in the filtered signal. During QRS detection, the ECG waves are to be detected which are composed of slopes and local maxima or minima at different scales, occurring at different time instants within the cardiac cycle. This establishes the need of using such a wavelet.

If The scale and the translation parameters are discretized such that $a = 2^k$ and $b = 2^k l$, the transform is then called the dyadic wavelet transform with the basis functions

$$\psi_{k,l}(t) = 2^{-k/2}\psi(2^{-k}t - l) \qquad k, l \in Z^+ \tag{5.17}$$

The dyadic wavelet transform for discrete time signals is equivalent, according to Mallat's Algorithm, to the octave filter bank, and can be implemented as a cascade of identical cells (low and high pass FIR filters) as shown below.

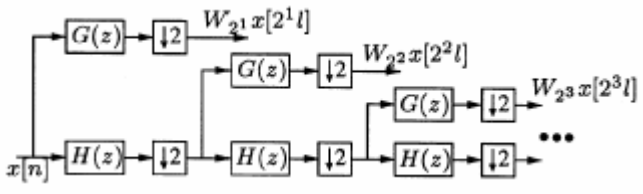

fig. 5-17 The Dyadic Wavelet Transform

The down samplers after each filter remove the redundancy of the signal representation. As side effects they make the signal representation time-variant, and reduce the temporal resolution of the wavelet coefficients for increasing scales. In order to overcome this problem, a modified version of this algorithm is used, which is shown below. In this algorithm , the decimation stages have been removed and the filter impulse responses of the previous scale are interpolated to contain twice as many points as in the previous scale.

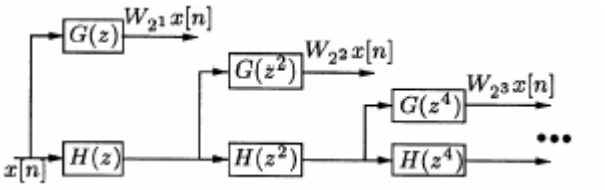

fig. 5-18 The Modified Algorithm for DWT (Algorithm a trous)

The FIR filter impulse responses for the above implementation are

$$h[n] = \frac{1}{8}\{\delta[n+2] + 3\delta[n+1] + 3\delta[n] + \delta[n-1]\}$$
$$g[n] = 2\{\delta[n+1] - \delta[n]\} \tag{5.18}$$

As these filters have linear phase, the outputs of the filters can be realigned in order to present the same delay with respect to the original ECG.

Various components of the ECG register themselves as maximas and minimas at different scales. The figure below shows several simulated waves similar to those in the ECG, together with the first five scales of their DWT.

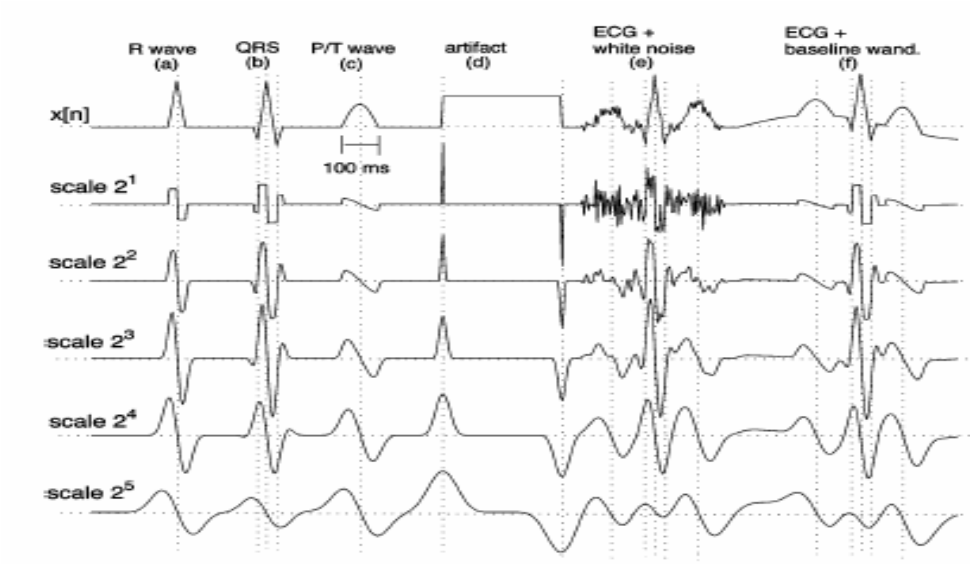

fig. 5-19 Response of the modified DWT algorithm to simulated waves of the ECG [14]

As exemplified by (a), monophasic waves produce a positive maximum-negative minimum pair along the scales, with a zero crossing between them. Each sharp change in the signal is associated to a line of maxima or minima across the scales. In wave (b), which simulates a QRS complex, it can be observed that the small Q and S wave peaks have zero crossings associated in the WT, mainly at scales 2^1 and 2^2. P or T-like waves (c) have their major component at scales 2^4 to 2^5, whereas artifacts like (d) produce isolated maximum or minimum lines which can be easily discarded. If the signal is contaminated with high-frequency noise (e), the most affected scales are 2^1 and 2^2, being higher scales essentially immune to this sort of noise. Baseline wander (f) affects only at scales higher than 2^4. The figure below shows the results of our implementation of the modified algorithm on a similar simulated signal and it compares quite accurately to the one from the original paper.

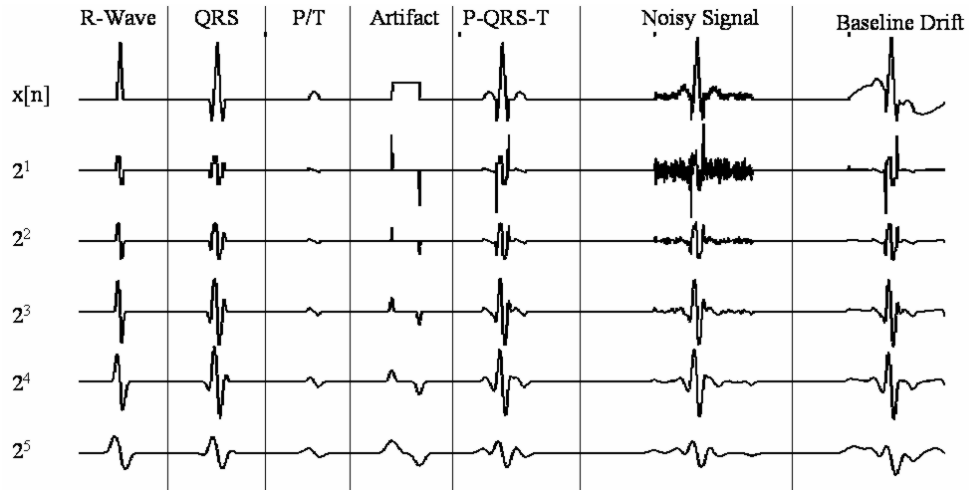

fig. 5-20 The response of our implementation of [14] DWT to the simulated ECG waves

Using the information of local maxima, minima and zero crossings at different scales the algorithm is able to detect the Fiducial points in the QRS complexes and obtain the location of the onset and offset along with that of the individual waves.

5.4.4.2 Detection of the QRS Complex Individual Waves and Determination of QRS Morphology

The QRS Detection process is based on simple thresholding of the WT (details) at scale 2^1. The threshold is computed for each window of 65535 samples (Sampling frequency of 250Hz) and is proportional to the RMS value of the WT, Mathematically

this threshold is given by $\in_{QRS}^{1} = \mathrm{RMS}\left(W_{2^1} x[n]\right)$. The thresholded result is then morphologically post processed, to obtain the QRS regions.

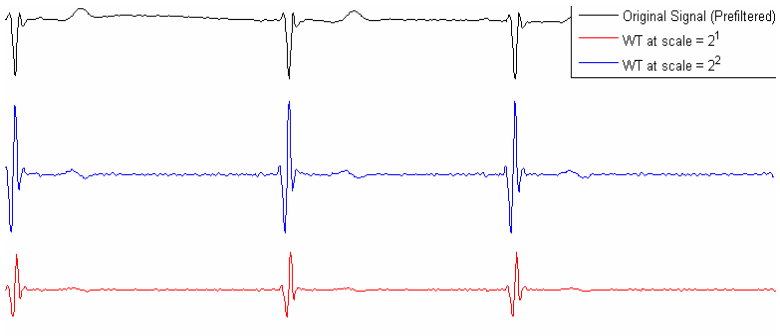

fig. 5-21 Response of the WT at the first two scales to the given ECG signal

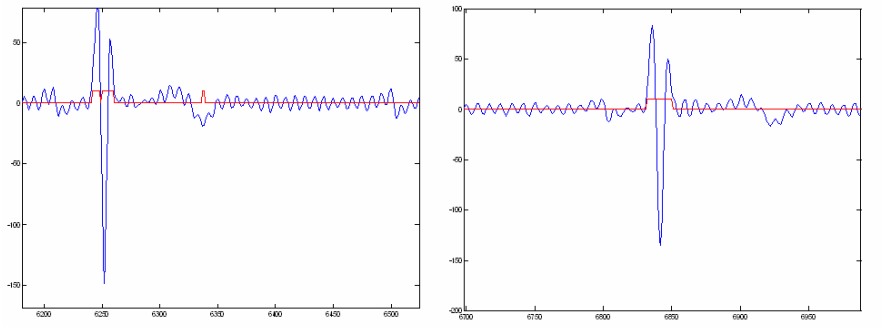

fig. 5-22 Effects of thresholding and morphological postprocessing

The QRS Fiducial point is flanked by a pair of maximum moduli with opposite signs at scale 2^2, namely at n_{pre} and n_{post} and is found out by searching for the root of the WT representation at scale 2^2 between n_{pre} and n_{post} within each extended QRS region. The extended QRS regions are obtained by widening the QRS regions obtained through the thresholding explained earlier. The delineator looks before n_{pre} and after n_{post} for significant maxima of $\left|W_{2^2} x[n]\right|$ accounting for other adjacent slopes within the QRS complex. To consider a local maximum modulus as significant, it must exceed the threshold, $\gamma_{QRS_{pre}}$ or $\gamma_{QRS_{post}}$ respectively for previous or subsequent waves. Small spikes in thresholding are removed using morphological opening. Moreover, the positive minimas and negative maximas are removed. If redundant modulus maximas occur than each such sequence is replaced by a single modulus maxima having the greatest value of all. The figures below show these steps in detail. The sequence of positive maximas (M^+s) and negative minimas (m^-s) thus obtained (called the maxima string representation) is used to determine the QRS morphology using a simple rule based

approach. Figure 5-24 shows this classification of the QRS Morphology is detail. If the maxima string obtained for a QRS region is not one of those shown in the figure, it is classified as 'Unknown' Morphology and subjected to a spike removal algorithm which includes protection measures, based on time interval and sign rules, to reject notches in waves and anomalous deflections in the ECG signal. If the morphology is QRS or RSR' then special checks are made to ascertain the initial classification result as both QRS and W-type complexes and the RSR' and M-type complexes have the same maxima string representation. The differentiation between these categories is done on the basis of signs of the signal values in the original signal. The zero crossings between the significant slopes at scale 2^1 are assigned to wave peaks, and labeled depending on the sign and the sequence of the maximum moduli.

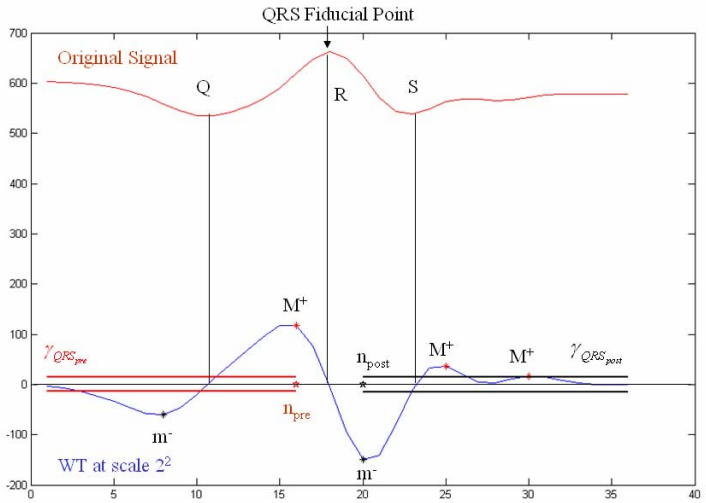

fig. 5-23 Detection of QRS Individual Waves and the QRS Morphology. It shows a single QRS region and different thresholds and zero crossings corresponding to the given signal. It also shows redundant modulus maxima (two M+). In such a case the one with the maximum absolute value is retained. Any positive minimas or negative maximas (if present) are also removed to produce the Maxima String Representation for a QRS region. In this case the string is $m^-M^+m^-M^+$, which corresponds to the morphology QRS.

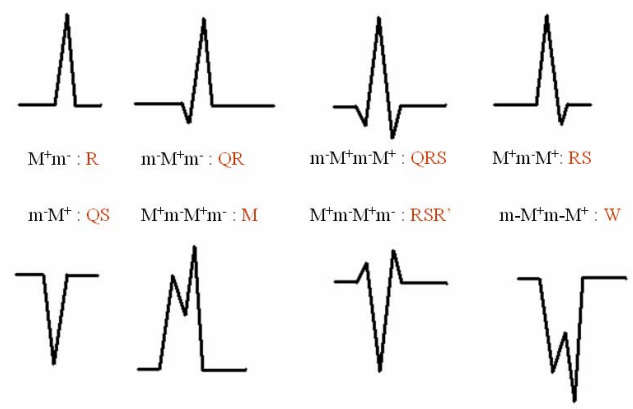

fig. 5-24 Classification of the QRS Morphology

5.4.4.3 Determination of the QRS Onset and Offset

The onset (end) of the QRS is before (after) the first (last) significant slope of the QRS, which is associated with a maximum of $\left|W_{2^2}x[n]\right|$. So, we first identify the samples of the first and last peaks associated with the QRS in $\left|W_{2^2}x[n]\right|$, say n_{first} and n_{last}. Then, candidates to onset and end are determined by applying two criteria:

i) searching for the sample where $\left|W_{2^2}x[n]\right|$ is below a threshold ($\xi_{QRS_{on}}$ or $\xi_{QRS_{end}}$) relative to the amplitude of the maximum modulus ($\left|W_{2^2}x[n_{first}]\right|$ or $\left|W_{2^2}x[n_{last}]\right|$);

ii) ii) searching for a local minimum of $\left|W_{2^2}x[n]\right|$ before n_{first} or after n_{last}. Finally the QRS onset and end are selected as the candidates that supply the nearest sample to the QRS fiducial point.

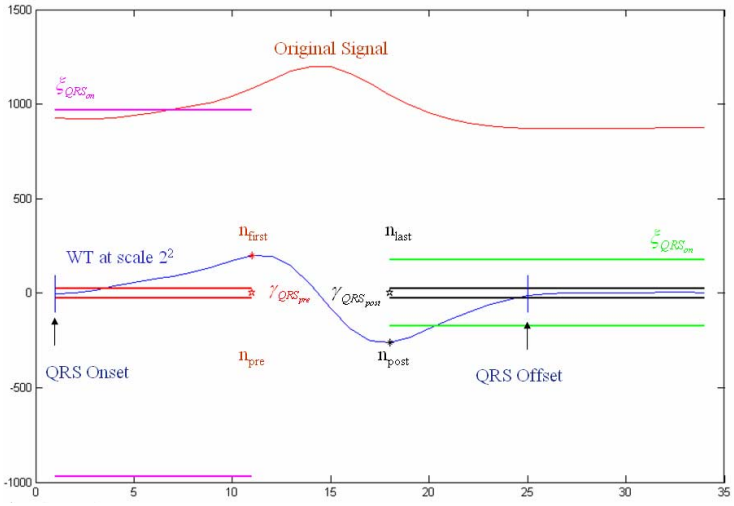

fig. 5-25 QRS Onset and Offset Detection

5.4.4.4 A Note About the Thresholds

The thresholds are given by

$$\begin{aligned}
\gamma_{QRS_{pre}} &= \chi_1 \max\left(\left|W_{2^2}x[n]\right|\right) \quad n \in S_{W_{QRS}} \text{ (Search Window before } n_{pre}) \\
\gamma_{QRS_{post}} &= \chi_2 \max\left(\left|W_{2^2}x[n]\right|\right) \quad n \in S_{W_{QRS}} \text{ (Search Window after } n_{post}) \\
\xi_{QRS_{on}} &= \begin{cases} \chi_3 W_{2^2}x[n_{first}] & \text{if } W_{2^2}x[n_{first}] > 0 \\ \chi_4 W_{2^2}x[n_{first}] & \text{if } W_{2^2}x[n_{first}] < 0 \end{cases} \\
\xi_{QRS_{end}} &= \begin{cases} \chi_5 W_{2^2}x[n_{last}] & \text{if } W_{2^2}x[n_{last}] > 0 \\ \chi_6 W_{2^2}x[n_{last}] & \text{if } W_{2^2}x[n_{last}] > 0 \end{cases}
\end{aligned} \tag{5.19}$$

The threshold multipliers $\chi = [\chi_2 \quad \chi_2 \quad \chi_3 \quad \chi_4 \quad \chi_5 \quad \chi_6]$ were tuned using Genetic Algorithms with the criterion function to reduce the sum of the mean of the error in onsets and offsets for a number of beats of different subjects from the QTDB. The original values in the paper are:

$$\chi = [0.06 \quad 0.09 \quad 0.05 \quad 0.07 \quad 0.125 \quad 0.71]$$

The error in segmentation using these parameter values was found to be 3.5 samples (onset), 2.67 samples (offset) at a sampling rate of 250Hz. These values were improved using Genetic Algorithms as detailed in results. Ten subjects from the QTDB were used for training. The mutation probability was set to be 5%. Two point cross-over operator was used along with elitism.

5.4.4.5 Function Reference

This function is implemented in the Matlab-7 function m-file `DetectQRS_Del2`.

```
[qrs_s qrs_e qrs_Absolute]=DetectQRS_Del2(S,FS,param)
% Author Name: Fayyaz ul Amir Afsar Minhas
% Date: 20Sep05
 % Description: DWT Based QRS Det and Deln: An implementation of
'A Wavelet-Based ECG Delineator: Evaluation on Standard Databases'
% Usage:
%     [indxon indxoff R]=detectQRS_LT(s,FS,NOISEFAC)
%     %s: Input ECG Signal (nx1)
%     %FS: Sampling Freq (Hz)
%     %param: Parameters [1 Xi] (see doc.)
%            Optional: Default Value are the original ones from
the paper i.e [1 0.06 0.09 0.05 0.07 0.125 0.17]
%     qrs_s: QRS Onsets (1 x number_of_qrs)
%     qrs_e: QRS Offsets (1 x number_of_qrs)
%   qrs_Absolute: the Fiducial Point (1 x number_of_qrs)
% Internal Parameters:
%   QRS_Size=0.12*FS; %Approx Size of QRS Complex (Samples)
%   Min_QRS_Size=0.04*FS; %Minimum QRS Size (Spike Removal)
% Note: Works only for FS=250Hz
```

5.4.4.6 Results

This algorithm gives excellent QRS delineation results i.e. a mean absolute error of 5 samples in the detection of QRS onsets (2.5 sample error) and offset (2.5 sample error) at 250Hz sampling frequency for the whole QTDB using annotations by the first expert cardiologist. The mean error (not absolute) is even lower. The mean error with standard deviation is 0 ± 8 ms and the offset error is 0 ± 9 ms, Which makes the QRS complex onsets and offsets detected by this algorithm perfect for use for all practical purposes.

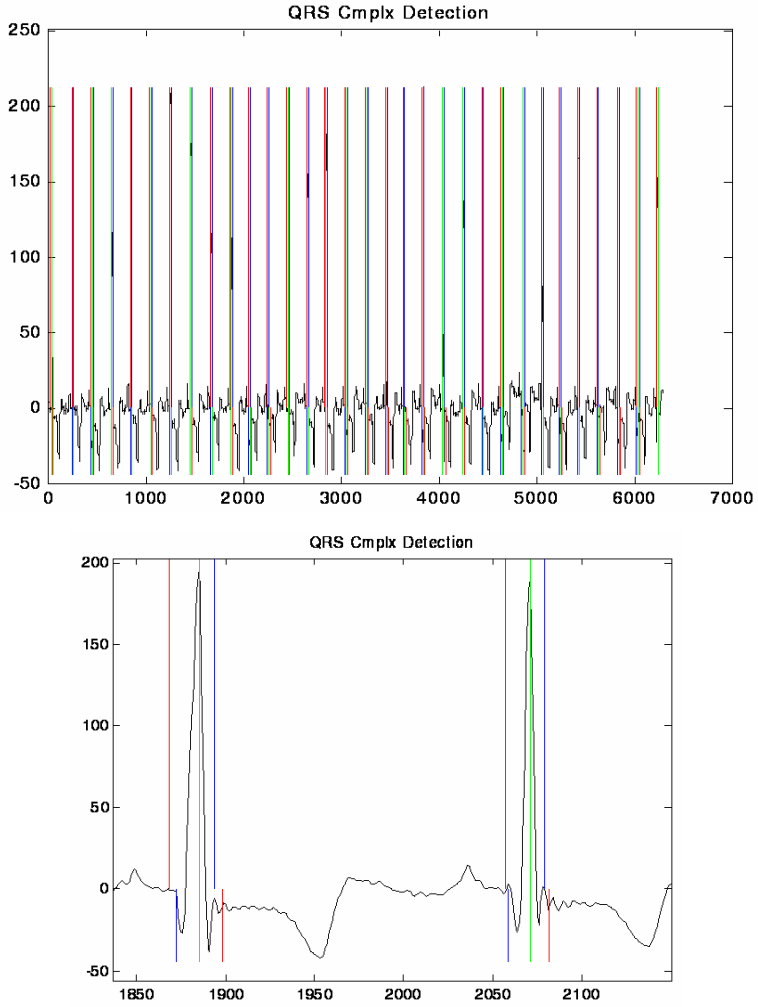

fig. 5-26 Results of DWT Based QRS Detection

However it's QRS detection accuracy is lower than that of the Pan and Tompkins's algorithm (Positive Predictive Values and sensitivity = ~99.1%). This is because of the presence of noise in some ECG signals of the QTDB since QRS detection is based on the WT at scale 2^1, which is severely affected by noise. The implantation of a noise reduction algorithm prior to this process can reduce this problem.

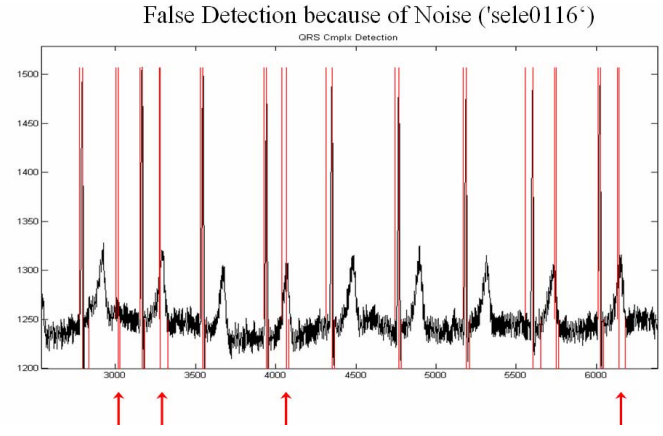

fig. 5-27 False Detection due to Noise

5.4.4.7 Limitations

This algorithms works for sampling frequency of 250Hz. In order to work with other sampling frequencies, the filters used in the WT need to be modified or the input signal be resampled.

CHAPTER 6
DETECTION OF THE P AND T WAVES

The detection of the T and P waves is the next step after the detection and delineation of the QRS complex. The P wave reflects Artrial depolarization whereas the T wave is the representation of the ventricular repolarization The detection and delineation of these waves is of critical importance in analyzing both the arterial and ventricular activity of the heart. In terms of disease classification, the P-wave is responsible for the classification of a majority of arterial disease whereas the T-wave is used in the classification of infarctions, ischemia and ventricular hypertrophies.

6.1 Problems in the Detection of the P and T waves

Many problems manifest themselves in the detection of the P and T waves, some of them are given below:

a. It is difficult to choose a search window in relation to the QRS reference for a beat. Especially for the P-wave, which may occur without a QRS (heart blocks).
b. The amplitude of the P-wave might be very small.
c. Both the P and T waves occur in a wide variety of morphologies, which makes the task of their detection difficult.
d. The P wave can occur very close to the T wave and also to the QRS, which makes its separation an issue.
e. In some cases a U-wave may also occur after the T-wave, which must be segmented from both the P and the T waves.

A P/T detection algorithm must be able to deal with all of the above mentioned problems.

6.2 Literature Survey

A variety of P-wave detection methodologies exist in the literature. In [45], a real time method for the detection of the P-waves is presented. This method first removes the baseline from the signal by using cubic function and parabolic corrections. After the

baseline removal process, the differential of the TQ interval is computed using the following operator:

$$y_i^{'} = \frac{f_s}{10}\left(-2y_{i-2} - y_{i-1} + y_{i+1} + 2y_{i+2}\right) \tag{6.1}$$

Where f_s is the sampling frequency. Afterwards the maxima of this differential within 5s is found and is designates as $D_{\max}$. On the basis of this value, two thresholds are setup i.e.

$$T_1 = \max(\mathrm{N}_1 D_{\max}, 1.0) \quad T_2 = \max(\mathrm{N}_2 D_{\max}, 0.25) \tag{6.2}$$

T_1 is for the detection of the P-wave and T_2 is for location of the onset and offset of the P-wave. Both these thresholds are in mv/s. The coefficients N_1 and N_2 can be determined by adjustment from many cases. The P-wave detection accuracy is reported at 92.6%. [46] gives a method for P-wave detection in high resolution ECG, which is based on the use of forward and reverse filtering of the Signal Averaged ECG using a HPF. [47] gives a P-wave detection method using the Wavelet transform. In this method a technique similar to the one proposed in [14] is proposed for P-wave detection, which uses the ratio of the WT of the signal at scale 2^3 and 2^3. Another WT based approach is given in [48] for the detection of the P and T waves along with the QRS complexes. Other methods include [48-53].

6.3 Implemented Schemes for T Wave Detection

Two schemes have been implemented for the detection of the T-wave i.e.

a. Use of Joeng's Differential Operator for T wave detection [54]
b. Use of DWT for T-wave detection [14]

Each of these methods is described below.

6.3.1 Use of Joeng's Operator for T wave detection

This approach is based upon the method given in [54]. T-wave detection is carried out by the following steps

a. Base line removal

Prior to the detection of the T-wave, the baseline is removed from the signal using techniques described in the next chapter.

b. Band Pass Filtering

The T-wave has its frequency content in the range 0.05-15Hz. Therefore a BPF FIR filter is used to BPF the given signal. This operation makes the algorithm more noise tolerant.

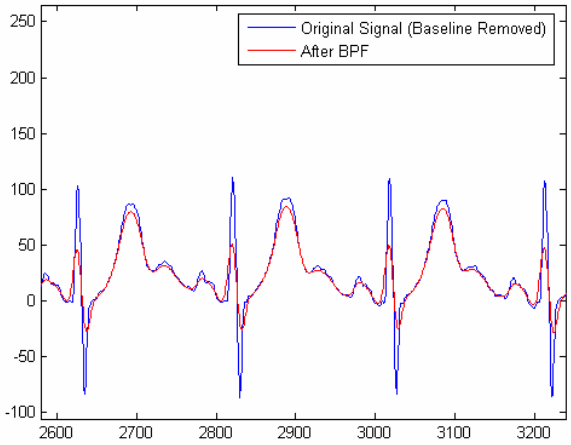

fig. 6-1 Effects of Band Pass Filtering

c. Determination of the search window

The algorithm searches for the T-wave, after a QRS complex has been detected. The T wave is expected within a specified time window. The start and duration of the window depends on the RR interval, as shown below.

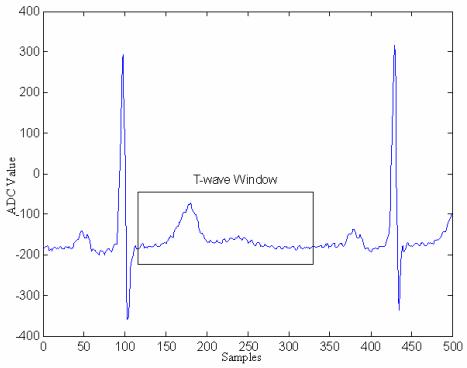

fig. 6-2 The T-wave Window

$$\left.\begin{aligned} T_{win_S} &= 0.08s + QRS_E \\ T_{win_E} &= 0.44s + QRS_E \end{aligned}\right\} \quad if\ \ bpm \le 85$$

$$\left.\begin{aligned} T_{win_S} &= 0.04s + QRS_E \\ T_{win_E} &= 0.7RR - 0.06s + QRS_E \end{aligned}\right\} \quad if\ \ bpm \ge 85 \qquad (6.3)$$

The above windowing scheme was the one originally given in the paper, however better results were obtained using the following window, which was developed by us through statistical analysis and curve fitting over the QTDB.

$$\left.\begin{aligned} T_{win_S} &= 0.05s + QRS_E \\ T_{win_E} &= 0.7RR - 0.42s + QRS_E \end{aligned}\right\} \quad if\ \ bpm \le 40$$

$$\left.\begin{aligned} T_{win_S} &= 0.03s + QRS_E \\ T_{win_E} &= 0.2RR + 0.3s + QRS_E \end{aligned}\right\} \quad if\ \ 40 < bpm \le 85 \qquad (6.4)$$

$$\left.\begin{aligned} T_{win_S} &= 0.02s + QRS_E \\ T_{win_E} &= 0.7RR - 0.044s + QRS_E \end{aligned}\right\} \quad if\ \ bpm > 85$$

d. Use of Joeng's Differential Operator

Within the window after a QRS, the Joeng's differential operator is applied, which is given by

$$F(n) = \frac{\sum_{k=-4}^{4} k\ x(n+k)}{60} \qquad (6.5)$$

where x(n) is the input ECG signal. This differentiator operator has a flatter frequency magnitude response at higher frequencies, thus effectively removal any noise artifacts. Smoothing using a moving window integrator (proposed in the original method) is not performed, because it decreases the temporal resolution of the detection process.

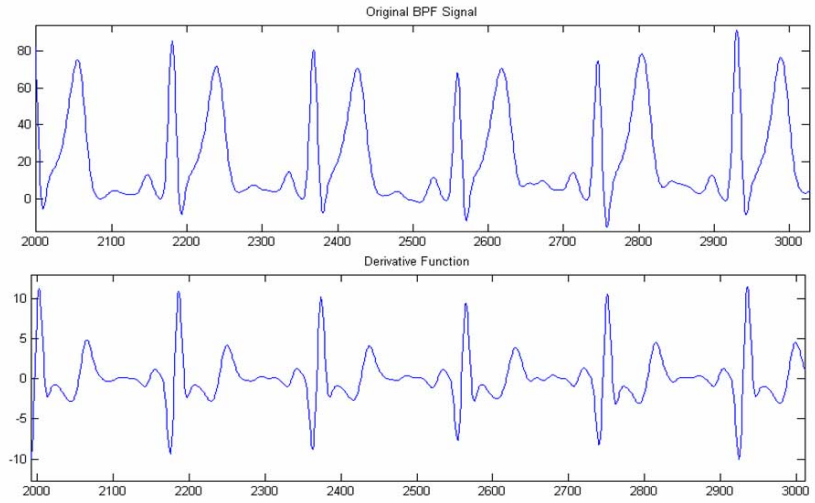

fig. 6-3 Application of the Joeng's Differential Operator

e. Detection of the T-wave fiducial point (peak)

The T-wave Fiducial point is flanked by a pair of maximum moduli with opposite signs in the derivative function $F(n)$ in a T-wave window, namely at n_{pre_T} and n_{post_T} and is found out by searching for the root of the derivative function between n_{pre_T} and n_{post_T} within each T-wave window. Also the slope magnitude needs to be at least 0.006mV/s for a T-wave to be detected.

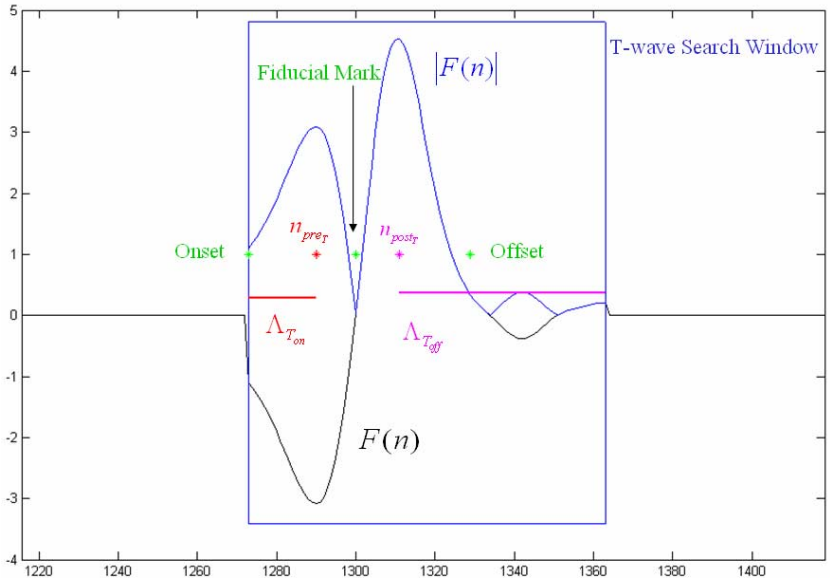

fig. 6-4 Determination of the QRS Onset, Offset and the Fiducial Point

f. Determination of the T-wave onsets and offsets

Then, candidates to onset and end are determined by applying two criteria: i) searching for the sample where the absolute value derivative function is below a threshold ($\Lambda_{T_{on}} = \chi_{1_T} \left| F\left(n_{pre_T}\right)\right|$ or $\Lambda_{T_{end}} = \chi_{2_T} \left| F\left(n_{post_T}\right)\right|$) ; ii) searching for the minimum absolute value of the derivative function before n_{pre_T} and n_{post_T}. Finally the QRS onset and end are selected as the candidates that supply the nearest sample to the QRS fiducial point. The parameters χ_{1_T} and χ_{2_T} need to be optimized using Genetic Algorithms.

6.3.1.1 Function Reference

This algorithm is implemented in the Matlab-7 function file `detectT.m`.

```
[T_on T_off T]=detectT(RRI,qrs_off,FS,blr)
% Author Name: Fayyaz ul Amir Afsar Minhas
% Date: 25Sep05, Modified: 18Oct05
% Description: QRS Detection using the Joeng's Operator
% Usage:
%     [T_on T_off T]=detectT(RRI,qrs_off,FS,blr)
%     %RRI: RR Intervals (2xn). n=number of QRS Complexes-1
%          The first row contains the location of the QRS The
second row contains the value of RR for the corresponding QRS
%     %qrs_off: QRS Offsets (1xno_of_qrs)
%     %FS: Sampling Freq (Hz)
%     %blr: Baseline Removed Prefiltered Input ECG
%     %param: Parameters [Xi1 Xi2]
%           Optional: Default Value are [0.09 0.08]
%     T_on: T-wave Onsets (1xno_of_qrs)
%     T_off: T-wave Offsets
```

```
%      T: Location of the Fiducial Point (1 x number_of_qrs)
```

6.3.1.2 Results

The results of this algorithm in terms of T-wave detection and onset/offset calculation have not been formalized due to the immediate implementation of the DWT based approach described next, which gives a better subjective performance. However it has been found to give a very good performance on the QTDB which has been observed through visual inspection. The figure below shows some examples of QRS detection over the QTDB.

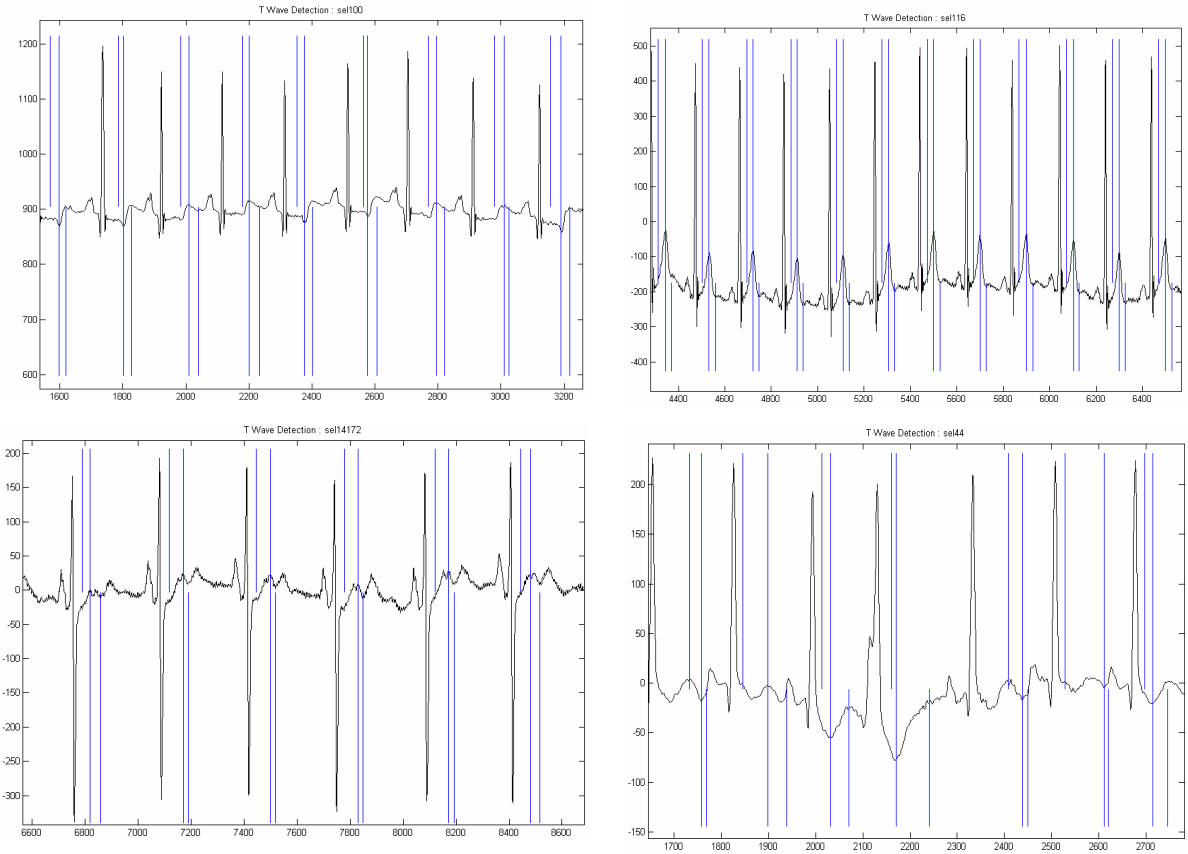

fig. 6-5 Some Examples of T-wave Detection on QTDB using Joen'g Differential Operator

6.3.1.3 Comments

This algorithm performs quite well in the detection and delineation of the T-wave. However, it currently gives no information about the morphology of the T-wave for which additional rules need to be added.

6.3.2 Use of DWT for T-wave detection

This method is based on the algorithm proposed by [14] and is quite similar to the QRS detection and delineation algorithm using DWT explained earlier in the previous chapter.

The process for multiscale T wave detection and delineation is as follows: first of all, we define a search window for each beat, relative to the QRS position and depending on a recursively computed RR interval. Within this window, we look for local maxima of $\left|W_{2^4}x[n]\right|$ obtained by applying the modified WT algorithm to the baseline removed ECG signal. If at least two of them exceed the threshold $\in_T$, a T-wave is considered to be present. In this case, the local maxima of WT with amplitude greater than γ_T are considered as significant slopes of the wave, and the zero crossings between them as the wave peaks. After this thresholding, morphological post processing is also carried out to remove spikes and to compute the T-wave region effectively. Depending on the number and polarity of the found maxima, we assign one out of six possible T wave morphologies: positive (+), negative (-), biphasic (+/- or -/+), only upwards, and only (figure below).

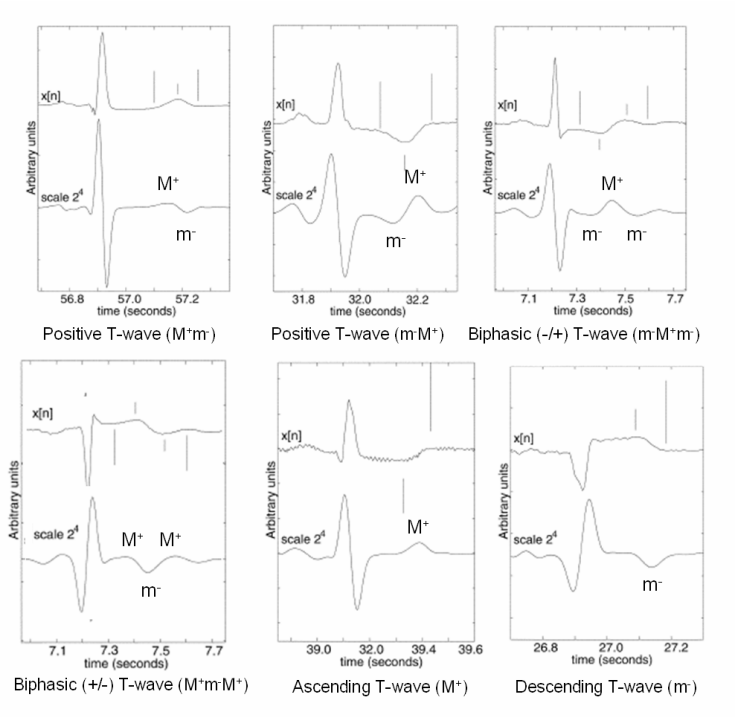

Fig. 6-6 Different T-wave Morphologies

To identify the wave limits, we used the same criteria as for QRS onset and end, with thresholds $\xi_{T_{ON}}$ and $\xi_{T_{END}}$ applied to scale 2^4. The thresholds are given as:

$$\begin{aligned} \in_T &= \chi_{1_T}\,\mathrm{RMS}\left(W_{2^4}x[n]\right) && \chi_{1_T} = 0.25 \\ \gamma_T &= \chi_{2_T}\max\left(\left|W_{2^4}x[n]\right|\right) && \chi_{2_T} = 0.125, n \in S_{W_T}\ (\text{T-wave search window}) \\ \xi_{T_{ON}} &= \chi_{3_T} W_{2^4}x\left[n_{first}\right] && \chi_{3_T} = 0.25 \\ \xi_{T_{end}} &= \chi_{4_T} W_{2^4}x\left[n_{last}\right] && \chi_{4_T} = 0.4 \end{aligned} \quad (6.6)$$

The RMS value above is calculated for each T-wave window

6.3.2.1 Function Reference

This algorithm is implemented in the Matlab-7 function file `DetectT_Del2.m`.

```
[T_s T_e]=DetectT_Del2(S,FS,RRI,qrs_s,qrs_e)
% Author Name: Fayyaz ul Amir Afsar Minhas
% Date: 25Sep05
% Description: T wave QRS Detection using the DWT
% Usage:
%     [T_s T_e]=DetectT_Del2(S,FS,RRI,qrs_s,qrs_e)
%     %S: Baseline Removed Prefiltered Input ECG
%     %FS: Sampling Freq (Hz)
%     %RRI: RR Intervals (2xn). n=number of QRS Complexes-1
%       The first row contains the location of the QRS
%           The second row contains the value of RR for the
corresponding QRS
%     %qrs_s: QRS Start (1xno_of_qrs)
%     %qrs_s: QRS End (1xno_of_qrs)
%     T_s: T-wave Onsets (1xno_of_qrs)
%     T_e: T-wave Offsets
%          All T_on,T_off and T vectors contain the location of
the corresponding siginifcant points adjacent to the related QRS
complexes. If no T-wave occurs adjacent to a complex the
corresponding entry in all these    vectors is zero.
% Internal Parameters:
%     T_Size=ceil(0.15*FS); %Approx Size of T Complex (Samples)
%          Min_T_Size=ceil(0.05*FS);  %Min  Size  of  T  Complex
(Samples)
%     Epsilon, kappa and T-wave window control parameters
```

6.3.2.2 Results

The figure below shows some examples of T-wave detection over the QTDB. The Mean error and the standard deviation in detecting the start of the T-wave using this algorithm are -0.4748 +/- 10.6 samples at 250Hz, for the QTDB. This corresponds to an error of 0ms +/- 42ms. The mean value of the absolute error is 7.2 samples (29ms).

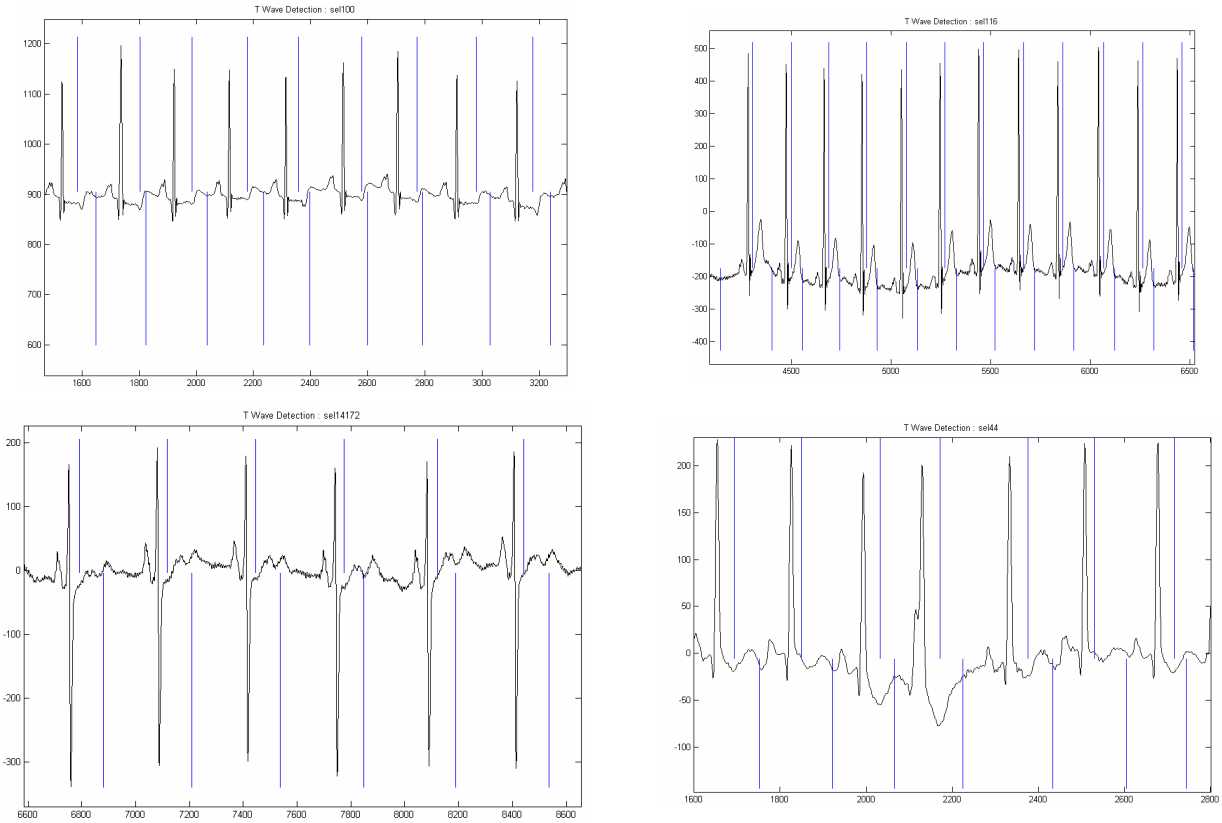

fig. 6-7 Some Examples of T-wave Detection using DWT

6.4 Implemented Schemes for P Wave Detection

The same methods used for T-wave detection can also be used for the detection of the P-waves. The search window for the P-wave in both the algorithms is taken as the TQ segment after a T-wave.

6.4.1 Use of DWT for P-wave Detection

The P-wave has the following morphologies, which can be detected using this algorithm positive (+), negative (-), and biphasic (+/-, -/+). The thresholds used are given below and they need to be optimized.

$$\begin{aligned}
&\epsilon_P = \chi_{1_P}\,\mathrm{RMS}\left(W_{2^4}x[n]\right) && \chi_{1_P} = 0.02 \\
&\gamma_P = \chi_{2_P}\max\left(\left|W_{2^4}x[n]\right|\right) && \chi_{2_P} = 0.125, n \in S_{W_P}\,(\text{P-wave search window}) \\
&\xi_{P_{ON}} = \chi_{3_P} W_{2^4}x\left[n_{first}\right] && \chi_{3_P} = 0.5 \\
&\xi_{P_{end}} = \chi_{4_P} W_{2^4}x\left[n_{last}\right] && \chi_{4_P} = 0.9
\end{aligned} \tag{6.7}$$

6.4.1.1 Function Reference

This algorithm is implemented in the Matlab-7 function file `DetectP_Del2`.

```
[P_s P_e]=DetectP_Del2(S,FS,RRI,qrs_s,qrs_e,T_off)
% Author Name: Fayyaz ul Amir Afsar Minhas
% Date: 25Sep05
% Description: P-wave Detection using the DWT
% Usage:
%     [P_s P_e]=DetectP_Del2(S,FS,RRI,qrs_s,qrs_e,T_off)
%     %S: Baseline Removed Prefiltered Input ECG
%     %FS: Sampling Freq (Hz)
%     %RRI: RR Intervals (2xn). n=number of QRS Complexes-1
%       The first row contains the location of the QRS
%           The second row contains the value of RR for the
corresponding QRS
%     %qrs_s: QRS Start (1xno_of_qrs)
%     %qrs_e: QRS End (1xno_of_qrs)
%     T_off: T-wave Offsets
%     %P_s: QRS Start (1xno_of_qrs)
%     %P_e: QRS End (1xno_of_qrs)
%           All P_s,P_e vectors contain the location of the
corresponding
%    siginifcant points adjacent to the related QRS complexes.
If no P-wave
%   occurs adjacent to a complex the corresponding entry in all
these
%   vectors is zero.
% Internal Parameters:
%     T_Size=ceil(0.15*FS); %Approx Size of P wave (Samples)
%     Min_T_Size=ceil(0.05*FS); %Min Size of P wave (Samples)
%     Epsilon, kappa and P-wave window control parameters
```

6.4.1.2 Results

The results of this algorithm in terms of P-wave detection and onset/offset calculation have not been formalized yet. However it has been found to give a satisfactory performance on the QTDB which has been observed through visual inspection. The figure below shows some examples of P-wave QRS detection over the QTDB.

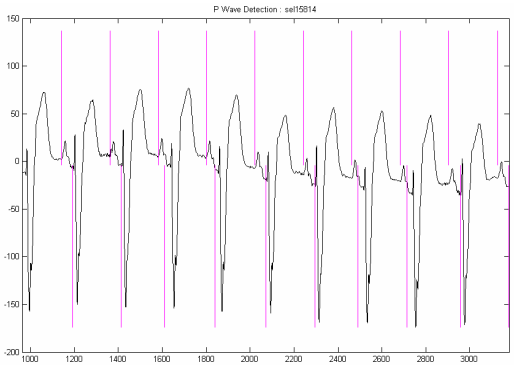

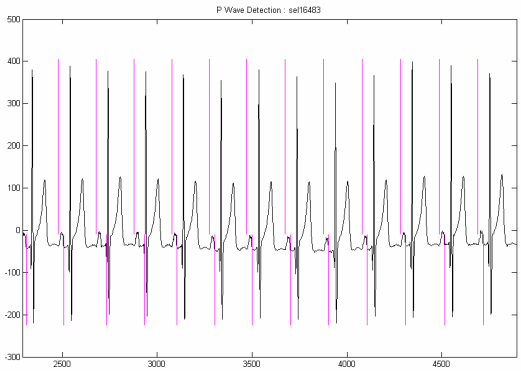

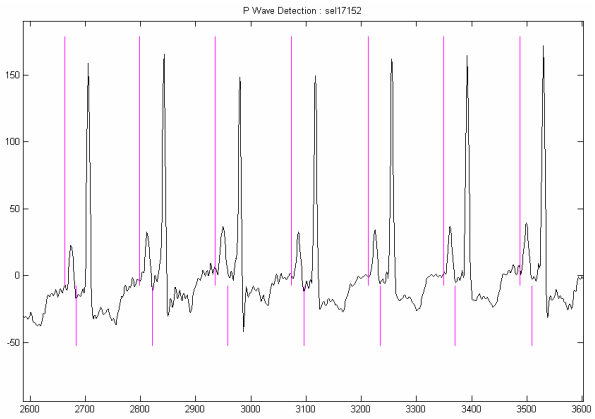

fig. 6-8 Some Examples of P-wave Detection

6.4.2 Problems in P-wave Detection

Currently none of algorithms implemented address the issue of isolated and multiple P-waves (which may occur in heart blocks).

6.5 Future Directions on P/T Detection

In order to make the detection of the P and T waves reliable, it is hereby proposed that the annotations in the QTDB for P/T waves be used along with the RR data for the corresponding beats to develop a rule for determining the start and endpoints of the windows for T and P waves in reference to the QRS end based on the RR interval employing clustering techniques.

CHAPTER 7
BEAT CLASSIFICATION

In this chapter we present the implemented techniques for the classification of different types of beats in the ECG. This component is of vital importance in the design and implementation of a practical Disease Classification System. This chapter presents the objectives and significance of beat classification and arrhythmia detection. A short review of different types of beats and arrhythmias is also given followed by a literature survey of techniques in use for detecting cardiac arrhythmias and beat classification. A description of the techniques implemented for beat classification is rendered along with the results.

7.1 Objectives and Significance of Beat Classification

Arrhythmias in the heart stem from irregular pacing in the heart due to improper electrical activity in the heart. As has been explained in chapter-2 the pacing of the heart is due to the electrical activity generated by the pacemaker sites (SA node under normal conditions) in the heart which regulate the rate at which the heart beats and the cardiac output. Any discrepancy in the pacemaker sites or any conduction blockage may cause arrhythmias which may or may not be life threatening.

Though some of the cardiac arrhythmias are mostly benign but they may also reflect the presence and/or after-effects of certain types of cardiac abnormalities. Therefore the detection of irregular beats resulting from arrhythmias is of prime importance to ensure proper diagnosis of cardiac abnormalities.

7.2 Types of Beats/Arrhythmias

In this section we describe different types of cardiac arrhythmias along with a brief description of their causes and effects on the ECG which can be used for their diagnosis. Some common types of heart rhythms are listed below.

7.2.1 Normal Sinus Rhythm (NSR)

During normal operation of the heart, the SA node acts as the trigger for the electric impulse that spreads across the heart. NSR is characterized by:

- Regular and Upright P-waves in leads II, III and aVF
- Heart rate of 60-100bpm

The ECG reflecting NSR is shown below.

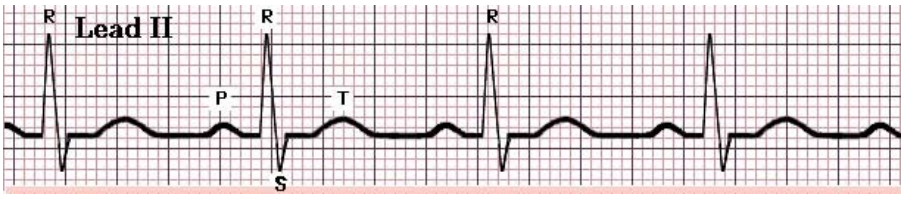

fig. 7-1 NSR with heart rate of 85bpm

7.2.2 Respiratory Sinus Arrhythmia (RSA)

Sinus arrhythmia is the mild acceleration followed by slowing of the normal rhythm that occurs with breathing as show below.

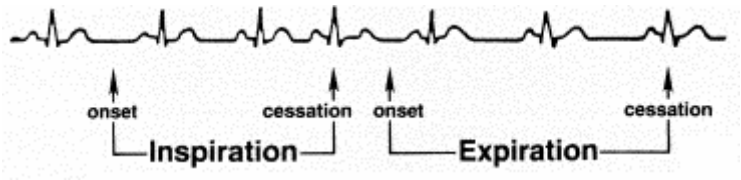

fig. 7-2 RSA

7.2.3 Sinus Tachycardia

A heart rate faster than 100bpm is considered a tachycardia. This number varies with age, as the heartbeat of a younger person is naturally faster than that of an older person's. With exercise the sinus node increases its rate of electrical activity to accelerate the heart rate. The normal fast rate that develops is called sinus tachycardia.

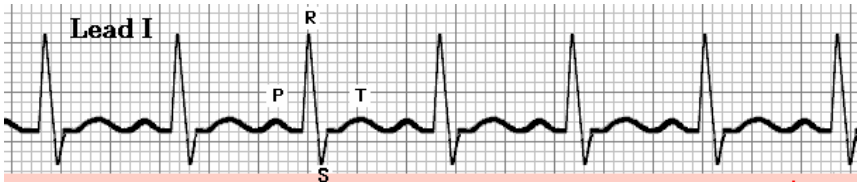

fig. 7-3 Sinus Tachycardia with a heart rate of 111bpm

7.2.4 Sinus Bradycardia

If the heart rate is less than 60bpm, Bradycardia is said to be present. This may be caused by increased vagal or parasympathetic tone or occur in the acute stages of myocardial infarction.

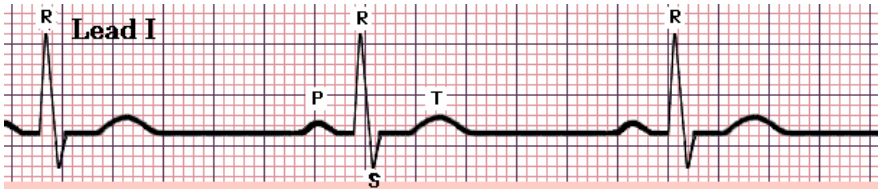

fig. 7-4 Sinus Bradycardia with a heart rate of 48bpm

7.2.5 Atrial Rhythms

Atrial rhythms result from irregular electrical activity in the atria of the heart. Some of these are described below.

i. Premature Atrial Contractions (PACs)

PACs are a type of arrhythmia which starts in the upper two chambers of the heart, also called atria. These aren't serious, and they frequently go away on their own. They are produced when an Atrial focus develops and fires before sinus beat is expected as shown below. This causes the P-wave to have a contour slightly different from sinus beats and the PR interval is prolonged. The QRS complex is narrow (<0.10s) and is similar to normal beats except for the timing.

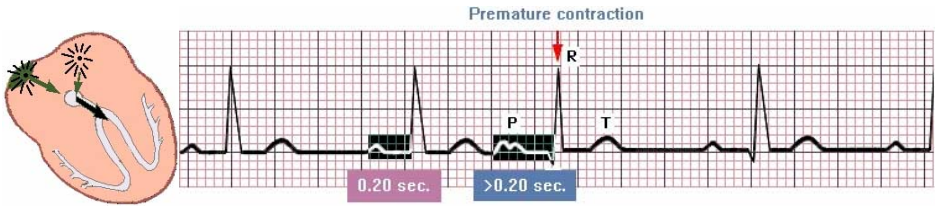

fig. 7-5 PAC

ii. Wandering Atrial Pacemaker (WAP)

If the contour or the shape of the P-waves in the ECG changes from beat to beat in a single lead often in association with variations in PP, PR and RR intervals it means that the site of Atrial depolarization is changing and the situation is termed as WAP.

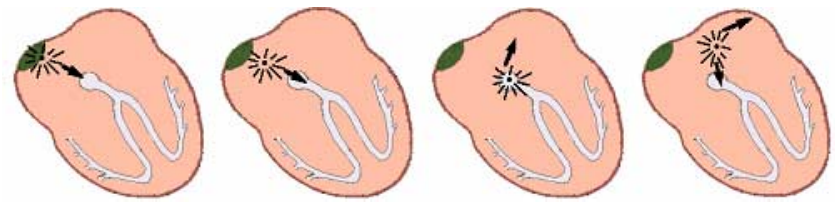

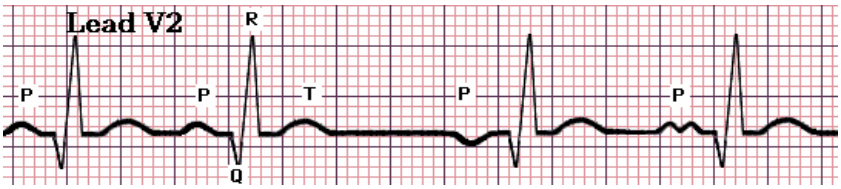

fig. 7-6 WAP

iii. Multifocal Atrial tachycardia (MAT)

During MAT, impulses generate irregularly and rapidly at different points in atria causing P-wave contours, PR intervals, PP and thus RR intervals all to vary. It is usually associated with severe pulmonary disease.

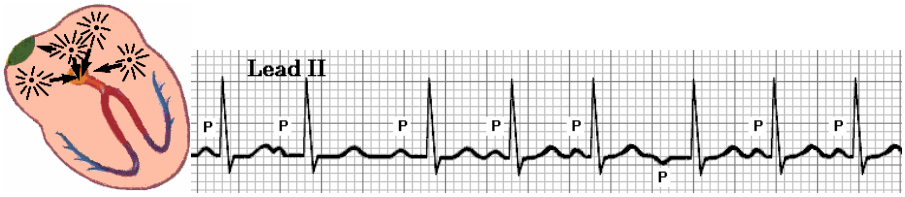

fig. 7-7 MAT

iv. Paroxysmal Supraventricular/Atrial tachycardia (SVT/PAT)

SVT or PAT results from impulses that recycle repeatedly in and near AV node due to slowing in area of unidirectional block with an atrial rate of 160-220 per minute. This is caused by the presence of a unidirectional blockage in the AV node. P waves are often regular and inverted with a QRS complex that can either be regular or irregular.

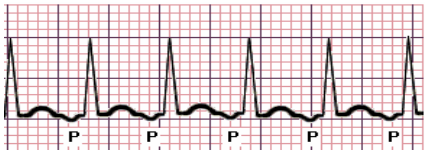

fig. 7-8 SVT

v. Atrial flutter

During atrial flutter impulse travels in a circular course in the atria, setting up a regular, rapid (200-300 per minute) flutter (F) waves without any isoelectric baseline. It is caused by the presence of some degree of AV block.

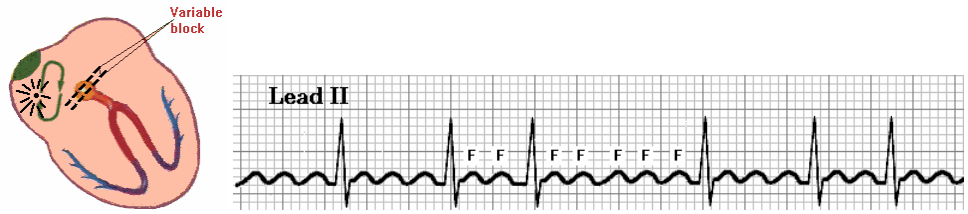

fig. 7-9 Atrial Flutter

vi. Atrial fibrillation (Afib)

During Atrial Fibrillation impulses take chaotic, random pathways in the atria, resulting in no organized electrical activity and no pumping action in the atria. The baseline in the ECG with Afib is coarsely or finely irregular with irregular QRS complexes and no P-waves.

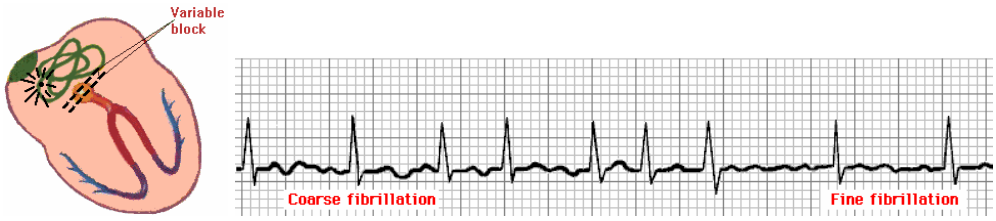

fig. 7-10 Atrial Fibrillation

7.2.6 Ventricular Rhythms

i. Premature Ventricular Contractions (PVC)

PVC is caused generation of an electric impulse within the ventricles before the sinus beat is expected. There is no P-wave associated with it and the QRS complex is wider than normal.

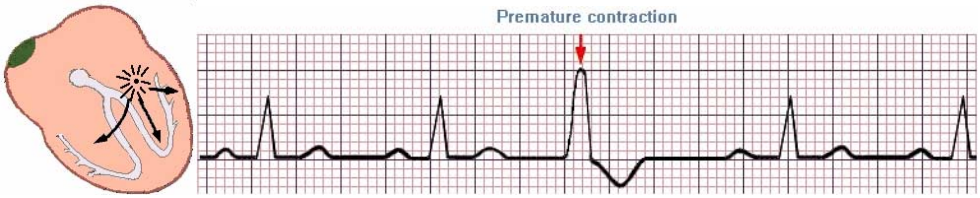

fig. 7-11 PVC

ii. Accelerated idioventricular rhythm (AIVR)

AIVR is characterized by wide QRS complexes (>0.1s) and an absence of normal, upright P-waves related to QRS complexes. It is usually asymptomatic and with no progression to VT or Vfib.

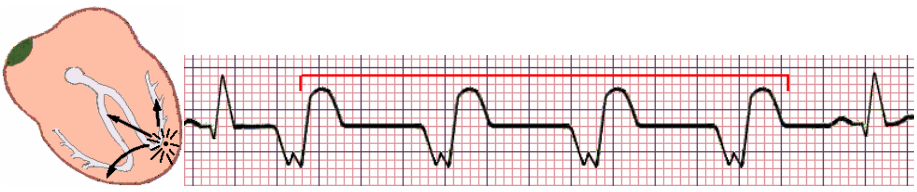

fig. 7-12 AIVR

iii. Ventricular tachycardia (VT)

VT is characterized by Wide QRS complexes (>0.10s), no P-wave and a high heart rate. A possible cause of VT is Myocardial Infarction as slowed conduction in the

margin of ischemic area permits circular course of impulse and reentry with repetitive depolarization.

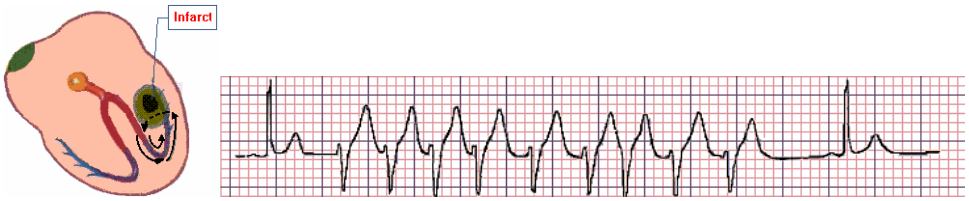

fig. 7-13 VT

iv. Ventricular fibrillation (Vfib)

Vfib may be associated with either coarse or fine chaotic modulations of the ECG baseline, but no true QRS complexes and indeterminate heart rate.

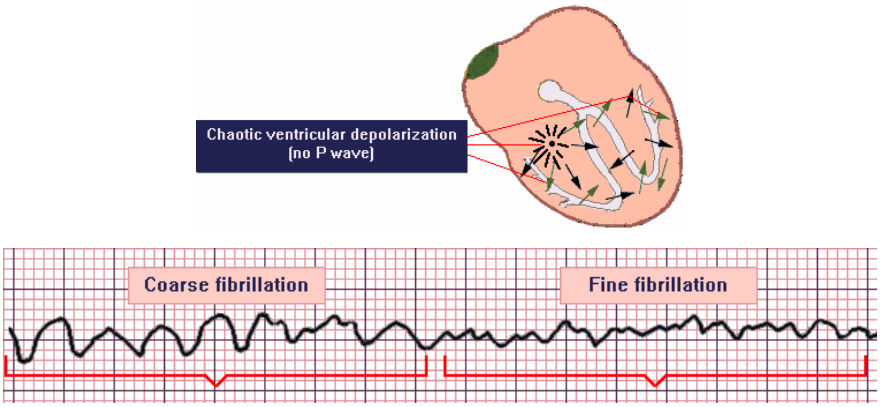

fig. 7-14 Vfib

v. Paced Rhythm

Paced rhythm is caused by an artifical pacemaker which sends out an impulse into the ventricles of the heart. It is characterized by wide QRS complexes and no P-wave.

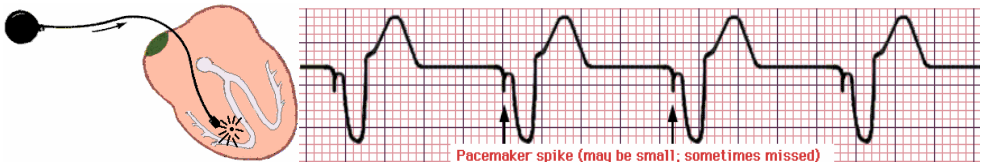

fig. 7-15 Paced Rhythm

7.2.7 Wolff-Parkinson-White (Pre-excitation) syndrome

In this syndrome impulses originating at the SA node preexcite the peripheral conduction system and ventricular muscle via bundle of Kent without delay at the AV node, thus producing an early slurred upstroke (the delta wave) of the QRS Complex. Impulses can also pass via posterior accessory bundle. QRS is prolonged as the impulse after delay through the AV node also arrives.

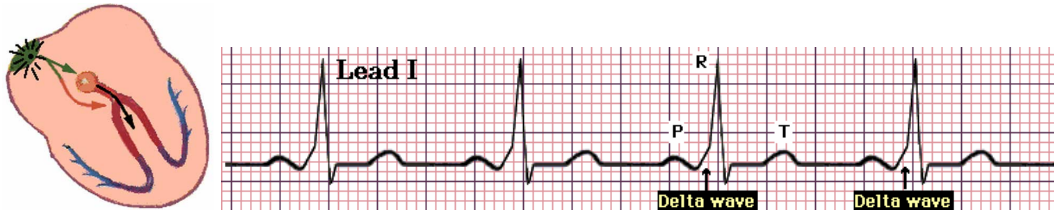

fig. 7-16 WPW Syndrome

7.2.8 Junctional rhythm

In junctional rhythm impulses originate in the AV-Node with retrograde and antegrade transmission. P-waves are often inverted and may be buried in QRS or follow narrower than normal QRS complexes at slow heart rates.

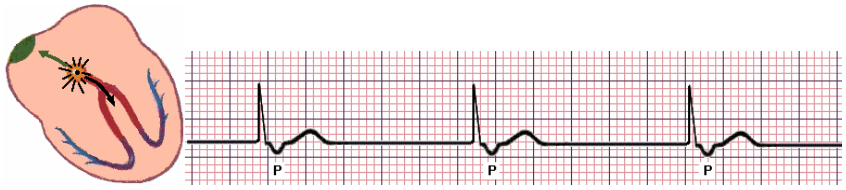

fig. 7-17 Junctional Rhythm

7.2.9 Escape Beats

Escape beats result when an electric impulse is not produced or not conducted from the SA node.

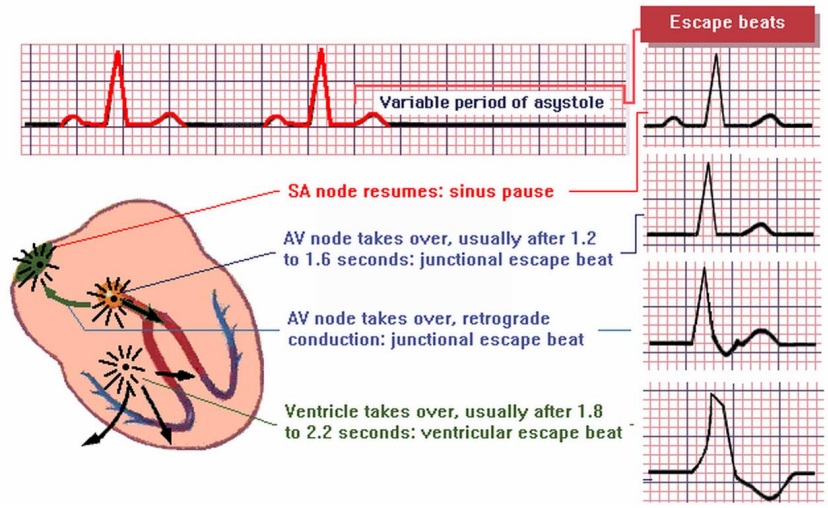

fig. 7-18 Escape Beats

7.2.10 Bundle Branch Blocks (BBB)

BBB results from a blockage in the path of the electrical activity as it passes through the Bundle Branch. There are two types of BBB:

i. Left BBB (LBBB)

LBBB is caused by a block of the left anterior or posterior fascicles or the left main bundle branch. It causes ST depression in leads I, aVL, V5 and V6 while producing wide QRS complexes (>0.12s).

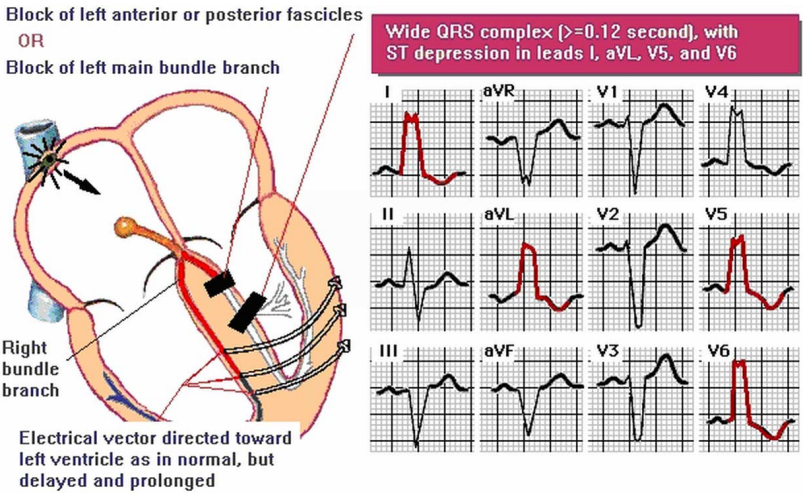

fig. 7-19 LBBB

ii. Right BBB (RBBB)

RBBB is caused by a blockage in the right bundle branch and it causes QRS to be prolonged (>0.12s), terminal broad S wave in lead I and RSR' complex in lead V1.

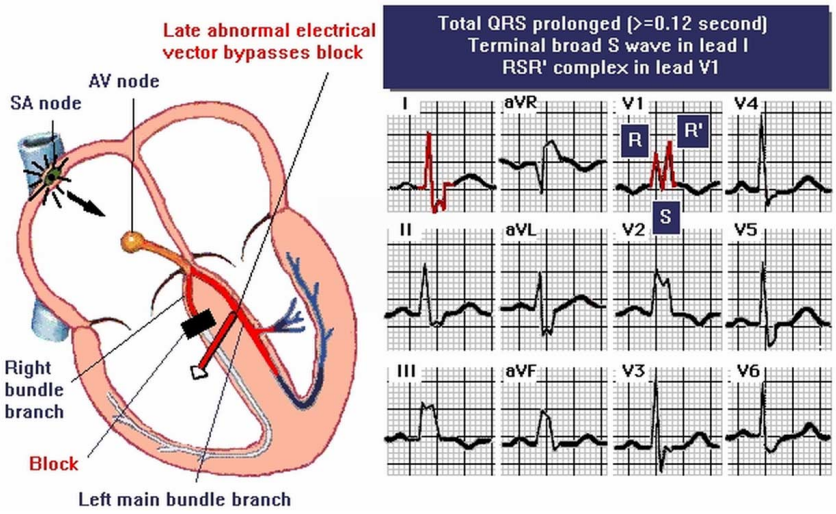

fig. 7-20 RBBB

7.2.11 Other Types

Other types include (heart) AV blocks, Junctional premature beats etc.

7.3 Literature Review

Major difficulties in the classification of cardiac rhythms include the presence of noise in the ECG signal and the large variations within each rhythm class due to person specific parameters in case of some of the rhythms.

Many researches have been conducted to explore effective signal analysis techniques for the classification of cardiac rhythms. There are primarily two components of such a computer aided diagnosis system i.e. Feature Extraction and Classification. A variety of feature extraction techniques exist in the literature for beat classification which can broadly be classified in terms of Time Domain Features, Frequency Domain Features, Time-Frequency (Wavelet) and Filter Banks, Blind Source Separation (BSS) and Independent Component Analysis, Higher Order Statistics, Hermite Basis, Phase Space Reconstruction and nonlinear dynamical modeling etc. For the purpose of classification efforts have been devoted to the development of classifier for these feature sets including Linear Discrimination, Neural Networks, Support Vector Machines, Fuzzy and Neuro-Fuzzy Expert Systems and Ensemble based Techniques. In this section we present a short review of some of the different methodologies in the literature for the purpose of beat classification in the ECG. However a discrete comparison of different techniques in the literature is not possible to the variations in the types of cardiac rhythms considered and the evaluation of the presented techniques on different number of subjects from different datasets.

Moraes et al. [55] have proposed an unsupervised method for the classification of different type of QRS Complexes through the extraction of 4 time domain features, i.e. width, total sum of areas under the positive and negative curves, total sum of the absolute value of the sample variations and total amplitude. These features are classified with the use of a Mahalanobis distance based classifier which calculates the distance Mahalanobis distance between its feature set and centroids of all existing classes to determine the class label. A new class is added if this distance exceeds a predefined distance threshold. This method achieves a Sensitivity (Se) /Positive Predictivity Value (PPV) of 90.74%/96.55%. Another time domain based technique for the classification of cardiac rhythms has been presented by De Chazal et al. [56] which is aimed at the classification of Normal, PVC and Fusion Beats. This method uses a variety of features derived from the RR interval and the presence, interval,

magnitude and area of P, QRS complex and T-waves of both leads in recordings of the MITBIH Database [3] for a single beat. These features are classified using Linear Discriminants and Neural Networks with an accuracy of 89.1%. Time domain features, although simple to calculate suffer from the presence of noise and errors in determining the onset and offset of the QRS complex which need to be approximated based on the location of the R-wave. Moreover these features may not be able to provide very good seperability among different types of QRS complexes due to the presence of large within-class variations.

Minami et al. [57] have proposed the use of Fourier Transform (FT) based Frequency Domain techniques for the classification of Supraventricular Rhythm, Ventricular Rhythm including VT and PVC, and Vfib. A QRS complex window of length 256ms of each beat is Fourier transformed and its power spectrum is computed after the application of hamming window to suppress discontinuities due to the adjacent T-wave and P-wave. Five spectral components with central frequencies of 3.9, 7.8, 11.7, 15.6 and 19.5Hz (shown below for different rhythms) were fed into a Neural Network Classifier. This method achieves a Se/PPV of ~98%.

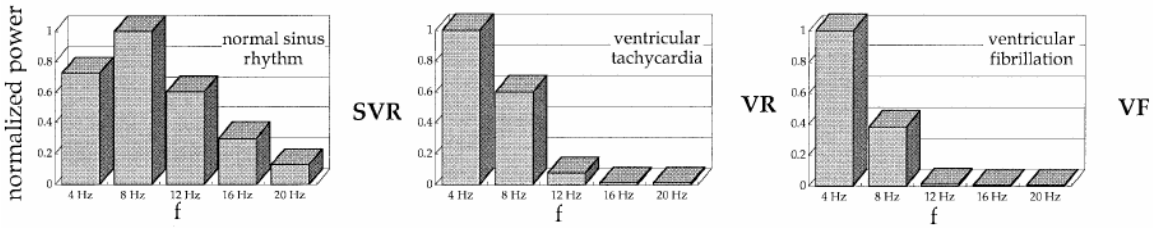

fig. 7-21 Using Fourier Transform Based Features for Classification

A related technique is the use of filter banks for the classification of QRS complexes as given by Alfonso et al. [58]. Frequency based techniques for the classification of cardiac rhythms offer more promising prospects as they are more robust to noise in comparison to time domain techniques and present a more effective model of the QRS complex. However, the use of time-frequency decomposition of the ECG signal using the wavelet transform offers a better alternative than the application of Fourier transform for beat classification due to the non-stationary nature of the ECG signal. A comparative study involving the use of Fourier Transform and the Wavelet Transform (WT) has been carried out by Dokur et al. [59] which demonstrates the efficacy of the use of WT as it provides a higher classification accuracy for ten types of beats from the MIT-BIH database in comparison to FT. Another method that uses the wavelet transform for beat classification is given by Al-Fahoum et al. [60] which extracts six

energy descriptors from the wavelet coefficients over a single beat interval from the ECG signal. These features are classified using a Radial Basis Function (RBF) Neural Network. This method achieves an accuracy of 97.5% with the use of Daubechies wavelet transform. Another method utilizing the wavelet transform for the detection of Vfib has been proposed by Addison et al. [61]. Another approach employing Wavelet Transform for Beat Classification has been formulated by Prasad et al. [62] which uses sym6 wavelets for classifying 12 different types of beats in the MIT-BIH database with a reported accuracy of 96.77% through a Neural Network Classifier. Inan et al. [63] have presented a method for the classification of PVCs using wavelet transform coupled with a neural network classifier achieving an accuracy of over 95% on 40 files of the MIT-BIH. Yu et al. [64] have presented a beat classification technique that extracts features from the wavelet decomposition sub-bands and applies a probabilistic neural network for classification of 6 types of beats from the MIT-BIH achieving accuracy greater than 99%. Enign [65] has used autoregressive (AR) model coefficients; higher-order cumulant and wavelet transform variances as features with a neuro-fuzzy classifier achieving an accuracy of 98% while classifying 4 types of beats over the MIT-BIH database. Güler et al. [66] have proposed a mixture of experts approach to discriminate five different types of beats employing wavelet transform coefficients and lyapunov exponents of the ECG as features and have achieved an accuracy of ~98%. Another technique proposed by Güler et al. [67] uses statistical features such as mean of the absolute values of the coefficients in each sub-band, Average power of the wavelet coefficients in each sub-band, standard deviation of the coefficients in each sub-band and the ratio of the absolute mean values of adjacent sub-bands extracted from the Wavelet Decomposition of the ECG signal with a cascaded neural network architecture for classification. This method has achieved an accuracy of ~97% in classifying four types of ECG beats (Normal, Congestive Heart Failure, VT, Afib) from the MIT-BIH database. Exarchos et al. [68] have utilized a rule mining approach for the classification of heart rhythms by developing a fuzzy inference system with an accuracy of 96% in discriminating 4 types of beats (VF, PVC, 2^{nd} degree heart block, and normal) in the MIT-BIH utilizing time domain features for each beat. This method provides a promising classifying technique as it removes a discrepancy of the neural network approaches by providing an easy to understand rule base for classification and has the potential to be extended further through the combination of frequency or wavelet domain features

and lead specific rules. A method based on the use of independent component analysis (ICA) has been proposed by Yu et al. [69] which uses 27 features for the classification of 6 types of beats over the MIT-BIH database with an accuracy of over 99%. ICA also presents an effective approach to the classification of cardiac rhythms as it separates out different basic components of the rhythms of the heart which can then be classified and discriminated to recognize these rhythms.

In this work, we have implemented the approach given by Yu et al. [64] as it provides an efficient and simple technique for classification of 6 types of beats in the ECG using features derived from the wavelet transform. This technique is described in the next section.

7.4 Implemented Technique

The adopted technique is able to classify the input beats into one of the six classes, i.e., Normal (N), Left Bundle Branch Block (LBBB), Right Bundle Branch Block (RBBB), Premature Ventricular Contraction (PVC), Atrial Premature Beat (APB) and Paced Beat (PB). For the purpose of this study 23 ECG records were selected from the MIT-BIH database for analysis and recognition. For the purpose of conformity, signals recorded with the MLII lead were used. The originality of the ECG beats is listed in the table below.

Table 7-1 The Data Set Used for Beat Classification

Type	MIT/BIH file	Training (#/file)	Testing (#/file)
N	103, 113, 115, 123, 220, 234	600	600
LBBB	109, 111, 207, 214	600	600
RBBB	118, 124, 212, 231	600	600
PVC	119	200	200
	221	150	150
	200, 233	400	400
APB	209	150	150
	222	100	100
	232	600	600
PB	107, 217	600	600
Total		11600	11600

The steps involved in this technique are shown below:

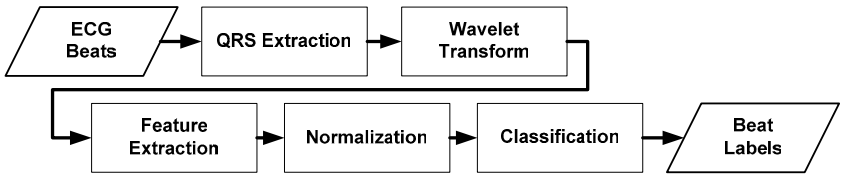

fig. 7-22 Steps Involved in DWT Based Beat Classification

Each of these steps is explained in detail below.

7.4.1 QRS Segmentation

Since the QRS complex is one of the most important ECG components in the sense that it is associated with electrical ventricular activation, QRS complexes were extracted. Based on the R-peak position identified in the associated MIT-BIH database annotation file, 64 point QRS segments centered at R-peaks were extracted from the record. The R-peak was taken to be the center of the 64 point window. The DC value of each 64 point ST-segment is removed.

7.4.2 Wavelet Transform

Due to the short length of the QRS segments, only two-level DWT is used with the haar wavelet. The two-level DWT (shown below) decomposes each QRS signal into three sets of wavelet coefficients, D_1, D_2 and A_2. These sets of coefficients are shown in the figure below.

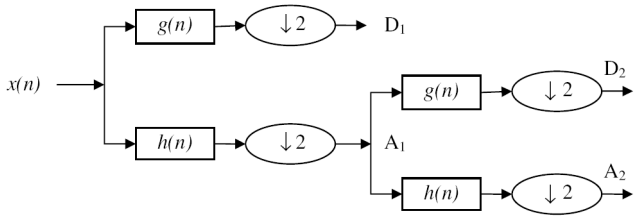

fig. 7-23 Mallat's Algortihm for DWT

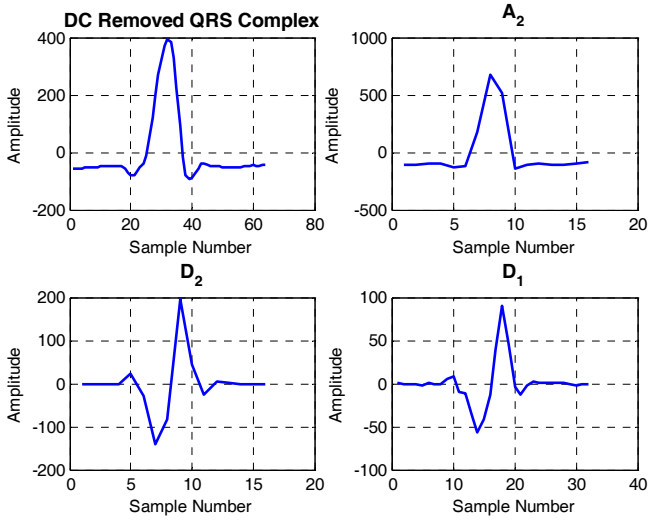

fig. 7-24 Wavelet Decomposition of an ECG Signal

7.4.3 Feature Extraction

Next, statistical features are extracted from the wavelet coefficients computed earlier. These features are divided into two feature sets FS1 and FS2. FS1 comprises of the following:

AC power of the original signal, i.e. variance of the original QRS complex signal denoted by σ_S^2. This feature measures the power in the original QRS complex signal.

AC power of the wavelet coefficients in each sub-band denoted by $\sigma_{A2}^2, \sigma_{D2}^2$ and σ_{D1}^2. This feature measures the power in each of the sub-bands.

AC power of the autocorrelation function of the wavelet coefficients in each sub-band denoted by $\sigma_{R(A2)}^2, \sigma_{R(D2)}^2$ and $\sigma_{R(D1)}^2$. This is a measure of the coherence in the sub-bands.

Ratio of the minimum to the maximum of the wavelet coefficient in each sub-band denoted by r_{A2}, r_{D2} and r_{D1}. These features represent the morphological characteristics of the sub-band coefficients.

The AC power of a signal, *x* with length *N,* is calculated by finding its variance as follows,

$$\sigma_x^2 = \frac{1}{N}\sum_{n=1}^{N}\left[x(n) - \bar{x}\right]^2 \tag{7.1}$$

The autocorrelation function is considered to be a measure of similarity between a signal $x(n)$ and its shifted version. Mathematically,

$$R_{xx}(l) = \sum_{n=i}^{N-|k|-1} x(n)x(n-l) \tag{7.2}$$

Where *l* is the time shift index, *i=l, k=0* for $l \geq 0$ and *i=0, k=l* for $l \leq 0$. The AC power of the autocorrelation function is calculated by determining the variance of the autocorrelation function.

The ratio of the minimum to the maximum value of a signal is given by,

$$r_x = \frac{\min\left(x(n)\right)}{\max\left(x(n)\right)} \tag{7.3}$$

These features are computed for each of the sub-band or the original signal as described earlier to form FS1, which for a single QRS complex can be expressed as, $\left\{\sigma_S^2, \sigma_{A2}^2, \sigma_{R(A2)}^2, r_{A2}, \sigma_{D2}^2, \sigma_{R(D2)}^2, r_{D2}, \sigma_{D1}^2, \sigma_{R(D1)}^2, r_{D1}\right\}$. FS2 combines all features in FS1

(explained above) and the instantaneous RR interval. Thus FS2 is given by the set $\left\{\sigma_S^2, \sigma_{A2}^2, \sigma_{R(A2)}^2, r_{A2}, \sigma_{D2}^2, \sigma_{R(D2)}^2, r_{D2}, \sigma_{D1}^2, \sigma_{R(D1)}^2, r_{D1}, RR\right\}$.

7.4.4 Normalization

As the quantities of the features can be quite different, a normalization process is necessary to standardize all the features to the same level. The relation used for normalization is defined as follows:

$$x_{ij}^{'} = \text{tansig}\left(\frac{x_{ij} - \overline{x}_j}{\sigma_{x_j}}\right) \tag{7.4}$$

where x_{ij} is the j^{th} component of the i^{th} feature vector, with $\overline{x}_j$ and σ_{x_j} being the mean and variance of the the j^{th} component of the i^{th} feature vector computed over the training set and used throughout the computation. The application of the tangent sigmoid function normalizes the range of features to [-1, 1]. The normalized features for some selected beats of different types are shown in the figure below.

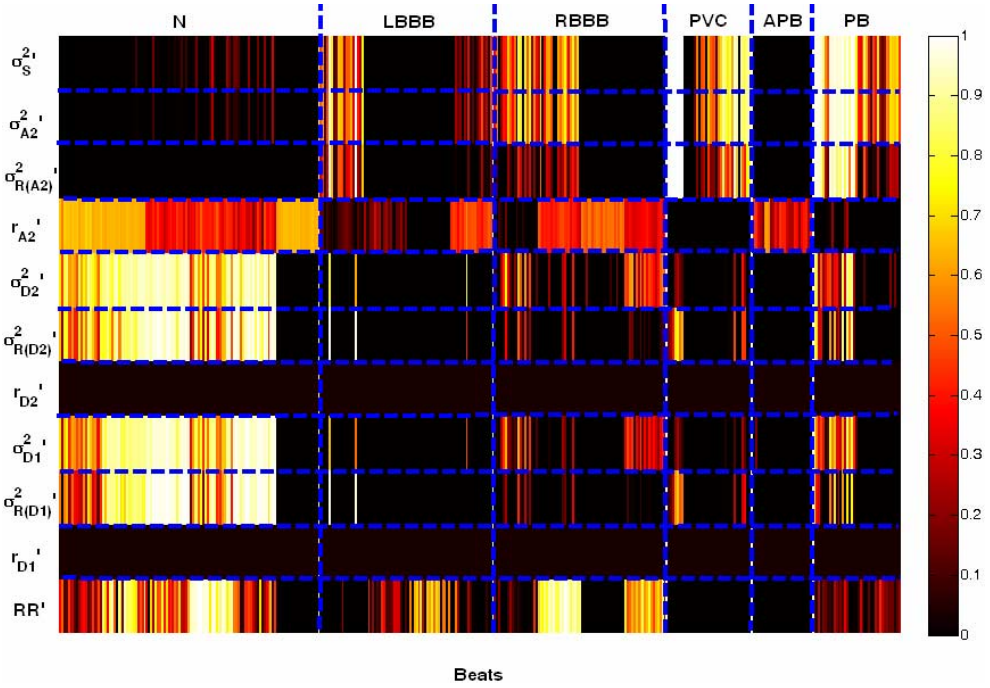

fig. 7-25 Normalized Features for Selected Beats of Different Types

7.4.5 Classification

For the purpose of classification the following classifiers were used:

i. LVQ Neural Network

The LVQ neural network was used with 200 hidden neurons.

ii. Probabilistic Neural Network (PNN)

PNN with smoothing factors of 0.1 and 0.02 was used.

iii. *k*-Nearest Neighbor Classifier (*k*-NN)

k-NN with *k=1* was used.

The performance of these classifiers was evaluated using both the feature sets, FS1 and FS2.

7.5 Results and Discussion

Below we present the results of beat classification with both FS1 and FS2 through LVQ, PNN and *k*-NN classifiers. This clearly demonstrates the effectiveness of using RR interval features in beat classification. The best reported results are a classification accuracy of 99.65% with FS2 using PNN (smoothing factor of 0.1). The best results that we have obtained through our implementation exhibit a beat classification accuracy of 99.1% with FS2 with *k*-NN classifier (k=1).

Table 7-2 Result with FS1 using LVQ

LVQ (Training Beats: 1450, Testing Beats: 11600) using Fs1 with 200 hidden neurons						
Beat Types	**N**	**LBBB**	**RBBB**	**PVC**	**PAC**	**PB**
N	2794	44	585	0	190	0
LBBB	1	1753	37	83	528	1
RBBB	61	230	2042	0	42	40
PVC	0	364	39	561	31	204
PAC	0	2	123	0	688	0
PB	5	139	77	77	0	859
Accuracy (%)	**97.6582**	**69.2338**	**70.3410**	**77.8086**	**46.5179**	**77.8080**
Net Accuracy (%)	**74.9741**					

Table 7-3 Result with FS1 using PNN

PNN (Training Beats: 1933, Testing Beats: 11600) using Fs1 with Smoothing factor = 0.02						
Beat Types	**N**	**LBBB**	**RBBB**	**PVC**	**PAC**	**PB**
N	3568	0	13	0	16	0
LBBB	3	2286	31	29	25	1
RBBB	2	24	2342	6	9	2
PVC	8	63	22	1031	2	22
PAC	1	14	18	1	815	0
PB	0	3	27	19	0	1197
Accuracy (%)	**99.6092**	**95.6485**	**95.4749**	**94.9355**	**94.0023**	**97.9542**
Net Accuracy (%)	**96.8879**					

Table 7-4 Result with FS1 using k-NN

k-NN (Training Beats: 11600, Testing Beats: 11600) using Fs1 with k = 1						
Beat Types	**N**	**LBBB**	**RBBB**	**PVC**	**PAC**	**PB**
N	3611	0	8	0	9	0
LBBB	1	2326	15	28	28	4
RBBB	6	7	2384	5	4	1
PVC	0	32	12	1052	0	11
PAC	3	17	13	3	761	0
PB	0	5	4	11	0	1239
Accuracy (%)	**99.7238**	**97.4445**	**97.8654**	**95.7234**	**94.8878**	**98.7251**
Net Accuracy (%)	**98.0431**					

Table 7-5 Result with FS2 using LVQ

LVq (Training Beats: 1450, Testing Beats: 11600) using Fs2 with 200 hidden neurons						
Beat Types	**N**	**LBBB**	**RBBB**	**PVC**	**PAC**	**PB**
N	2848	11	560	0	252	0
LBBB	1	2107	116	7	146	34
RBBB	57	43	2223	0	78	13
PVC	0	131	11	858	128	2
PAC	0	2	122	0	667	0
PB	4	183	69	9	0	918
Accuracy (%)	**97.8694**	**85.0626**	**71.6866**	**98.1693**	**52.4784**	**94.9328**
Net Accuracy (%)	**82.9397**					

Table 7-6 Result with FS2 using PNN (spread = 0.1)

PNN (Training Beats: 1450, Testing Beats: 11600) using Fs2 with Smoothing factor = 0.1						
Beat Types	**N**	**LBBB**	**RBBB**	**PVC**	**PAC**	**PB**
N	3580	2	27	0	9	0
LBBB	8	2298	34	20	11	5
RBBB	36	17	2349	1	11	9
PVC	0	15	2	1121	5	2
PAC	0	3	5	1	848	0
PB	0	1	15	10	0	1155
Accuracy (%)	**98.7859**	**98.3733**	**96.5872**	**97.2246**	**95.9276**	**98.6336**
Net Accuracy (%)	**97.8534**					

Table 7-7 Result with FS2 using PNN (spread = 0.02)

PNN (Training Beats: 1450, Testing Beats: 11600) using Fs2 with Smoothing factor = 0.02						
Beat Types	**N**	**LBBB**	**RBBB**	**PVC**	**PAC**	**PB**
N	3546	0	18	0	11	0
LBBB	11	2308	37	34	13	2
RBBB	9	19	2359	1	8	4
PVC	8	14	3	1150	0	4
PAC	2	4	3	10	850	0
PB	0	6	15	12	0	1139
Accuracy (%)	**99.1611**	**98.1710**	**96.8789**	**95.2775**	**96.3719**	**99.1297**
Net Accuracy (%)	**97.8621**					

Table 7-8 Result with FS2 using k-NN (Best Results)

k-NN (Training Beats: 11600, Testing Beats: 11600) using Fs2 with k = 1						
Beat Types	**N**	**LBBB**	**RBBB**	**PVC**	**PAC**	**PB**
N	3538	0	13	0	2	0
LBBB	0	2404	18	18	4	3
RBBB	2	9	2390	0	3	1
PVC	0	10	3	1129	1	0
PAC	1	4	1	0	838	0
PB	0	1	2	8	0	1197
Accuracy (%)	**99.9153**	**99.0115**	**98.4755**	**97.7489**	**98.8208**	**99.6669**
Net Accuracy (%)			***99.1034***			

7.6 Evaluation Using DFT

In order to illustrate the effectiveness of the use of DWT instead of the DFT, we adopted a similar approach for the classification of different beats which is shown in the figure below.

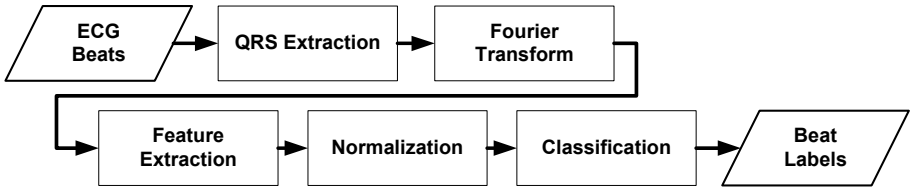

fig. 7-26 Steps in DFT Based Disease Classification

In this method we take the N-point DFT using FFT and compute the amplitude of the Fourier Coefficients thus obtained. These coefficients are normalized in the same way as in the DWT based method. These features are shown below.

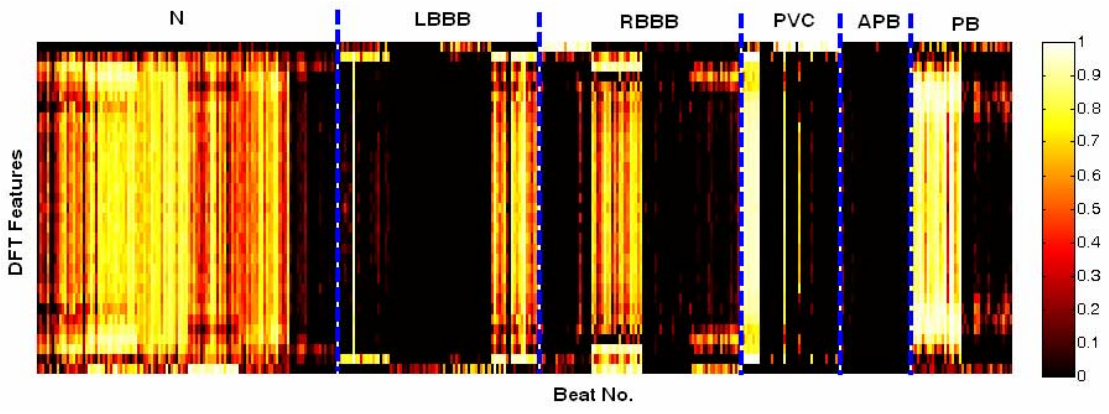

fig. 7-27 Normalized 32 point DFT Features

For classification, we employ a k-NN with k=1. Results of evaluation of this method using N=16 and N=32 both with and without Heart Rate are shown below.

Table 7-9 Result with 16 point DFT Features

k-NN* (Training Beats: 11600, Testing Beats: 11600) with k = 1						
Beat Types	N	LBBB	RBBB	PVC	PAC	PB
N	3180	102	165	5	46	71
LBBB	190	1852	17	209	4	119
RBBB	269	24	1561	26	352	201
PVC	12	227	30	764	3	113
PAC	61	3	382	8	307	96
PB	105	185	222	139	86	484
Accuracy (%)	83.3115	78.0447	65.6710	66.3771	38.4712	44.6494
Net Accuracy (%)	70.2414					

Table 7-10 Result with 16 point DFT and Instantaneous Heart Rate Features

k-NN* (Training Beats: 11600, Testing Beats: 11600) with k = 1						
Beat Types	N	LBBB	RBBB	PVC	PAC	PB
N	3464	47	78	4	4	44
LBBB	52	2159	19	23	2	85
RBBB	142	19	2150	7	71	76
PVC	4	17	10	1078	12	3
PAC	13	2	68	4	708	9
PB	86	90	84	0	11	955
Accuracy (%)	92.1032	92.5021	89.2487	96.5950	87.6238	81.4846
Net Accuracy (%)	90.6379					

Table 7-11 Result with 32 point DFT Features

k-NN* (Training Beats: 11600, Testing Beats: 11600) with k = 1						
Beat Types	N	LBBB	RBBB	PVC	PAC	PB
N	3609	4	3	1	8	8
LBBB	4	2300	3	34	20	1
RBBB	3	5	2343	13	17	4
PVC	4	29	6	1147	6	1
PAC	35	10	28	1	766	0
PB	11	0	2	0	1	1173
Accuracy (%)	98.4452	97.9557	98.2390	95.9030	93.6430	98.8203
Net Accuracy (%)	97.7414					

Table 7-12 Result with 32 point DFT and Instantaneous Heart Rate Features (Best Results with DFT)

k-NN* (Training Beats: 11600, Testing Beats: 11600) with k = 1						
Beat Types	N	LBBB	RBBB	PVC	PAC	PB
N	3546	0	2	0	4	3
LBBB	8	2388	9	13	9	1
RBBB	10	5	2389	7	5	2
PVC	0	8	2	1103	10	0
PAC	25	7	5	1	821	0
PB	1	2	1	0	0	1213
Accuracy (%)	98.7744	99.0871	99.2110	98.1317	96.7020	99.5078
Net Accuracy (%)	98.7931					

The results obtained above (98.7931%) compare well with the best results obtained with DWT (99.1034%) but the number of features being used for the DWT is only 11 whereas DFT requires 33 features. These features can also be reduced through different pruning techniques [59]. Other studies [70] also demonstrate the effectiveness of the use of DWT over that of DFT in beat classification. This stems from the fact that DWT is able to handle non-stationary signals like the ECG in a much better way than DFT.

CHAPTER 8
DETECTION OF ISCHEMIC ST SEGMENT DEVIATIONS

ST Segment elevation and depression in the ECG form a basis for the diagnosis of Coronary Heart Disease (CHD). In this chapter we describe the causes and mechanism of developing CHD and its relation with the ECG along with a detailed description of the techniques present in the literature for the automatic detection of Myocardial Ischemia. We also render the methodologies implemented under this project for the detection of ST level changes in the ECG, which can used in the diagnosis of CHD, along with their results.

8.1 Introduction to CHD

Coronary heart disease (CHD) [71], also called Coronary Artery Disease (CAD), ischaemic heart disease (IHD), Atherosclerotic heart disease, is the end result of the accumulation of atheromatous plaques within the walls of the arteries that supply the myocardium (the muscle of the heart) with oxygen and nutrients. While the symptoms and signs of coronary heart disease are noted in the advanced state of disease, most individuals with coronary heart disease show no evidence of disease for decades as the disease progresses before the first onset of symptoms, often a "sudden" heart attack, finally arise. After decades of progression, some of these atheromatous plaques may rupture and (along with the activation of the blood clotting system) start limiting blood flow to the heart muscle. The disease is the most common cause of sudden death, and is also the most common reason for death of men and women over 20 years of age. According to present trends in the United States, half of healthy 40-year-old males will develop CHD in the future, and one in three healthy 40-year-old women. According to the Guinness Book of Records, Northern Ireland is the country with the most occurrences of CHD.

Atherosclerotic heart disease can be thought of as a wide spectrum of disease of the heart. At one end of the spectrum is the asymptomatic individual with atheromatous

streaks within the walls of the coronary arteries (the arteries of the heart). These streaks represent the early stage of atherosclerotic heart disease and do not obstruct the flow of blood. A coronary angiogram performed during this stage of disease may not show any evidence of coronary artery disease, because the lumen of the coronary artery has not decreased in calibre.

Over a period of many years, these streaks increase in thickness. While the atheromatous plaques initially expand into the walls of the arteries, eventually they will expand into the lumen of the vessel, affecting the flow of blood through the arteries. While it was originally believed that the growth of atheromatous plaques was a slow, gradual process, recent evidence suggests that the gradual buildup may be complemented by small plaque ruptures which cause the sudden increase in the plaque burden due to accumulation of thrombus material.

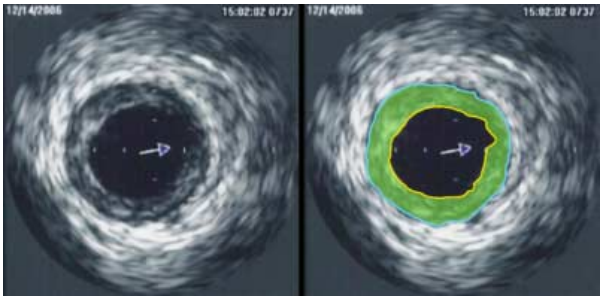

fig. 8-1 Intravascular ultrasound image of a coronary artery (left), with color coding on the right, delineating the lumen (yellow), external elastic membrane (blue) and the atherosclerotic plaque burden (green). As the plaque burden increases, the lumen size will decrease [71].

Atheromatous plaques that cause obstruction of less than 70 percent of the diameter of the vessel rarely cause symptoms of obstructive coronary artery disease. As the plaques grow in thickness and obstruct more than 70 percent of the diameter of the vessel, the individual develops symptoms of obstructive coronary artery disease. At this stage of the disease process, the patient can be said to have ischemic heart disease. The symptoms of ischemic heart disease are often first noted during times of increased workload of the heart. For instance, the first symptoms include exertional angina or decreased exercise tolerance.

As the degree of coronary artery disease progresses, there may be near-complete obstruction of the lumen of the coronary artery, severely restricting the flow of oxygen-carrying blood to the myocardium. Individuals with this degree of coronary heart disease typically have suffered from one or more myocardial infarctions (heart

attacks), and may have signs and symptoms of chronic coronary ischemia, including symptoms of angina at rest and flash pulmonary edema.

A distinction should be made between myocardial ischemia and myocardial infarction. Ischemia means that the amount of oxygen supplied to the tissue is inadequate to supply the needs of the tissue. When the myocardium becomes ischemic, it does not function optimally. When large areas of the myocardium become ischemic, there can be impairment in the relaxation and contraction of the myocardium which causes the variation in the ST level and T-wave in the ECG. If the blood flow to the tissue is improved, myocardial ischemia can be reversed. Infarction means that the tissue has undergone irreversible death due to lack of sufficient oxygen-rich blood.

An individual may develop a rupture of an atheromatous plaque at any stage of the spectrum of coronary heart disease. The acute rupture of a plaque may lead to an acute myocardial infarction (heart attack).

8.2 Stages of Development of IHD

Insufficient blood supply to the myocardium can result in myocardial ischemia, injury or infarction, or all three. Atherosclerosis of the larger coronary arteries is the most common anatomic condition to diminish coronary blood flow. The branches of coronary arteries arising from the aortic root are distributed on the epicardial surface of the heart. These in turn provide intramural branches that supply the cardiac muscle. Myocardial ischemia generally appears first and is more extensive in the sub-endocardial region since these deeper myocardial layers are farthest from the blood supply, with greater intramural tension and need for oxygen.

8.2.1 Subendocardial ischemia

Ischemia in this area prolongs local recovery time. Since repolarization normally proceeds in an epicardial-to-endocardial direction, delayed recovery in the subendocardial region due to ischemia does not reverse the direction of repolarization but merely lengthens it. This generally results in a prolonged QT interval or increased

amplitude of the T wave or both as recorded by the electrodes overlying the subendocardial ischemic region.

8.2.2 Subepicardial or transmural ischemia

Transmural ischemia is said to exist when ischemia extends subepicardially. This process has a more visible effect on recovery of subepicardial cells compared with subendocardial cells. Recovery is more delayed in the subepicardial layers, and the subendocardial muscle fibers seem to recover first. Repolarization is endocardial-to-epicardial, resulting in inversion of the T waves in leads overlying the ischemic regions.

8.2.3 Injury

Injury to the myocardial cells results when the ischemic process is more severe. Subendocardial injury on a surface ECG is manifested by ST segment depression, and subepicardial or transmural injury is manifested as ST segment elevation. In patients with coronary artery disease, ischemia, injury and myocardial infarction of different areas frequently coexist, producing mixed and complex ECG patterns.

8.2.4 Myocardial infarction

The term infarction describes necrosis or death of myocardial cells. Atherosclerotic heart disease is the most common underlying cause of myocardial infarction. The left ventricle is the predominant site for infarction; however, right ventricular infarction occasionally coexists with infarction of the inferior wall of the left ventricle. The appearance of pathological Q waves is the most characteristic ECG finding of transmural myocardial infarction of the left ventricle. A pathological Q wave is defined as an initial downward deflection of a duration of 40 msec or more in any lead except III and aVR. The Q wave appears when the infarcted muscle is electrically inert and the loss of forces normally generated by the infarcted area leaves unbalanced forces of variable magnitude in the opposite direction from the remote region, for example, an opposite wall. These forces can be represented by a vector directed away from the site of infarction and seen as a negative wave (Q wave) by electrodes overlying the infarcted region.

During acute myocardial infarction, the central area of necrosis is generally surrounded by an area of injury, which in turn is surrounded by an area of ischemia. Thus, various stages of myocardial damage can coexist. The distinction between ischemia and necrosis is whether the phenomenon is reversible. Transient myocardial ischemia that produces T wave, and sometimes ST segment abnormalities, can be reversible without producing permanent damage and is not accompanied by serum enzyme elevation. Two types of myocardial infarction can be observed electrocardiographically:

Q wave infarction, which is diagnosed by the presence of pathological Q waves and is also called transmural infarction. However, transmural infarction is not always present, hence the term Q-wave infarction may be preferable for ECG description

Non-Q wave infarction, which is diagnosed in the presence of ST depression and T wave abnormalities.

Elevation of serum enzymes is expected in both types of infarction. In the absence of enzyme elevation, ST and T wave abnormalities are interpreted as due to injury or ischemia rather than infarction.

8.3 Site of infarction

The ECG has been used to localize the site of ischemia and infarction. Some leads depict certain areas; the location of the infarct can be detected fairly accurately from analysis of the 12-lead ECG. Leads that best detect changes in commonly described locations are classified as follows:

- Inferior (or diaphragmatic) wall: II, II and aVF
- Septal: V1 and V2
- Anteroseptal: V1, V2, Vf3 and sometimes V4
- Anterior: V3, V4 and sometimes V2
- Apical: V3, V4 or both
- Lateral: I, aVL, V5 and V6
- Extensive anterior: I, aVL and V1 through V6

These details are also shown in the table below.

Table 8-1 Localization of Myocardial Infarction [72]

Wall Affected	Leads Showing ST Segment Elevation	Leads Showing Reciprocal ST Segment Depression	Suspected Culprit Artery
Septal	V_1, V_2	None	Left Anterior Descending (LAD)
Anterior	V_3, V_4	None	Left Anterior Descending (LAD)
Anteroseptal	V_1, V_2, V_3, V_4	None	Left Anterior Descending (LAD)
Anterolateral	V_3, V_4, V_5, V_6, I, aVL	II, III, aVF	Left Anterior Descending (LAD), Circumflex (LCX), or Obtuse Marginal
Extensive anterior (Sometimes called Anteroseptal with Lateral extension)	V_1, V_2, V_3, V_4, V_5, V_6, I, aVL	II, III, aVF	Left main coronary artery (LCA)
Inferior	II, III, aVF	I, aVL	Right Coronary Artery (RCA) or Circumflex (LCX)
Lateral	I, aVL, V_5, V_6	II, III, aVF	Circumflex (LCX) or Obtuse Marginal
Posterior (Usually associated with Inferior or Lateral but can be isolated)	V_7, V_8, V_9	V_1, V_2, V_3, V_4	Posterior Descending (PDA) (branch of the RCA or Circumflex (LCX))
Right ventricular (Usually associated with Inferior)	II, III, aVF, V_1, V_4R	I, aVL	Right Coronary Artery (RCA)

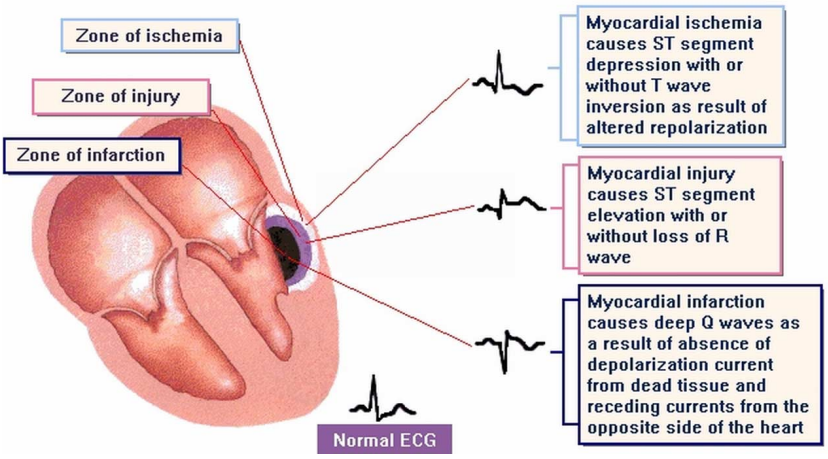

fig. 8-2 ST and T Wave Deviation in Ischemia

Posterior wall infarction does not produce Q wave abnormalities in conventional leads and is diagnosed in the presence of tall R waves in V1 and V2. The classic changes of necrosis (Q waves), injury (ST elevation), and ischemia (T wave inversion) may all be seen during acute infarction. In recovery, the ST segment is the earliest change that normalizes, then the T wave; the Q wave usually persists. Therefore, the age of the infarction can be roughly estimated from the appearance of the ST segment and T wave. The presence of the Q wave in the absence of ST and T wave abnormality generally indicates prior or healed infarction. Although the presence of a Q wave with a 40 msec duration is sufficient for diagnosis, criteria defining the abnormal depth of Q waves in various leads have been established. For example, in lead I, the abnormal Q wave must be more than 10 percent of QRS amplitude. In leads II and aVF, it should exceed 25 percent, and in aVL it should equal 50 percent of R wave amplitude. Q waves in V2 through V6 are considered abnormal if greater than 25 percent of R wave amplitude. fig. 8-2 shows the effects of various stages of IHD on the ECG.

8.4 Cause of ST Deviation in IHD patients

Under normal conditions, the ST segment is relatively isoelectric (i.e., flat along the baseline), because all healthy myocardial cells attain about the same potential during repolarization. Ischemia has complex time-dependent effects on the electrical properties of the affected myocardial cells. Severe, acute ischemia lowers the resting membrane potential, shortens the duration of the action potential, and changes the shape of the plateau (phase 2) of the action potential in the ischemic area. These changes cause a voltage gradient between normal and ischemic zones, leading to current flow between these regions during both systolic and diastolic portions of the cardiac cycle. These so-called currents of injury are represented on the surface ECG by deviation of the ST segment. The injury current can thus be thought to originate as the result of depolarization of the cellular resting membrane potential due to ischemia which causes a potential difference to develop between the normal and ischemic tissue producing the resultant current [73]. According to current-of-injury theory, ST-segment elevation occurs when the injured muscle is located between normal muscle and the corresponding precordial electrode. On the other hand, ST-segment depression occurs when normal muscle is located between the injured tissue and the corresponding electrode.

Other causes of ST segment elevation, apart from IHD, include the following:

- Acute pericarditis: ST elevation in acute pericarditis is generally diffuse and does not follow the pattern of blood supply. As a rule these changes are not accompanied by reciprocal depression of the ST segment in other leads.
- Early repolarization: In some patients without known heart disease, particularly young patients, early takeoff of the ST segment may be seen.
- Ventricular aneurysm: After acute myocardial infarction, the ST segment usually normalizes. However, in the presence of a persistent aneurysm in the region of infarction, ST segment elevation may persist indefinitely.

Abnormal T waves can be seen in a variety of conditions other than myocardial ischemia, including:

- Hyperventilation
- Cerebrovascular disease
- Mitral valve prolapse
- Right or left ventricular hypertrophy
- Conduction abnormalities (right or left bundle branch block)
- Ventricular preexcitation
- Myocarditis
- Electrolyte imbalance
- Cardioactive drugs such as digitalis and antiarrhythmic agents
- No obvious cause, particularly in women

8.5 Standard Datasets and Evaluation Methods

Standard datasets for the detection of ischemia include the European Society of Cardiology Database (ESC-ST-T DB) and the Long term ST database (LTST DB). These databases are available at physiobank.

Ischemia detection techniques either focus on the detection of ischemic beats or on the detection of ischemic episodes. The accuracy of the former methods is given by the classification accuracy whereas the latter methods use sensitivity, TP/(TP+FN), and positive predictive values ,TP/(TP+FP), for presenting the accuracy with TP, FN and FP representing number of True-Positive, False-Negative and False Positive episodes. A distinction of average and gross statistics must also be made. Aggregate gross statistics weights each event (episode) equally by pooling all the events over all records together, and models how the system behaves on a large number of events. Aggregate average statistics weights each record equally, and models how the system behaves on randomly chosen records. All techniques for ischemic episode detection implemented in this work use the 48 freely available files of the ESC-ST-T database and use aggregate gross statistics.

8.6 Literature Review

A variety of techniques exist in the literature for the detection of myocardial ischemia and ST segment change episodes. These include the use of Time Domain

Approaches, Artificial Neural Networks, Principal Component Analysis, Wavelet Transform, Fuzzy and Neuro-Fuzzy Systems etc.

Maglaveras et al. (1998) [74] have presented a 3 layer adaptive Backpropagation Neural Network for detection of Ischemic episodes and achieve Sensitivity/PPV of 88.62%/78.38% for episode detection using Average statistics and 85%/68.69% using gross statistics using the ESC-ST-T Database. The neural net operates on an estimate of the baseline corrected ST segment taken to start 40ms after the R-peak with duration of 160ms which is down-sampled by a factor of two for further processing as a means of dimensionality reduction. The neural net is trained on the deviation of the ST segment estimate from a normal template.

Jager et al. (1998) [75] have presented a technique based on the use of lead independent KLT components for the detection of ST-segment episodes and with a Sensitivity/PPV of 87.1%/87.7%(average), 85.2%/86.2%(gross) over the ESC-ST-T database. Principal Component Bases are obtained by first dividing the input database into a number of pattern classes and then applying KLT.

Frenkel et al. (1999) [76] have proposed an Artificial Neural Network based Approach for ST-T segment classification with Sensitivity/PPV of 84.15%/72.63%.

Garcia et al. (2000) [77] propose a method based which uses a detection algorithm to the filtered root mean square (RMS) series of differences between the beat segment (ST segment or ST-T complex) and an average pattern segment. This method gives a (average) sensitivity/PPV of 85%/86% and 85%/76%, for ST segment deviations and ST-T complex changes respectively over the ESC-ST-T Database. An evaluation of this method on the LTST [78] gives Sensitivity/PPV of 75%/71%.

Papaloukas et al. (2000) [19] proposed A knowledge based approach for ischemia detection through application rules employing evaluation of ST Segment level and slope along with T wave polarity. This paper does not describe results on the whole of ESC-ST-T Database. It presents a simple and effective method for the removal of baseline variations without introducing significant distortion in the ST Segment.

Papaloukas et al. (2002) [79] have proposed a technique for the detection of myocardial ischemia using a Neural Network trained using Bayesian Regularization method. The proposed system uses a 400ms long estimate of the ST Segment. Lead independent principal components (5) of the ST segment estimates are obtained for the entire database and used for dimensionality reduction. This method gives a

Sensitivity/PPV of 90%/89% for aggregate gross statistics and 86%/87% for average statistics using ESC-ST-T Database.

Bezerianos et al. (2001) [80] propose a Network Self Organizing Map (NetSOM) model for the detection of ST-T episodes. The Sensitivity/PPV of ischemic beats for this method over the ESC-ST-T database is given as 77.7%/74.1%.

Papadimitriou et al. (2001) [81] have reported a episode detection Sensitivity/PPV of 82.8%/82.4% over the ESC-ST-T database through the use of a supervising network self-organizing map with SVM using an RBF kernel.

Papaloukas et al. (2001) [82] present a rule based approach for ST Segment and T-wave abnormality detection using the J+60/80ms (dependent upon heart rate) point as an estimate of the ST segment and application of rules over the slope and level of the ST-segment and T-wave followed by window characterization for episode detection. The accuracies presented in the paper in terms of Sensitivity/PPV for ST Segment deviation and T-wave episode detection is 92.02%/93.77% and 91.09%/80.09% on the ESC-ST-T database respectively.

Zimmerman et al. (2003) [83] propose a reconstructed phase space approach for distinguishing Ischemic from Nonischemic ST changes through Gaussian Mixture Models. The Sensitivity/Specificity of this method is given as 81%/88.1% over the LTST Database.

Langley et al. (2003) [84] use ST Segment Deviations and their Principal Components for detection of ischemic ST episodes. The Sensitivity/Specificity of this technique is given as 99%/88.8% with an accuracy of 91.1% over the LTST Database. Zimmerman (2004) [85] has improved the method proposed by Langley et al. to give an accuracy of 94.80% over the LTST database using Support Vector Machine classifier coupled with the original method.

Smrdel et al. (2004) [86] use ST deviation time series for the detection of ST episodes. The presented Sensitivity/PPV of this method over ESC-ST-T database is 81.3%/89.2%.

An ischemia detection method using Genetic Algorithms and Multicriterion Decision Analysis has been proposed by Goletsis et al. (2004) [87]. This method uses ST deviation defined at the J+60/80ms point, ST Segment slope, T-wave amplitude, T-wave normal amplitude and polarity and age. The Sensitivity/Specificity of this algorithm for ischemic beat classification over ESC-ST-T Database is 91%/91%.

A technique using Nonlinear PCA Neural Networks for Ischemia Detection was proposed by Stamkopoulos et al. (2004) [88] giving correct classification rate of approximately 80% for the normal beats and higher than 90% for the ischemic beat for ST segment deviations on ESC-ST-T Database. Moreover [89] conjectures that linear dimensionality reduction methods, e.g. Linear PCA can perform better in comparison to Nonlinear techniques on real datasets.

Another method using PCA and Artificial Neural Networks for episode detection is given by Tasoulis et al. (2004) [90] which gives an episode detection accuracy of 80.4% over the ESC-ST-T Database.

A Hidden Markov Model (HMM) based approach has been proposed by Andreao et al. (2004) [91] which gives a Sensitivity/PPV of 83%/85% over 48 files out of 90 from the ESC-ST-T Database.

A real time Ischemia detection system is presented in the paper by Pang et al. (2005) [92] which employs a real time R peak detector and combined time domain and KLT features along with an adaptive neuro-fuzzy system for classification. This method achieves Sensitivity/PPV of 81.29%/74.65% over ESC-ST-T database.

Sales et al. (2005) [93] present an implementation of an ischemia detection system using wavelets along with its evaluation on a limited number of subjects of LTST.

A method that uses decision trees for detection of ischemia was proposed by Dranca et al. (2006) [94] and it has achieved a Sensitivity/PPV of 89.89%/70.03% over the LTST database.

Exarchos et al. (2006) [95] have proposed a method using a rule mining approach for ischemia detection. This method uses ECG features such as ST Segment Deviation, slope, area, T-wave deviation (from normal template) amplitude along with patient's age. This method then uses specially mined rules for detection of ischemia. The Sensitivity/Specificity of this method for ischemic beat classification over the ESC ST-T database is 87%/93%.

Exarchos et al. (2007) [68] give a fuzzy expert system based technique for ischaemic beat classification that relies on the extraction and application of fuzzy rules and optimization of membership functions parameters. The ischemic beat detection accuracy of this method is given by a Sensitivity/Specificity of 91%/92%.

Table 8-2 Results of Literature Survey

Reference	Year	Accuracy Assessment		Detection Type
ESC-ST-T DB Cardiologists	1992	Se=70-83%	PPV=85-93%	
Maglaveras et al.	1998	Se_A = 88.6%	PPV_A =78.4%	Ischemic Episodes
		Se_G = 85.0%	PPV_G =68.7%	Ischemic Episodes
Jager et al.	1998	Se_A = 87.1%	PPV_A =87.7%	ST Segment Episodes
		Se_G = 85.2%	PPV_G =86.2%	ST Segment Episodes
Frenkel et al.	1999	Se=84.2%	PPV=72.6%	ST Segment Episodes
Garcia et al.	2000	Se_A = 85.0%	PPV_A =86.0%	ST Segment Episodes
		Se_G = 85.0%	PPV_G =76.0%	Ischemic Episodes
Papaloukas et al.	2001	Se_A = 86.0%	PPV_A =87.0%	Ischemic Episodes
		Se_G = 90.0%	PPV_G =89.0%	Ischemic Episodes
Vladutu et al.	2001	Se=77.7%	PPV=74.1%	Ischemic Episodes
Papadimitriou et al.	2001	Se=82.8%	PPV=82.4%	Ischemic Episodes
Papaloukas et al.	2002	Se=92.1%	PPV=93.8%	ST Segment Episodes
		Se=91.1%	PPV=80.1%	T Wave Episodes
Smrdel et al.	2004	Se=81.3%	PPV=89.2%	ST Segment Episodes
Goletsis et al.	2004	Se=91.0%	Sp=91.0%	Ischemic Beats
Andreao et al.*	2004	Se=83.0%	PPV=85.0%	ST Segment Episodes
Pang et al.	2005	Se=81.3%	PPV=74.6%	Ischemia Episode
Exarchos et al.	2006	Se=87.0%	Sp=93.0%	Ischemic Beats
Exarchos et al.	2007	Se=91.0%	Sp=92.0%	Ischemic Beats

8.7 Implemented Schemes

Automated ST Deviation Episode Detection is based upon the following major steps as shown below. :

- Preprocessing
- Feature Extraction
- Classification
- Post Processing

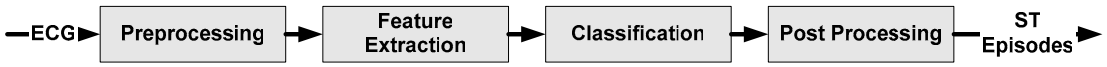

fig. 8-3 Steps Involved in ST Segment Deviation Episode Detection

These steps are explained in detail henceforth.

8.7.1 Preprocessing

Preprocessing involves the removal of noise and baseline artifacts from the input ECG signal. It also includes the detection of the QRS reference points for the

extraction of features for ST segment deviation detection, which appears as the next stage in the system. Here we describe, in detail, the preprocessing stage for use with the consequent stages.

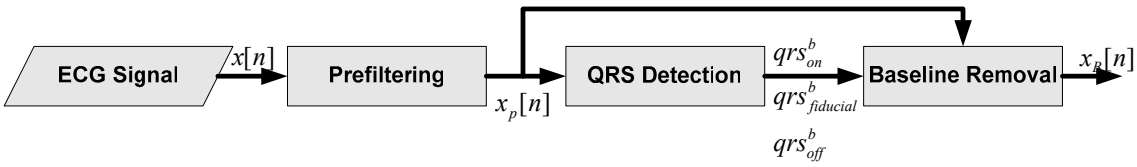

fig. 8-4 Preprocessing for ST Segment Deviation Episode Detection

A given input ECG signal $x[n],\ n = 1 \cdots N$ with a sampling frequency of f_s (250Hz for ESC-ST-T Database) belonging to lead l is taken as input and is passed through a pre-filtering stage which is responsible for the removal of high frequency noise and minimization of effects of baseline variation. This is done by passing $x[n]$ through the cascade of a high pass and a low pass filter to obtain $x_p[n]$. A 6^{th} order Butterworth IIR high pass filter with cutoff frequencies of $f_{pass} = 0.6Hz$ and $f_{stop} = 0.4Hz$ for the pass and stop bands respectively is employed through zero-phase (forward-backward) filtering to reduce the effects of baseline variation which lies up to ~0.5Hz while minimizing distortion in the ST segment. Effects of high frequency noise are reduced by the use of zero-phase filtering through a 12^{th} order Butterworth IIR low pass filter with a cutoff frequency of $f_c = 45Hz$.

The pre-filtered signal $x_p[n]$ is subjected to QRS detection using a Genetic Algorithm Optimized Wavelet Transform based QRS Detection and delineation system [96] that gives a triple $\left\{qrs^b_{on}, qrs^b_{fiducial}, qrs^b_{off}\right\}$ corresponding to the onset, fiducial point and offset for each beat $b = 1 \cdots N_b$ (number of beats).

The QRS delineation information and the pre-filtered signal $x_p[n]$ is used for baseline removal using a two stage linear interpolation based technique proposed in [19] to obtain the baseline removed signal $x_B[n]$. For the Rule Based Technique described below, a cubic spline based baseline removal technique (see chapter 3) was used with the knot amplitude being defined through averaging the signal values lying between $[qrs^b_{on} - 40ms, qrs^b_{on} + 4ms]$ and the knot position to be defined at qrs^b_{on} for each beat. These baseline removal methodologies works in conjunction with the High Pass Filter

used during pre-filtering to remove baseline variations while introducing minimum distortion in the ST Segment. This baseline removed ECG signal is used in subsequent processing.

8.7.2 Feature Extraction and Classification

The following schemes were implemented for detection of feature extraction:

- Using Time Domain Features
- Using KLT Features

Below we describe in details these approaches.

8.7.2.1 Using Time Domain Features and a Rule Based Classifier

This method originally proposed by Papaloukas et al. [82] requires the extraction of the following features for each beat in the input signal.

a. Isoelectric Level

The isoelectric level defined for the knot in the cubic spline interpolation based baseline removal procedure by averaging signal values in the range $[qrs_{on}^{b} - 40ms, qrs_{on}^{b} + 4ms]$ is used. This isoelectric level was removed through the baseline removal procedure.

b. ST Reference Point (J80 or J60) Amplitude

The ST deviation is measured at the J80 (heart rate < 120bpm) or the J60 point (heart rate ≥ 120bpm). The J point amplitude used is the averaged amplitude in the interval [J-4ms, J + 4ms]. Similarly, for the J80 (or J60) point, the interval [J80+4 ms, J80- 4 ms] (or [J60+4ms, J60-4ms]) is applied.

c. ST Reference Amplitude for a Subject

The average of the ST point amplitudes of the first 50 beats is used as a reference level for each subject and subtracted from the rest of the ST point amplitudes.

d. ST Point (J80 or J60) Slope

The ST slope is defined as the slope of the line connecting the J and J80 (or J60) points.

e. T-peak Amplitude

T wave detection is carried out prior to the extraction of these features through the DWT based approach described in Chapter-6 and the peak T-wave amplitude is determined. If the T-wave detection methodology fails, an estimate of the T-wave peak amplitude is obtained by finding the amplitude of the point that has maximum variation in amplitude from the J80 point in a 350ms window starting at the J80 point.

The beat classification was based on the following rules (see figure below):

a. Negative ST deviation: ≤ 0.8 mm (0.08mV) below the isoelectric line and with a slope $\geq 65°$ from the vertical line, or in other words with signal slope at the ST segment ≤ 1.87 mV ms^{-1})

b. Positive ST deviation: ≥ 0.8 mm (0.08mV) above the isoelectric line

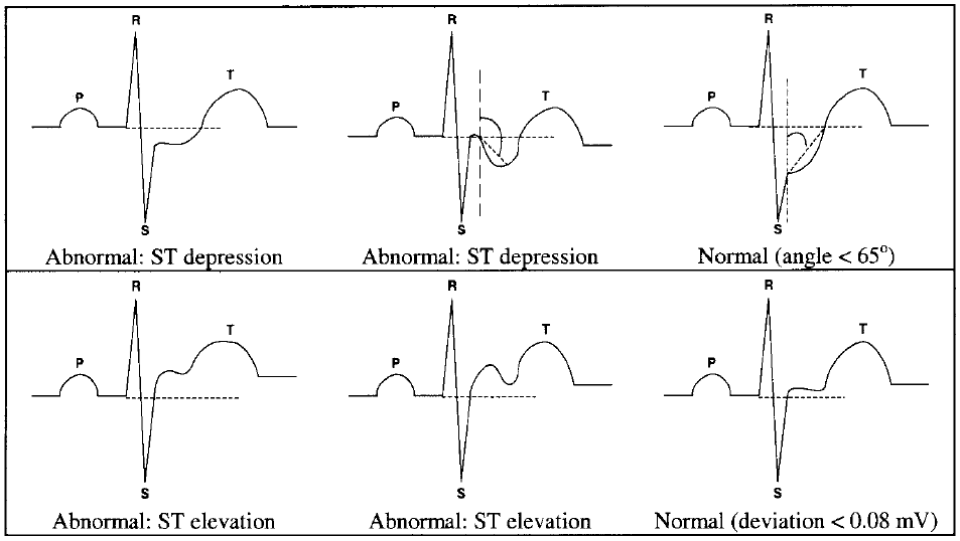

fig. 8-5 Rules for ST Segment Deviation Detection

The figure below shows the ST deviation plot along with the associated thresholds for two different subjects of the ESC-ST-T Database.

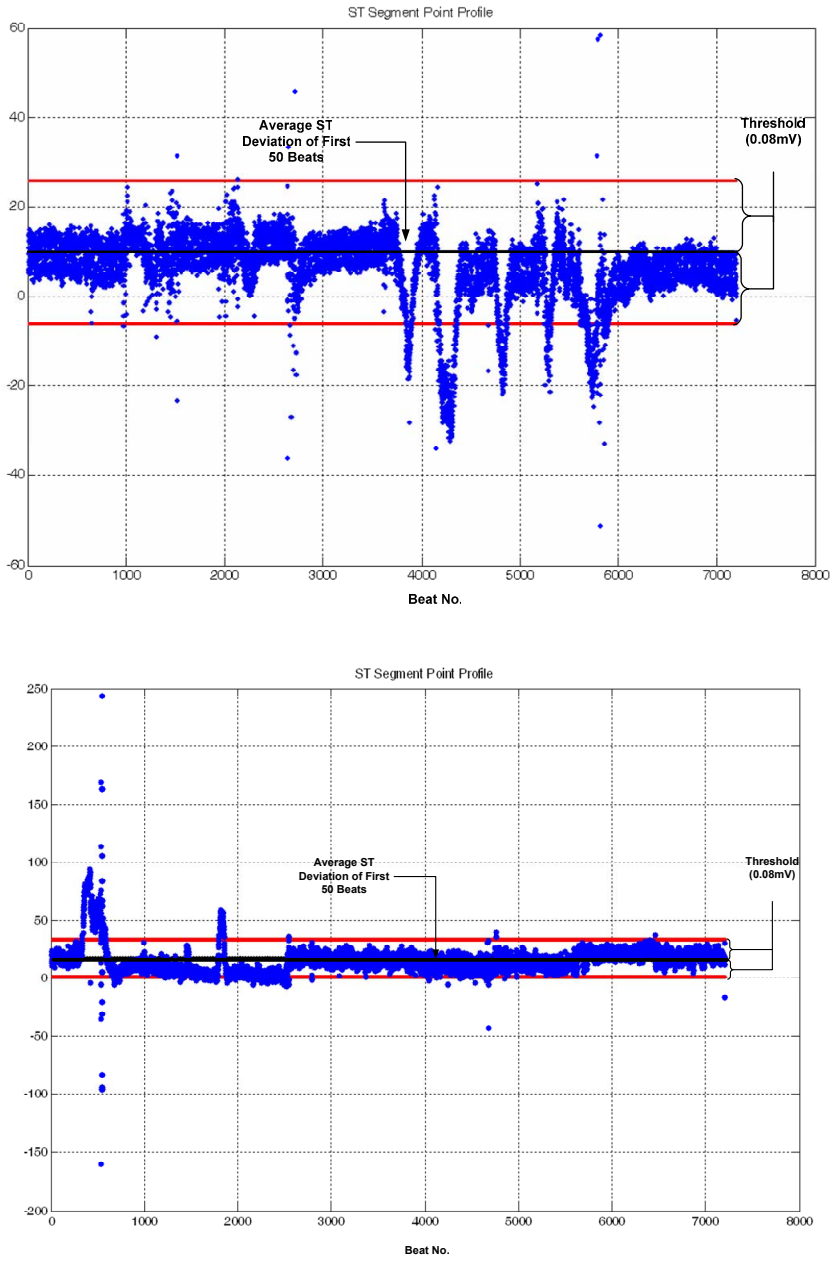

fig. 8-6 ST Segment profiles for two selected ESC DB Subjects

8.7.2.2 Using KLT Features

In this method we use lead specific Principal Component Analysis for the detection of ST Segment episodes as shown below.

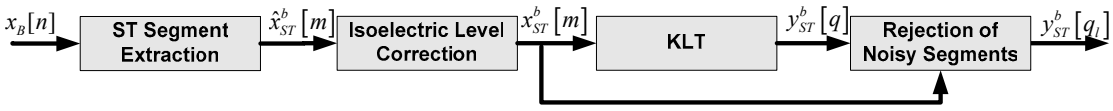

fig. 8-7 Feature Extraction using KLT

An estimate of the ST Segment, $\hat{x}_{ST}^{b}[m]$, $m=1\cdots M$ taken to start at qrs_{off}^{b} and ending at $qrs_{off}^{b}+100ms$ is extracted for each beat from the baseline removed signal. Isoelectric level is then estimated by finding the average value of the flattest 20ms long region starting 80ms before qrs_{on}^{b} and ending at qrs_{on}^{b} for each beat. This value for each beat is subtracted from the corresponding $\hat{x}_{ST}^{b}[m]$ to obtain a more precise estimate of the true ST deviation $x_{ST}^{b}[m]$.

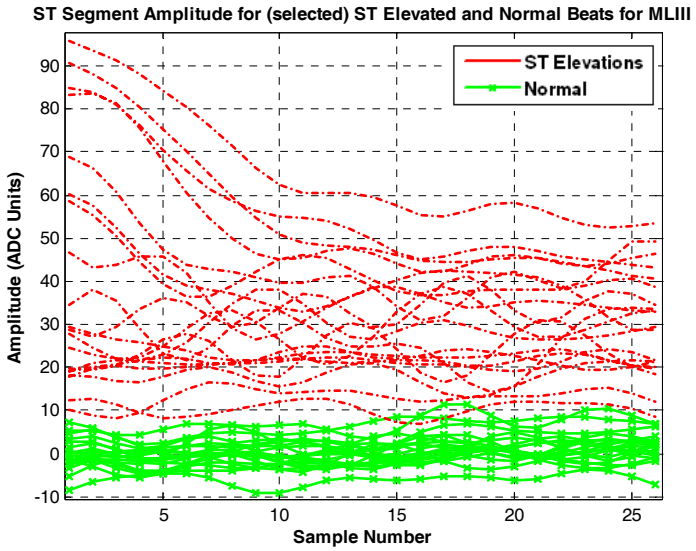

fig. 8-8 Normal and Elevated ST Segments for lead MLIII

The ST deviation estimate $x_{ST}^{b}[m]$ is projected onto lead-specific Karhunen-Loève Transform (KLT) bases Φ_{l}^{q}, $q=1...(Q=5)$ to obtain the principal coefficients $y_{ST}^{b}[q]$corresponding to ST deviation for each beat. These bases are obtained by selecting a subset of ST segments of non-noisy beats for the lead l using the manual noise level annotations in the database and finding the Eigen Vectors and Eigen values corresponding to the Covariance (or dispersion) matrix R_l formed by these non-noisy beat ST segments. The covariance matrix is given by,

$$R_l=\frac{1}{N_t^l}\sum_{n_t=1}^{N_t^l}\left(x_{ST}^{n_t}-\mu_l\right)\left(x_{ST}^{n_t}-\mu_l\right)^T \qquad (8.1)$$

Where $N_t^{l_i}$ is the number of ST segments chosen (randomly) from the non-noisy beats for l_i for determining the KLT bases and $\mu_{l_i}[m]$ is the mean of these beats given by,

$$\mu_{l_i}[m] = \frac{1}{N_t^{l_i}} \sum_{n_t=1}^{N_t^{l_i}} \left(x_{ST}^{n_t}[m] \right), \qquad m = 1 \cdots M \tag{8.2}$$

The Eigen values and vectors are obtained by solving the Eigen value problem,

$$R_l \Phi_l^q = \lambda_l^q \Phi_l^q, \qquad q = 1 \cdots M \tag{8.3}$$

The Eigen values λ_l^q are sorted in descending order $\lambda_l^1 \geq \lambda_l^2 \geq \ldots \geq \lambda_l^M$ and the highest $Q = 5$ out of M are taken as they contribute the maximum variance (energy) [40].

The bases corresponding to different leads are different as is illustrated in the figure below.

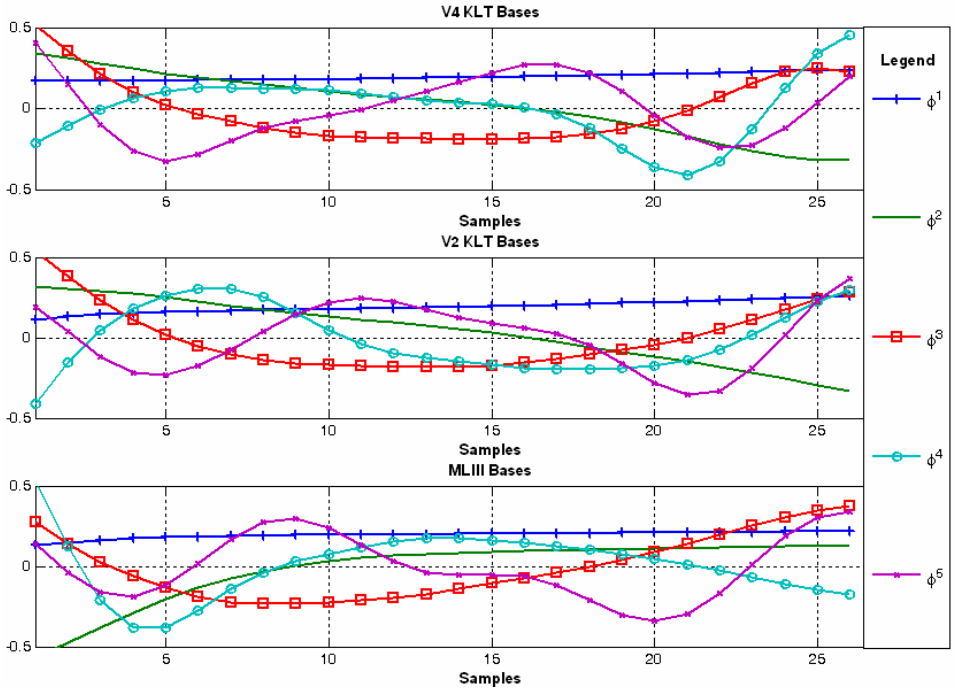

fig. 8-9 KLT Bases for Different leads

Let Φ_l be the matrix of the Eigen vectors as given below,

$$\Phi_l = \left[\Phi_l^1 \quad \Phi_l^2 \quad \cdots \quad \Phi_l^Q \right] \tag{8.4}$$

This matrix is used to obtain y_{ST}^b for each beat as follows,

$$y_{ST}^b = \Phi_l^T \left(x_{ST}^b - \mu_l \right) \tag{8.5}$$

The reconstruction of the ST segment deviation of a beat is given by,

$$\tilde{x}_{ST}^b = \left(\sum_{q=1}^{Q} y_{ST}^b[q] \Phi_l^q \right) + \mu_l \tag{8.6}$$

This reconstruction is used to find the normalized reconstruction error as follows,

$$r(b) = \frac{\left\| \tilde{x}_{ST}^{b} - x_{ST}^{b} \right\|}{x_{ST}^{b}} \tag{8.7}$$

This normalized reconstruction error is used to detect noisy beats. ST segments having $r(b) > 0.3$ are taken as noisy and rejected in further processing [40].

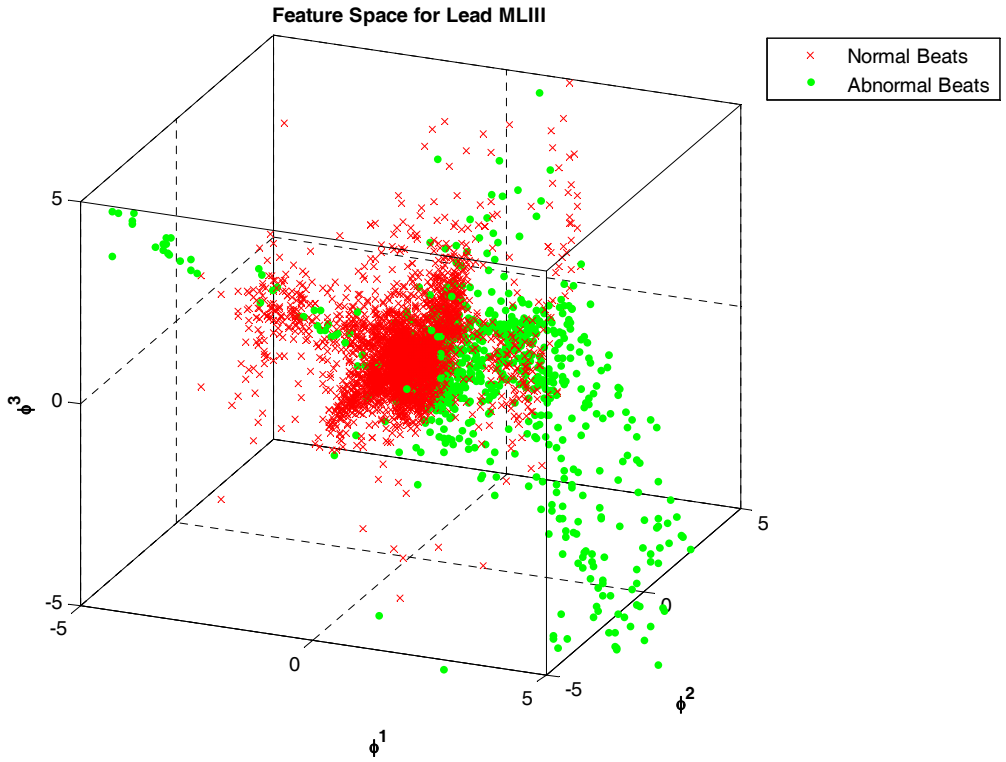

fig. 8-10 A reduced Feature Space showing discrimination between normal and abnormal ST Segments

Four different types of classifiers were used for solving the classification problem. These techniques are described below in detail.

a. Using Feed-Forward Backpropagation Neural Network

In this method a single Backpropagation Neural Network was used for the detection of ST deviation in the ECG. The non noisy ST deviations $y_{ST}^{b}[q_l]$ $(q_l = 1 \cdots Q_l)$ with $b = 1 \cdots N_{nnb}$ (number of non noisy beats) and Q_l being the number of principal components used in classification of ST episodes for lead l are applied at the input of a Neural Network. The output of the neural networks for a beat is given by $z(b)$. A moving average filter of length $L = 40$ is applied (through zero phase filtering) on all of $z(b)$ to obtain $fz(b)$ to introduce temporal linking in the output of the neural network. Thresholding is then performed on $fz(b)$ as below,

$$t_{k^+}(b)=\begin{cases}1 & if\ fz(b)>\Theta_l^+\\ -1 & if\ fz(b)\le\Theta_l^-\\ 0 & else\end{cases} \tag{8.8}$$

Thus $t(b)=1$ implies that the Neural Network classifier has conjectured the input ST segment as a $\left(ST^+\right)$ segment. $t(b)=0$ implies that this classifier has classified the input ST segment as a non-deviated ST segment. Similarly $t(b)=-1$ labels the input ST segment as a depressed ST segment. The thresholds Θ_l^+ and Θ_l^- are lead specific and are given in the table below. This method was utilized for the detection of ST segment deviation only in the MLIII lead before moving on to the more effective method of using a Neural Network Ensemble for classification, which is described in the next section.

Table 8-3 Parameters for NN Based Classification

Lead (l)	(Q_l) **Bases**	(S_l) **NN Structure**	$\left(\Theta_l^+\right)$ ST^+ **Threshold**	$\left(\Theta_l^-\right)$ ST^- **Threshold**
MLIII	5	12,12,1	0.65	0.7

For each lead a training set of approximately equal number of ST deviated (if present) and normal beats is selected (<6% of total number of beats for that lead). The training class labels are taken as C_t with,

$$C_t\ (b)=\begin{cases}1 & \text{for } ST^+\\ -1 & \text{for } ST^-\\ 0 & \text{else}\end{cases} \tag{8.9}$$

Some of these beats form the cross validation set over which different parameters of this system, such as the neural network architecture and different thresholds used are optimized empirically. Tangent sigmoid activation functions were used throughout in the design of all neural networks for all layers.

b. Using Neural Network Ensemble

In this method we used an ensemble of neural networks with k-fold training and majority voting for classification as shown below.

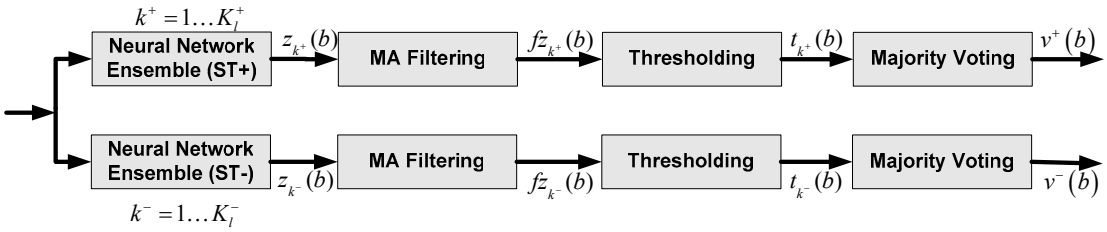

fig. 8-11 Use of NN Ensemble for Classification

The non noisy ST deviations $y_{ST}^b[q_l]$ $(q_l = 1 \cdots Q_l)$ with $b = 1 \cdots N_{nnb}$ (number of non noisy beats) and Q_l being the number of principal components used in classification of ST episodes for lead l are applied at the input of two sets of Neural Networks, one each for the detection of ST elevation $\left(ST^+\right)$ (having K_l^+ neural networks) and ST depression $\left(ST^-\right)$ episodes (having K_l^- neural networks). The output of these neural networks for a beat is given by $z_{k^+}(b)$, $k^+ = 1 \ldots K_l^+$ and $z_{k^-}(b)$, $k^- = 1 \ldots K_l^-$. A moving average filter of length $L = 40$ is applied (through zero phase filtering) on all of $z_{k^+}(b)$ and $z_{k^-}(b)$ to obtain $fz_{k^+}(b)$ and $fz_{k^-}(b)$ to introduce temporal linking in the output of the neural networks. Thresholding is then performed on each of $fz_{k^+}(b)$ and $fz_{k^-}(b)$ as below,

$$t_{k^+}(b) = \begin{cases} 1 & if\ fz_{k^+}(b) > \Theta_l^+ \\ 0 & if\ fz_{k^+}(b) \le \Theta_l^+ \end{cases} \tag{8.10}$$

$$t_{k^-}(b) = \begin{cases} 1 & if\ fz_{k^-}(b) > \Theta_l^- \\ 0 & if\ fz_{k^-}(b) \le \Theta_l^- \end{cases} \tag{8.11}$$

Thus $t_{k^+}(b) = 1$ implies that the Neural Network classifier number k^+ has conjectured the input ST segment as a $\left(ST^+\right)$ segment. $t_{k^+}(b) = 0$ implies that this classifier has classified the input ST segment as a non-elevated ST segment. Similarly $t_{k^-}(b)$ labels the input ST segment as depressed or non-depressed ST segments. The thresholds Θ_l^+ and Θ_l^- are lead specific and are given in table below. Majority voting is then used to combine the results of different Neural Network based Classifiers for detecting ST elevation vs. non-elevated ST segments and ST depressions vs. non-depressed ST segments. For a given beat, $v^+(b)$ is taken as the label for which maximum number of

classifiers, out of the K_l^+ classifiers used for discerning ST elevations and normal ST segments, has voted. Similarly $v^-(b)$ is taken as the label for which maximum number of classifiers, out of the K_l^- classifiers used for classifying ST depressions and normal ST segments, has voted.

The training of these neural networks is carried out using *k-fold training* [97] (see fig. below). For each lead a training set of approximately equal number of ST elevated (if present) and normal beats is selected (<6% of total number of beats for that lead) and *k-fold training* is used to train K_l^+ back propagation neural networks each having . The training class labels are taken as $C_t^+(b)$ with,

$$C_t^+(b) = \begin{cases} 1 & \text{for ST}^+ \\ 0 & \text{else} \end{cases} \tag{8.12}$$

Some of these beats form the cross validation set over which different parameters of this system, such as the neural network architecture and different thresholds used are optimized empirically.

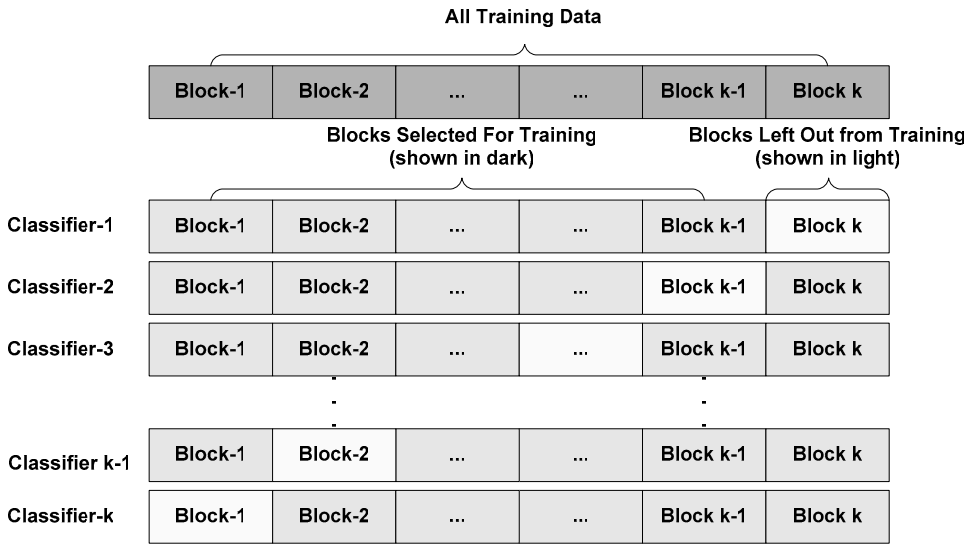

fig. 8-12 k-fold Training [97]

The same holds for the set of Neural Network detecting ST depressions where we train the neural networks with equal number of ST depressed (if present) and normal beats and class labels given by

$$C_t^-(b) = \begin{cases} 1 & \text{for ST}^- \\ 0 & \text{else} \end{cases} \tag{8.13}$$

The structure of each of the Neural Network for a lead is taken to be the same for a lead and is represented by S_l as given in the table below. Tangent sigmoid activation functions were used throughout in the design of all neural networks for all layers.

Table 8-4 Lead Specific Paramters for NN Ensemble

Lead (l)	$\left(K_l^+\right)$	$\left(K_l^-\right)$	$\left(Q_l\right)$ **Bases**	$\left(S_l\right)$ **NN Structure**	$\left(\Theta_l^+\right)$ ST^+ **Threshold**	$\left(\Theta_l^-\right)$ ST^- **Threshold**
MLI	5	5	5	10,12,1	0.65	0.7
MLIII	5	5	5	10,12,1	0.65	0.7
D3	5	0	5	10,12,1	0.725	-NA-
V1	5	5	5	8,8,1	0.8	0.825
V2	5	5	5	8,8,1	0.8	0.8
V3	0	5	5	8,8,1	-NA-	0.785
V4	5	5	5	8,8,1	0.8	0.8
V5	7	7	5	10,12,1	0.8	0.725

c. Using SVM Ensemble

In this method we investigated the use of a SVM Ensemble classifier for detecting ST segment elevation and depression. The method adopted is much the same as for the Neural Network Ensemble. The training patterns were selected in the same manner as for the Neural Network Ensemble except that the labels are taken as follows,

$$C_t^+(b) = \begin{cases} 1 & \text{for } ST^+ \\ -1 & \text{else} \end{cases} \tag{8.14}$$

$$C_t^-(b) = \begin{cases} 1 & \text{for } ST^- \\ -1 & \text{else} \end{cases} \tag{8.15}$$

The structure of the classification system is shown below.

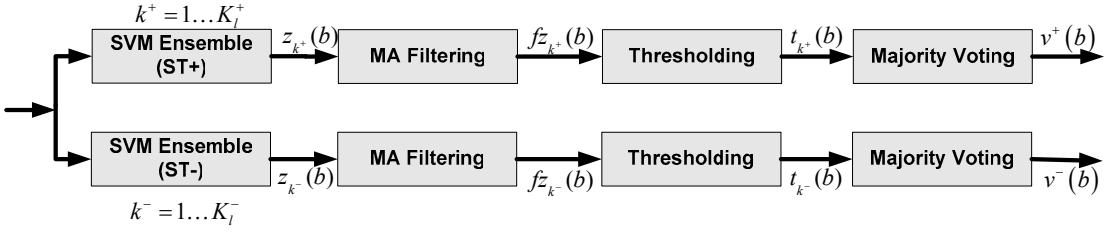

fig. 8-13 SVM Ensemble for Classification

The details of the number of SVM classifiers used and their structure is given below. SVM Ensemble based classification has been implemented only for leads MLI and MLIII.

Table 8-5 Lead Specific Paramters for SVM Ensemble

Lead (l)	(K_l^+)	(K_l^-)	(Q_l) Bases	Value of C for SVM Classifiers	Kernel	(Θ_l^+) ST^+ Threshold	(Θ_l^-) ST^- Threshold
MLI	5	5	5	10^{-7}	RBF (Spread = 1.1)	0	0
MLIII	5	5	5	10^{-7}	RBF (Spread = 1.1)	0	0

8.7.3 Post Processing

This procedure takes the outputs of the classifier for a number $(N_{episode})$ of beats and acknowledges it as an ST deviation episode if a certain percentage $(P_{\min})$ of these beats has are labeled as showing ST deviations. Episodes smaller then a specific length $(L_{\min})$ are removed and episodes that are spaced by a normal duration less than $(D_{\min})$ are combined. The output of the window characterization stage is taken as $C(b)$. $C(b)=1$ employs that the beat has been labeled as ST depressed or elevated, otherwise it is taken to be normal. These values were tuned empirically using a cross validation dataset for different classification systems explained earlier and are given in the table below. It should be noted that episode annotations for the two separate leads of the ECG are not combined as a practical implementation of the system may involve the use of only a single ECG lead.

Table 8-6 Postprocessing Parameters for different Classifiers

CLASSIFIER/PARAMETERS	$N_{episode}$	$P_{\min}$	$L_{\min}$	$D_{\min}$
Using Rule Based Classifier	15	60	30	50
Using KLT Features (BPNN, NN Ensemble, SVM Ensemble)	35	75	15	40

8.8 Results

Here we describe the results for all the above techniques.

8.8.1 Rule Based Technique

This method gives a Sensitivity/PPV of 85%/82% over 48 subjects of the ESC-ST-T Database for ST segment deviation episode detection. These results are considerably lower than those reported (92.1%/93.8%) by the original author. The

major issue with the use of this method is the presence of noise and its sensitivity to the accuracy of the baseline removal or isoelectric level detection procedure.

8.8.2 Using KLT Features with BPNN

With the use of the BPNN approach over the MLIII lead we achieved a Sensitivity/PPV of 96%/81% for the detection of ST segment episodes in the ESC-ST-T Database. These results demonstrate the effectiveness of the use of BPNN for classification of ST segment deviation episodes. This method was then extended to the use of NN ensemble.

8.8.3 Using NN Ensemble

The results for ST deviation episode detection using this method are shown in the figure below for lead MLIII.

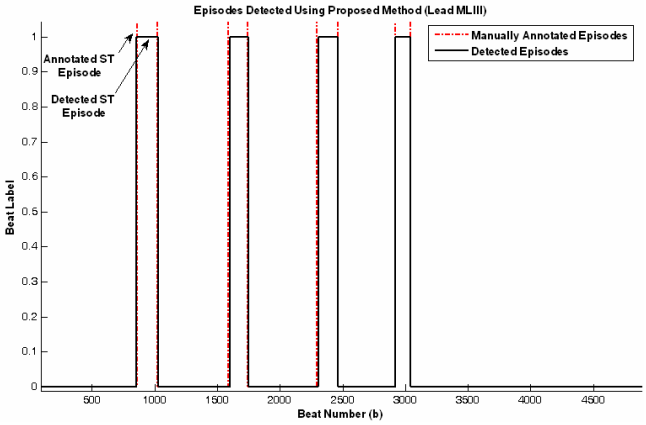

fig. 8-14 Episode Detection using NN Ensemble

The results for each lead are given below in terms of Sensitivity/PPV.

Table 8-7 Results with NN Ensemble

Lead (l)	Number Of ST Episodes	TP	FP	FN	PPV (%)	Se (%)
MLI	6	6	0	0	100	100
MLIII	45	40	3	5	93.02	88.89
D3	2	2	0	0	100	100
V1	9	9	1	0	90	100
V2	10	10	2	0	83.3	100
V3	4	4	0	0	100	100
V4	44	39	3	5	92.86	88.64
V5	53	47	10	6	82.46	88.68
ALL	**173**	**157**	**19**	**16**	**89.20**	**90.75**

These results rank amongst the best reported in the literature and they clearly demonstrate the effectiveness of the use of a NN ensemble for detecting ST segment episodes.

8.8.4 Using SVM Ensemble

The results of the use of SVM based ensemble over MLI and MLIII are shown below.

Table 8-8 Results with NN Ensemble

Lead (l)	**Number Of ST Episodes**	**TP**	**FP**	**FN**	**PPV (%)**	**Se (%)**
MLI	6	5	0	1	100	83.3
MLIII	45	36	4	9	90	80

CHAPTER 9
CONCLUSIONS AND FUTURE WORK

This work was aimed at the design of a decision support system for cardiac diseases with a particular focus on the design and implementation of algorithms for removal of artifacts from the ECG, ECG Segmentation, Arrhythmia classification and detection of ischemic ST segment deviation episodes. In this chapter we present our conclusions about different techniques implemented in this work along with issues related to system integration and development of system hardware. Different pointers to future research are also given along with a projection of the direction of future work for practical system development.

The ECG signal obtained from the ECG machine is prone to a variety of artifacts which can stem from different physiological and electrical components. These include Noise (Electromyographic, Electrical Interferences etc.) and Baseline variations. These artifacts can reduce the performance of the overall system thus making their removal an integral system component. We have implemented different methods for the removal of baseline variations from the ECG. These methods include the use of IIR and FIR high pass filters with a cutoff frequency of ~0.5Hz, curve fitting techniques such as Cubic Spline Interpolation, Median Filtering and a Two Stage Linear Interpolator. The desired characteristics for such a system include minimization of the distortion introduced into the ECG while effectively compensating for possibly large baseline variations. We conclude that these characteristics are achieved through the cascade implementation of a Zero Phase IIR low pass filter and the two stage linear interpolator. This procedure introduces the minimum amount of distortion especially in the highly sensitive region of the ST segment.

For the purpose of noise removal we have implemented different noise removal techniques based on the use of digital filters, Independent Component Analysis and locally projective principal component based nonlinear filtering. These techniques were evaluated on ECG generated synthetically by using a dynamical model for ECG generation and adding noise to it. This noise was removed using the implemented

techniques and parameters like Noise Reduction Factor and Correlation Coefficient were used to assess the quality of the noise removal procedure. We conclude that nonlinear noise filtering performs more effectively in removing noise that is orthogonal to the ECG signal (such as electrical interferences and a great deal of Electromyographic noise) as it offers a higher noise reduction factor. Due to the great computational complexity of this noise removal technique, a noise detection mechanism based on the thresholding of the PCA reconstruction error can be employed. ICA can be used to effectively compensate noise that is independent but not orthogonal to the ECG signal source. We have, in this work identified a number of difficulties and research pointers for using ICA for noise reduction which are described in Chapter-4. A method that combines ICA with locally projective filtering offers a more effective alternate to the use of noise filtering implemented in this work.

A fundamental component of any ECG based analysis and decision support system is Segmentation of the ECG signal into its constituent parts, i.e. QRS Complex, P and T-waves. For the purpose of QRS detection and delineation we have implemented methods based upon the use of Length Transform and the classical Pan-Tompkins Algorithm. However these method though giving very high detection accuracy (>99.9% over the QT-Database) do not give good results in terms of the error in detecting the onset and offset of the QRS complex. We have implemented an existing Discrete Wavelet Transform (DWT) based approach and optimized its parameters in a novel way through the use of Genetic Algorithms to achieve a Detection Sensitivity/Specificity of ~99.1% with a 10ms error in marking the onset and offset of the QRS complex. This method though having very low delineation error has much lower detection accuracy. We have implemented a novel Continuous Wavelet Transform (CWT) based technique for the detection and delineation of the QRS complex which gives a detection Sensitivity/Specificity of ~99.8% with ~10-12ms error in marking the onset and offset of the QRS complex. Moreover the CWT approach is more effective in terms of execution time than the DWT based approach. However the DWT coefficients extracted in the DWT based technique can also be used for the detection and delineation of the P and T-waves which makes it more effective in overall in terms of execution time. The delineation accuracy given above has been determined through comparison with manually annotated beats through expert cardiologists. Further improvement in these values can cause the system to be

over trained to the annotations as there always exists an inter-person variation in the markings of the onset and offset.

For the purpose of arrhythmia classification, we have compared the performance of approaches based on the DWT and DFT over the classification of six types of heart rhythms (Normal, Atrial Premature Beat, Ventricular Premature Contraction, Paced Rhythms, Left and Right Bundle Branch Blocks) from the MIT-BIH Arrhythmia Database. We conclude that DWT based features used in this work along with the Instantaneous Heart Rate perform better than the use of DFT based approaches as the former offer a high classification accuracy of ~99.1 with a k-NN classifier with the latter giving a comparable accuracy of ~98.9% but using three times more features. A possible candidate for future work is the use of Fuzzy Expert Systems for Arrhythmia classification with rules obtained from data through Evolutionary Algorithms which can improve the interpretability of the classification procedure along with allowing potential for reduction in the number of features required. From a practical system implementation perspective DFT may offer a computationally more efficient method due to the existence of high speed DFT hardware, but it may require the number of features to be reduced through the use of feature reduction or selection techniques such as Davies-Bouldin Index.

We have also implemented different approaches for ischemic ST Segment deviation episode detection such as the use of a Rule Based Classifier with Time Domain Features and the application of novel lead independent Karhunen-Loeve Transform (KLT) bases with a variety of classifiers (Backpropagation Neural Networks, Support Vector Machines and Neural Network Ensemble). We have evaluated the performance of our techniques over the ESC-ST-T database and conclude that the use of lead specific KLT features with a Neural Network Ensemble classifier offer much higher episode detection accuracy (Sensitivity/Positive Predictive Value of ~90%). We can also apply automatic fuzzy rule extraction techniques from data and use the consequent fuzzy inference system for classification.

The integrated system design obtained through this research is shown below:

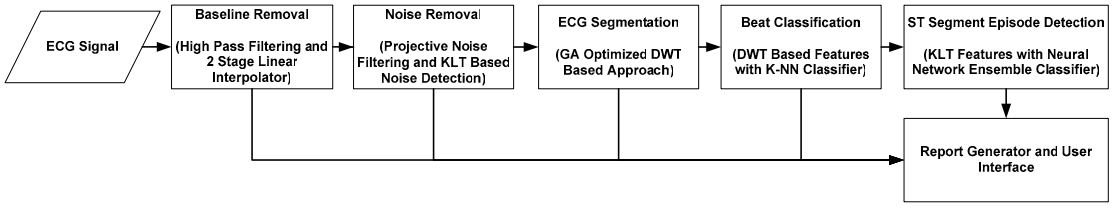

fig. 9-1 Proposed Systm Design

The implemented techniques for the base for the purpose of practical system development, which requires the integration of these modules and parameter tuning in the system to customize this system for operation with the ECG acquisition device and the environment in which it is to operate. Two types of practical system implementations can be envisioned:

a. Portable Device

A portable device can be helpful for the long term and remote monitoring of cardiac patients. Such a device can involve the use of a portable Holter monitor, a data-logging system and the developed algorithms implemented on a PDA or dedicated hardware. Such a system can transmit abnormalities in the ECG through a separate communication system or through a simple cell phone to a medical expert for immediate action.

b. Non-Portable System

Such a system can be used for the offline or online analysis of the ECG of single or multiple patients in hospitals and involves the interfacing of an ECG machine to a laptop through specially designed interface ADC cards.

The approaches implemented in this thesis can thus offer a promising automated patient monitoring system which can be helpful both to the cardiac expert and the patient. It can result in improvement of the life style of a cardiac patient by allowing him more freedom in activities. It can also make the life of a cardiac expert easier by presenting automatically calculated ECG parameters and decision support.

REFERENCES

1. Wikipedia. *Action Potential*. 2007 [cited; Available from: http://en.wikipedia.org/wiki/Action_potential.
2. Wikipedia. *Electrocardiogram*. 2007 [cited; Available from: http://en.wikipedia.org/wiki/Electrocardiogram.
3. Goldberger, A.L., et al., *PhysioBank, PhysioToolkit, and PhysioNet: Components of a New Research Resource for Complex Physiologic Signals.* Circulation, 2000. **101**(23): p. e215--e220.
4. Laguna, P., et al., *A Database for Evaluation of Algorithms for Measurement of QT and Other Waveform Intervals in the ECG.* Computers in Cardiology 1997. **24**: p. 673-676
5. Taddei, A., et al., *The European ST Database: Standard for Evaluating Systems for the Analysis of ST-T Changes in Ambulatory Electrocardiography. Eur Heart J* European Heart Journal, 1992. **13**: p. 1164-1172.
6. Mark, R. and G. Moody, *MIT-BIH Arrhythmia Database Directory*. 1988: Cambridge, MA: MIT Press.
7. Jager, F., et al. *The Long-Term ST database: a research resource for algorithm development and physiologic studies of transient myocardial ischemia*. in *Computers in Cardiology 2000*. 2000.
8. Friesen, G.M., et al., *A comparison of the noise sensitivity of nine QRS detection algorithms.* Biomedical Engineering, IEEE Transactions on, 1990. **37**(1): p. 85-98.
9. Gholam-Hosseini, H., H. Nazeran, and K.J. Reynolds. *ECG noise cancellation using digital filters*. in *Bioelectromagnetism, 1998. Proceedings of the 2nd International Conference on*. 1998.
10. Laguna, P., R. Jane, and P. Caminal. *Adaptive Filtering Of ECG Baseline Wander*. in *Engineering in Medicine and Biology Society, 1992. Vol.14. Proceedings of the Annual International Conference of the IEEE*. 1992.
11. Pandit, S.V. *ECG baseline drift removal through STFT*. in *Engineering in Medicine and Biology Society, 1996. Bridging Disciplines for Biomedicine. Proceedings of the 18th Annual International Conference of the IEEE*. 1996.
12. Donghui, Z. *Wavelet Approach for ECG Baseline Wander Correction and Noise Reduction*. in *Engineering in Medicine and Biology Society, 2005. IEEE-EMBS 2005. 27th Annual International Conference of the*. 2005.
13. Sayadi, O. and M.B. Shamsollahi, *Multiadaptive Bionic Wavelet Transform: Application to ECG Denoising and Baseline Wandering Reduction.* EURASIP Journal on Advances in Signal Processing, 2007: p. Article ID 41274, 11 pages.

14. Martinez, J.P., et al., *A wavelet-based ECG delineator: evaluation on standard databases.* Biomedical Engineering, IEEE Transactions on, 2004. **51**(4): p. 570-581.
15. Kossmann, C.E., D.A. Brody, and G.E. Burch, *Report of committee on Electrocardigraphy, American Hear Association.* Circulation, 1967. **35**: p. 583.
16. Clifford, G.D., *ECG Statistics, Noise, Artifacts and Missing Data*, in *Advanced Methods and Tools for ECG Analysis*, G.D. Clifford, F. Azuaje, and P.E. McSharry, Editors. 2006, Artech House Publishing: London.
17. Meyer, C.R. and H.N. Keiser, *Electrocardiogram baseline noise estimation and removal using cubic splines and state-space computation techniques.* Comput. Biomed. Res. , 1977. **10**: p. 459-470.
18. Chouhan, V.S. and S.S. Mehta. *Total Removal of Baseline Drift from ECG Signal*. in *Computing: Theory and Applications, 2007. ICCTA '07. International Conference on*. 2007.
19. Papaloukas, C., et al. *A robust knowledge-based technique for ischemia detection in noisy ECGs*. in *Knowledge-Based Intelligent Engineering Systems and Allied Technologies, 2000. Proceedings. Fourth International Conference on*. 2000.
20. Ma, W.K., Y.T. Zhang, and F.S. Yang, *A fast recursive-least-squares adaptive notch filter and its applications to biomedical signals.* Med Biol Eng Comput. , 1999. **37**(1): p. 99-103.
21. Levkov, C., et al., *Removal of power-line interference from the ECG: a review of the subtraction procedure.* Biomed Eng Online, 2005. **4**(50).
22. Martens, S.M.M., et al., *An Improved Adaptive Power Line Interference Canceller for Electrocardiography.* Biomedical Engineering, IEEE Transactions on, 2006. **53**(11): p. 2220-2231.
23. Lee, J.-W. and G.-K. Lee, *Design of an Adaptive Filter with a Dynamic Structure for ECG Signal Processing.* International Journal of Control, Automation and Systems, 2005. **3**(1): p. 137-142.
24. Nikolaev, N., et al. *Wavelet domain Wiener filtering for ECG denoising using improved signal estimate*. in *Acoustics, Speech, and Signal Processing, 2000. ICASSP '00. Proceedings. 2000 IEEE International Conference on*. 2000.
25. Barros, A.K., A. Mansour, and N. Ohnishi, *Removing artifacts from electrocardiographic signals using independent components analysis* Neurocomputing, 1998. **22**(1): p. 173-186.
26. He, T., G.D. Clifford, and L. Tarassenko, *Application of ICA in removing arte facts from the ECG*, in *Neural Processing Letters.*
27. Patrick, E.M. and D.C. Gari. *A comparison of nonlinear noise reduction and independent component analysis using a realistic dynamical model of the electrocardiogram*. 2004: SPIE.
28. Schreiber, T. and D. Kaplan, *Nonlinear noise reduction for electrocardiograms.* CHAOS, 1996. **6**(87).
29. Kotas, M., *Projective filtering of time-aligned ECG beats.* Biomedical Engineering, IEEE Transactions on, 2004. **51**(7): p. 1129-1139.
30. McSharry, P.E., et al., *A dynamical model for generating synthetic electrocardiogram signals.* Biomedical Engineering, IEEE Transactions on, 2003. **50**(3): p. 289-294.

31. McSharry, P.E. and G.D. Clifford. *ECGSYN - a realistic ECG waveform generator*. [cited; Available from: http://www.physionet.org/physiotools/ecgsyn/.
32. Hayes, M.H., *Welch's Method*, in *Statistical Digital Signal Processing and Modelling*. 2004, John Wiley & Sons, Inc. p. 415-420.
33. James, C.J. and D. Lowe, *Extracting Multisource Brain Activity from a Single Electromagnetic Channel.* Artificial Intelligence in Medicine, 2003. **28**(1): p. 89-104.
34. Wikipedia. *Box Counting Dimension*. 2007 [cited; Available from: http://en.wikipedia.org/wiki/Box_counting_dimension.
35. Kantz, H. and T. Schreiber, *Nonlinear Time Series Analysis*. 2004: Cambridge University Press.
36. Richter, M. and T. Schreiber, *Phase space embedding of electrocardiograms.* 1998.
37. Hyvärinen, A. *Fast and Robust Fixed-Point Algorithms for Independent Component Analysis*. IEEE Transactions on Neural Networks 1999 [cited 10 3]; 626-634]. Available from: http://www.cis.hut.fi/projects/fastica.
38. Cardoso, J.F. *Multidimensional independent component analysis*. in *Acoustics, Speech and Signal Processing, 1998. Proceedings of the 1998 IEEE International Conference on*. 1998.
39. Kern, A., D. Blank, and R. Stoop. *Projective noise reduction with dynamic neighborhood selection*. in *Circuits and Systems, 2000. Proceedings. ISCAS 2000 Geneva. The 2000 IEEE International Symposium on*. 2000.
40. Jager, F., *Introduction to Feature Extraction*, in *Advanced Methods and Tools for ECG Data Analysis*, G.D. Clifford, F. Azuaje, and P. McSharry, Editors. 2006, Artech House: London.
41. Kohler, B.U., C. Hennig, and R. Orglmeister, *The principles of software QRS detection.* Engineering in Medicine and Biology Magazine, IEEE, 2002. **21**(1): p. 42-57.
42. Makki, M., *Design of an Online ECG Analyzer*, in *Department of Electrical Engineering*. 2005, Pakistan Institute of Engineering and Applied Sciences: Islamabad.
43. Pan, J. and W.J. Tompkins, *A Real-Time QRS Detection Algorithm.* Biomedical Engineering, IEEE Transactions on, 1985. **BME-32**(3): p. 230-236.
44. Gutierrez, A., et al. *A QRS detection algorithm based on Haar wavelet*. in *Computers in Cardiology 1998*. 1998.
45. Li-Gao, Z., L. Hui-Jun, and H. Guang-Shu. *Real-time base-line drift correction and P-wave detection of ECG signal*. in *Engineering in Medicine and Biology Society, 1989. Images of the Twenty-First Century. Proceedings of the Annual International Conference of the IEEE Engineering in*. 1989.
46. Escalona, O., L. Gavidia, and G. Wright. *A robust procedure for P-wave detection and segmentation in high resolution 12-lead ECG*. in *Engineering in Medicine and Biology Society, 1996. Bridging Disciplines for Biomedicine. Proceedings of the 18th Annual International Conference of the IEEE*. 1996.
47. Sovilj, S., M. Jeras, and R. Magjarevic. *Real time P-wave detector based on wavelet analysis*. in *Electrotechnical Conference, 2004. MELECON 2004. Proceedings of the 12th IEEE Mediterranean*. 2004.

48. Cuiwei, L., Z. Chongxun, and T. Changfeng, *Detection of ECG characteristic points using wavelet transforms.* Biomedical Engineering, IEEE Transactions on, 1995. **42**(1): p. 21-28.

49. Stamkopoulos, T., et al. *Wave segmentation using nonstationary properties of ECG*. in *Computers in Cardiology 2000*. 2000.

50. Lepage, R., et al. *ECG segmentation and P-wave feature extraction: application to patients prone to atrial fibrillation*. in *Engineering in Medicine and Biology Society, 2001. Proceedings of the 23rd Annual International Conference of the IEEE*. 2001.

51. Tan, K.F., K.L. Chan, and K. Choi. *Detection of the QRS complex, P wave and T wave in electrocardiogram*. in *Advances in Medical Signal and Information Processing, 2000. First International Conference on (IEE Conf. Publ. No. 476)*. 2000.

52. Reddy, B.R.S., et al. *Detection of P waves in resting ECG: a preliminary study*. in *Computers in Cardiology 1992. Proceedings.* 1992.

53. Gritzali, F., G. Frangakis, and G. Papakonstantinou. *DECGAP: an automatic ECG analysis program*. in *Computers in Cardiology 1989. Proceedings.* 1989.

54. Hee-Kyo, J., et al. *A new algorithm for P-wave detection in the ECG signal*. in *Engineering in Medicine and Biology Society, 1989. Images of the Twenty-First Century. Proceedings of the Annual International Conference of the IEEE Engineering in*. 1989.

55. Moraes, J.C.T.B., et al. *A real time QRS complex classification method using Mahalanobis distance*. in *Computers in Cardiology, 2002*. 2002.

56. Chazal, P.d. and R.B. Reilly. *Automatic classification of ECG beats using waveform shape and heart beat interval features*. in *Acoustics, Speech, and Signal Processing, 2003. Proceedings. (ICASSP '03). 2003 IEEE International Conference on*. 2003.

57. Minami, K., H. Nakajima, and T. Toyoshima, *Real-time discrimination of ventricular tachyarrhythmia with Fourier-transform neural network.* Biomedical Engineering, IEEE Transactions on, 1999. **46**(2): p. 179-185.

58. Afonso, V.X., et al. *Filter bank-based ECG beat classification*. in *Engineering in Medicine and Biology society, 1997. Proceedings of the 19th Annual International Conference of the IEEE*. 1997.

59. Dokur, Z., T. Olmez, and E. Yazgan, *Comparison of discrete wavelet and Fourier transforms for ECG beat classification.* ELECTRONICS LETTERS, 1999. **35**(18): p. 1502-1504.

60. A.S. Al-Fahoum, I.H., *Combined Wavelet Transform and Radial Basis Neural Networks for the classifying Life Threatening Cardiac arrhythmias.* Med. Bio. Eng. Comput., 1999. **37**: p. 566-573.

61. Addison, P.S., et al., *A Novel wavelet based analysis reveals hidden structure in ventricular fibrillation.* IEEE Engineering in Medicine and Biology, 2000. **19**(4): p. 383-392.

62. Prasad, G.K., Sahambi, J.S. *Classification of ECG arrhythmias using multiresolution analysis and Neural Networks*. in *Conference on Convergent Technologies*. 2003. Bangalore, India.

63. Inan, O.T., L. Giovangrandi, and G.T.A. Kovacs, *Robust Neural-Network-Based Classification of Premature Ventricular Contractions Using Wavelet Transform and Timing*

Interval Features. Biomedical Engineering, IEEE Transactions on, 2006. **53**(12): p. 2507-2515.

64. Sung-Nien, Y. and C. Ying-Hsiang, *Electrocardiogram beat classification based on wavelet transformation and probabilistic neural network.* Pattern Recogn. Lett., 2007. **28**(10): p. 1142-1150.
65. Engin, M., *ECG beat classification using neuro-fuzzy network.* Pattern Recognition Letters, 2004. **25**: p. 1715 - 1722.
66. Güler, İ. and E.D. Übeylı, *A modified mixture of experts network structure for ECG beats classification with diverse features.* Eng. Appl. Artificial Intell., 2005. **18**: p. 845-856.
67. Güler, İ. and E.D. Übeylı, *ECG Beat Classifier designed by Combined Neural Network Model.* Pattern recognit., 2005. **38**: p. 199-208.
68. Exarchos, T.P., et al., *A methodology for the automated creation of fuzzy expert systems for ischaemic and arrhythmic beat classification based on a set of rules obtained by a decision tree.* Artificial Intelligence in Medicine, 2007. **40**: p. 187-200.
69. Sung-Nien, Y. and C. Kuan-To, *A switchable scheme for ECG beat classification based on independent component analysis.* Expert Syst. Appl., 2007. **33**(4): p. 824-829.
70. Dokur, Z. and T. Olmez, *ECG beat classification by a novel hybrid neural network.* Computer Methods and Programs in Biomedicine, 2001. **66**(2-3): p. 167-181.
71. Wikipedia. *Coronary Heart Disease*. 2007 [cited; Available from: http://en.wikipedia.org/wiki/Coronary_heart_disease.
72. Wikipedia. *Localization of Myocardial Infarction*. 2007 [cited; Available from: http://en.wikipedia.org/wiki/Myocardial_infarction.
73. Gettes, L.S. and W.E. Cascio, *Effect of acute ischemia on cardiac electrophysiology*. The Heart and cardiovascular System, ed. H. Fozzard. 1991: Raven Press. 2021-2054.
74. Maglaveras, N., et al., *An adaptive backpropagation neural network for real-time ischemia episodes detection: development and performance analysis using the European ST-T database.* Biomedical Engineering, IEEE Transactions on, 1998. **45**(7): p. 805-813.
75. Jager, F., G.B. Moody, and R.G. Mark, *Detection of transient ST segment episodes during ambulatory ECG monitoring.* Comput. Biomed. Res., 1998. **31**(5): p. 305-322.
76. Frenkel, D. and J. Nadal. *Ischemic episode detection using an artificial neural network trained with isolated ST-T segments*. in *Computers in Cardiology 1999*. 1999.
77. Garcia, J., et al., *Automatic detection of ST-T complex changes on the ECG using filtered RMS difference series: application to ambulatory ischemia monitoring.* Biomedical Engineering, IEEE Transactions on, 2000. **47**(9): p. 1195-1201.
78. Minchole, A., et al. *Evaluation of a root mean squared based ischemia detector on the long-term ST database with body position change cancellation*. in *Computers in Cardiology, 2005*. 2005.
79. Papaloukas, C., et al., *An ischemia detection method based on artificial neural networks.* Artificial Intelligence in Medicine, 2002. **24**(2): p. 167-178

80. Bezerianos, A., L. Vladutu, and S. Papadimitriou, *Hierarchical State Space Partitioning with the Network Self-Organizing Map for the effective recognition of the ST-T Segment Change.* IEE Medical and Biological Engineering and Computing, 2000. **38**(4): p. 406-415.
81. Papadimitriou, S., et al., *Ischemia detection with a self-organizing map supplemented by supervised learning.* Neural Networks, IEEE Transactions on, 2001. **12**(3): p. 503-515.
82. Papaloukas, C., et al., *A Knowledge -based Technique for the Detection of Ischemic Episodes in Long Duration ECGs.* Medical and Biological Engineering and Computing, 2001. **39**(1): p. 105-112.
83. Zimmerman, M.W., et al. *A reconstructed phase space approach for distinguishing ischemic from non-ischemic ST changes using Holter ECG data*. in *Computers in Cardiology, 2003*. 2003.
84. Langley, P., et al. *An algorithm to distinguish ischaemic and non-ischaemic ST changes in the Holter ECG*. in *Computers in Cardiology, 2003*. 2003.
85. Zimmerman, M.W. and R.J. Povinelli. *On improving the classification of myocardial ischemia using Holter ECG data*. in *Computers in Cardiology, 2004*. 2004.
86. Smrdel, A. and F. Jager., *Automated detection of transient ST segment episodes in 24-hour electrocardiograms.* Med. Biol. Eng. Comput.,, 2004. **42**: p. 303-311.
87. Goletsis, Y., et al., *Automated ischemic beat classification using genetic algorithms and multicriteria decision analysis.* Biomedical Engineering, IEEE Transactions on, 2004. **51**(10): p. 1717-1725.
88. Stamkopoulos, T., et al., *ECG analysis using nonlinear PCA neural networks for ischemia detection.* Signal Processing, IEEE Transactions on [see also Acoustics, Speech, and Signal Processing, IEEE Transactions on], 1998. **46**(11): p. 3058-3067.
89. Maaten, L.v.d., E. Postma, and H.v.d. Herik, *Dimensionality Reduction: A Comparative Review*. 2007.
90. Tasoulis, D.K., et al., *Online Neural Network Training for Automatic Ischemia Episode Detection.* Lecture Notes in Artificial Intelligence, 2004. **LNAI 3070**: p. 1062-1068.
91. Andreao, R.V., et al. *ST-segment analysis using hidden Markov Model beat segmentation: application to ischemia detection*. in *Computers in Cardiology, 2004*. 2004.
92. Pang, L., et al. *Real time heart ischemia detection in the smart home care system*. in *Engineering in Medicine and Biology Society, 2005. IEEE-EMBS 2005. 27th Annual International Conference of the*. 2005.
93. Sales, F.J.R., et al. *An ischemia detector based on wavelet analysis of electrocardiogram st segments*. in *Computers in Cardiology, 2005*. 2005.
94. Dranca, L., A. Goni, and A. Illarramendi. *Using DecisionTrees for Real-Time Ischemia Detection*. in *Computer-Based Medical Systems, 2006. CBMS 2006. 19th IEEE International Symposium on*. 2006.
95. Exarchos, T.P., et al., *An Association Rule Mining Based Methodology for the Automated Detection of Ischemic ECG Beats.* IEEE Trans Biomed Eng., 2007. **53**(8): p. 531-1540.

96. Afsar, F.A. and M. Arif, *QRS Detection and Delineation Techniques for ECG Based Robust Clinical Decision Support System Design*, in *National Science Conference*. 2007: Lahore, Pakistan.

97. Polikar, R., *Ensemble Based Systems in Decision Making.* IEEE Circuits and Systems Magazine, 2006. **6**(3): p. 21-45.

Fayyaz ul Amir Afsar Minhas was born in Murid, District Chakwal, Pakistan on 28th August 1983. He did his matriculation from District Public School, Chakwal and his FSc. from P.A.F. Intermediate College, Kallar-Kahar. He joined Pakistan Institute of Engineering and Applied Sciences (PIEAS), Islamabad in 2001 under the degree program for BS in Computer and Information Sciences. After the completion of his BS degree with distinction, he enrolled in the MS program in Systems Engineering also at PIEAS in 2005 under the Fellowship program by the Pakistan Atomic Energy Commission. He has published numerous papers in the field of Biometrics (Fingerprint Recognition and Signature Verification), Robotics (Path Planning), and Biomedical Signal Processing and Disease Classification. His research interests include Biomedical Signal Processing, Machine Learning, Pattern Classification, Image Processing, Robotics and Intelligent Applied Control.

Contact Information:

Department of Electrical Engineering
Pakistan Institute of Engineering and Applied Sciences (PIEAS)
PO Box Nilore 45650
Islamabad, PAKISTAN.

Cell: +92-345-5770844
Webpage: http://fayyazafsar.bravehost.com
Email: fayyazafsar@gmail.com